UNIVERSITA' POLITECNICA DELLE MARCHE

FACOLTA' DI **INGEGNERIA**

Corso di Laurea magistrale **Meccanica – Curriculum Energia**

MODELLAZIONE DINAMICA DEI SISTEMI DI STOCCAGGIO DELL'ENERGIA TRAMITE SUPERCONDENSATORI PER L'APPLICAZIONE NELLA RETE "EUROFUSION"

DYNAMIC MODELING OF SUPER-CAPACITOR ENERGY STORAGE SYSTEMS FOR EUROFUSION NETWORK APPLICATION

Relatore: Chiar.mo/a

Prof. **Gabriele Comodi**

Tesi di Laurea di:

Carlo Rinaldi

A.A. **2023** / **2024**

Outline

List of Figures

List of Tables

Acknowledgments

First of all, I would like to thank my supervisors at UNIVPM and TU/e.

Prof. Mosé Rossi and Gabriele Comodi for giving me the opportunity to do my thesis internship in Eindhoven;

I would like to thank Christina Papadimitriou for taking the role of my supervisor at TU/e, and for having routed me at the beginning of my period abroad, when I went there without knowing anyone; it could be a bit intimidating at first, but it wasn't in fact.

I would like to thank PHD student Jeroen Markus and post-doc student Kha Nguyen for being always available and giving me precious advice for the thesis.

Furthermore, I would like to thank all the people I met over these months in the Netherlands, especially Lingkang, Giacomo, Emma, Juan, Hande, Mark and the guys from Pusphaira team, who made this experience not only educational but also enjoyable and funny.

Moreover, deep gratitude to my family, for their support during the whole University period, and for giving inspiration and motivation, never being overwhelming.

Further, I would like to thank all my group of friends in Jesi, for constantly keeping in touch during my period abroad, not making me feel distant at all.

Finally, a big thank to my girlfriend Francesca, for always being there for me, even when separated by hundreds of kilometers.

Abstract

This graduation project finds its place in between two other projects about DEMOfusion Plant Electrical System network, assigned to Technische Universiteit of Eindhoven (TU/e), Netherlands.

DEMOnstration Power Plant (DEMO) is part of EUROfusion, an ambitious european project with the aim to pave the way towards commercial nuclear fusion energy. Since its schedule foresees still several decades for the project to be commissioned, some data are still indicatives and different paths could be chosen during its development.

DEMO, as the word suggests, should demonstrate a complete implementation of fusion technology: from fuel to electric power for the transmission grid. Inherent to the fusion power plant design, both the production of power as well as power consumption vary throughout the cycle: therefore, mitigation is required to ensure that the stability of the grid is not compromised. To this aim, mitigation is supposed to be fournished by an electric Energy Storage System.

Before this graduation project, a former Master of Science thesis work has been carried out at TU/e about this topic, dealing with energy balance of the DEMOfusion Plant Electrical System, followed by a multi-criteria analysis of several electrical Energy Strorage Systems in order to assess which one could be the most suitable for DEMOfusion operation.

As a conclusion of this project it tourned out that, as present, Super Capacitor Energy Storage is the most favourable one, followed by Superconducting Magnetic Energy Storage.

The other project, not yet performed at the time of writing this thesis, is assigned to a post-doctoral student at TU/e as well, who is supposed to model a simplified Plant Electrical System network, including the Energy Storage System (most likely Supercapacitor), for dynamic simulations of the network. The simulation tool chosen for this aim is MATLAB Simulink.

This thesis project, after a relatively detailed introduction about DEMOnstration Power Plant, deals with Supercapacitors and their modeling.

The main goal is to find a model of Supercapacitors which best represents their physical and electrical features, in order for the up-coming project to include into simulations a Supercapacitor Simulink block which works properly, as a black box.

In order to do this, an introduction about Supercapacitors is presented, followed by a detailed description of their construction, working principle and physical processes happening inside of them in order to understand how to build a model, *i.e.* an equivalent circuit that behaves as similarly as possible to a real Supercapacitor.

The model should properly simulate the behaviour of the Supercapacitor in the time-span of seconds, minutes and hours. Different test simulations in MATLAB Simulink, Simscape and Specialized Power Systems are carried out to this aim.

A comparison between three different model is presented towards the end of the thesis concerning the time-span of hours, namely the self-discharge profile of the Supercapacitor. Experimental results are taken from literature for different Supercapacitors, in order to assess the robustness of the models for a variety of Supercapacitors' key parameters.

On this project, Electric Double Layer Capacitors (EDLCs) are taken into account as they are the most widely used at present, but either Pseudo-Capacitors or Hybrid Capacitors should not be discarded a priori for DEMOfusion application.

Sintesi

Questo progetto di laurea si colloca tra due altri progetti relativi al DEMOnstration Power Plant, assegnati alla Technische Universiteit Eindhoven (TU/e), Olanda.

Il DEMOnstration Power Plant (DEMO) fa parte di EUROfusion, un ambizioso progetto europeo con l'obiettivo di spianare la strada verso l'energia da fusione nucleare commerciale. Poiché il suo programma prevede ancora diversi decenni prima che il progetto sia completato, alcuni dati sono ancora indicativi e durante il suo sviluppo potrebbero essere scelti percorsi diversi da quelli proposti al momento della scrittura di questa tesi.

DEMO, come suggerisce il termine, dovrebbe dimostrare una completa implementazione della tecnologia di fusione: dal reattore all'energia elettrica per la rete di trasmissione. Internamente alla rete, sia la produzione che il consumo di energia subiscono grandi variazioni durante il ciclo: pertanto, è necessaria una mitigazione per garantire che la stabilità della rete non venga compromessa. A tal fine, la mitigazione dovrebbe essere fornita da un sistema di accumulo di energia elettrica.

Prima di questo progetto di laurea, un precedente lavoro di tesi magistrale è stato svolto presso la TU/e su questo argomento, trattando il bilancio energetico del Sistema Elettrico dell'Impianto DEMOfusion, seguito da un'analisi a più criteri di diversi Sistemi di Accumulo di Energia elettrica per valutare quale potesse essere il più adatto per l'applicazione nella rete DEMOfusion.

Come conclusione di questo progetto, è emerso che, allo stato attuale, il SuperCapacitor Energy Storage System (SCES) risulta essere il migliore, seguito dal Superconducting Magnetic Energy Storage (SMES).

L'altro progetto, non ancora realizzato al momento della scrittura di questa tesi, è assegnato anch'esso a uno studente post-dottorato presso la TU/e, che avrà il compito modellare una rete semplificata del Sistema Elettrico dell'Impianto, includendo il Sistema di Accumulo di Energia (più probabilmente Supercondensatori), per simulazioni dinamiche della rete. Lo strumento di simulazione scelto a tale scopo è MATLAB Simulink.

Questo progetto di tesi, dopo un'introduzione relativamente dettagliata sul DEMOnstration Power Plant, tratta dei Supercondensatori e della loro modellazione.

L'obiettivo principale è trovare un modello di Supercondensatori che rappresenti al meglio le loro caratteristiche fisiche ed elettriche, in modo che il prossimo progetto possa includere nelle simulazioni un blocco Simulink del Supercondensatore, a scatola chiusa, che funzioni correttamente.

A tal fine, viene presentata un'introduzione sui Supercondensatori, seguita da una descrizione dettagliata della loro costruzione, del principio di funzionamento e dei processi fisici che avvengono al loro interno per capire come costruire un modello, ovvero un circuito equivalente che si comporti il più simile possibile a un vero Supercondensatore.

Il modello dovrebbe simulare correttamente il comportamento del Supercondensatore nel lasso di tempo di secondi, minuti e ore. Per questo scopo, vengono effettuate diverse simulazioni di test in MATLAB Simulink, Simscape e Specialized Power Systems.

Occorre specificare che sono stati presi in considerazione i Condensatori a Doppio Strato Elettrico (EDLC) poiché sono i più ampiamente utilizzati al momento, ma gli Pseudo-Capacitori o i Condensatori Ibridi non dovrebbero essere scartati a priori per l'applicazione DEMOfusion.

I modelli presi in cosiderazione in questa tesi sono principalmente tre: il modello di Stern, il modello di Zubieta, e un altro modello a quattro rami costruito durante questo progetto.

La scelta del modello da utilizzare nelle future simulazioni della rete del PES deve essere un compromesso tra accuratezza e costo computazionale. Il modello di Stern è il più semplice da usare, poiché può ricevere come input tutti i parametri principali, reperibili in ogni datasheet commerciale di supercondensatori, nonché i dati sperimentali di test di carica/scarica a corrente costante e di self-discharge.

Al contrario, i modelli di Zubieta e a quattro rami richiedono una parametrizzazione preliminare, cioè è necessario trovare tutti i valori dei parametri dei loro circuiti equivalenti prima di utilizzarli per le simulazioni. La parametrizzazione utilizzata per i modelli di Zubieta e a 4 rami è stata implementata in uno script MATLAB interfacciato a Simulink/Simscape, ed ha portato a risultati soddisfacenti.

Per simulazioni brevi, quindi nell'arco di pochi secondi o minuti, tutti i modelli forniscono risultati con sufficiente accuratezza. La robustezza dei risultati è stata confermata per una varietà di diversi supercondensatori e condizioni iniziali differenti.

Tuttavia, l'analisi della self-discharge (lasso di tempo di alcune ore) ha portato a differenze tra i modelli; il modello di Stern, sebbene gli siano stati dati i risultati dei test sperimentali come input, non rappresenta correttamente l'andamento della tensione del supercondensatore: poiché la sua risposta è caratterizzata da una pendenza costante, il cui errore viene accumulato dopo circa mezz'ora di circuito aperto.

Pertanto, il modello di Stern è adeguato per simulazioni brevi e come prima approssimazione, e il suo costo computazionale è piuttosto basso.

Al contrario, il modello di Zubieta rappresenta la self-discharge in maniera accettabile, almeno per le prime due ore di circuito aperto, ovvero il ciclo di tempo del reattore nucleare. Il costo computazionale, non eccessivo, è comparabile a quello del modello di Stern.

Risultati ancora più accurati sulla self-discharge sono emersi dal modello a quattro rami, che ha fornito risultati molto precisi per quasi tutte le simulazioni, ma che ha un costo computazionale piuttosto elevato, poiché al suo interno contiene due sensori di tensione i cui segnali entrano in un loop di Simulink che calcola la resistenza e capacità dipendenti dalla tensione; questo ovviamente porta a durate più lunghe per le simulazioni. Nel prossimo progetto relativo a DEMO, verranno eseguite delle simulazioni sulla rete Plant Electrical System (PES): la rete PES è un sistema estremamente complesso, e il suo modello Simulink, anche se semplificato, richiederà un costo computazionale molto elevato: sarebbe meglio non appesantirlo ulteriormente collegandoci un blocco del sistema d'accumulo eccessivamente complesso.

In fin dei conti, il modello di Zubieta offre un buon compromesso tra complessità e accuratezza. In questi termini, la scelta migliore sarebbe utilizzare questo modello per i lavori futuri, con la cura di effettuare una corretta parametrizzazione del modello prima di utilizzarlo per le simulazioni.

1. Introduction

1.1 Energy challenge

Energy is the milestone of civilization. Human progress is undoubtedly intertwined with the availability of energy sources. Innovations over thousands of years in human existence have increased the availability of energy to mankind as well as shifted the supply of energy from muscle to machine [1]. Since the industrial revolution, energy usage per capita worldwide has increased three-fold, and in Europe this figure has increased six-fold [1]. The availability of energy was provided by fossil fuels. Over the last century, the supply of energy has been complicated by the issue of climate change. Climate change is driven by the usage of carbon deposits such as coal, oil, and gas which after usage end up in ecosystems (e.g. atmosphere, oceans). These three fossil fuels account for 80.9% of the world's primary energy supply (2021) [2]. Since around three-quarters of greenhouse gas emissions are tied to the use of energy [3], it is evident that an alternative supply of energy is required. These alternatives can be divided into three main categories: renewable energy sources, nuclear fission, and nuclear fusion [4].

This thesis project is related to the development of nuclear fusion technology.

So far, man has been able to control fusion reactions for very short periods of time, a few seconds at most; this technology has been by far the least used one until now, in fact almost untapped at all, due to its extreme physical and engineering complexity, which results in high costs and long timelines for design and construction [5]. However, something has been changing in the last few years.

Fusion technology has inherent characteristics that could make it superior to both renewable energy sources and nuclear fission. The former ones are useful as a support of energy supply, but they cannot be considered as a stand-alone source of energy on large scale yet, mostly because of two of their shortcomings: space efficiency and, especially, dependency on weather conditions, which make them uncontrollable and difficult to predict [6].

Furthermore, nuclear fission has several limitations. First, Radioactive waste is extremely dangerous and long lasting; expensive measures must be taken to store it. In some cases, the waste is stored deep underground and must be kept for tens of thousands of years. Over time, this could leak and cause underground water and soil pollution. Second, like fossil fuels, nuclear fuels used for fission, such as uranium ore, are non-renewable energy resources since supplies will not last forever, and although nuclear fission is a non-polluting process, the mining, transport and purification of uranium ore releases significant amounts of greenhouse gases into the atmosphere. But the main aspect that limits public acceptance is undoubtedly safety [4]. Although substantial safety precautions are taken, in an unlikely event, a meltdown could occur which could spread radioactive particles over an entire continent, as well as people's concerns about living close to a nuclear power plants.

Due to inherent plasma physics, such an event cannot occur with fusion. Another disadvantage of fission is long-lived radioactive waste products. These need to be stored safely in some cases for many thousands of years [7]. Fusion also produces radioactive products but is favourable over fission on radioactivity, cardiotoxicity, and radioactive waste [7], so that the environmental impact is considered low to very low [8].

The prospect of Fusion Energy shows that it would be a valuable resource to society. The technology boasts inherent safety properties, minimal environmental impacts and will likely become economically competitive [9]. It could provide virtually limitless clean, safe, and affordable energy to meet the world's demand.

Fusion technology as of now is not mature; the European roadmap foresees that fusion technology will need several decades of development [10].

1.2 Nuclear fusion

Nuclear fusion is the process by which two light atomic nuclei combine to form a single heavier one while releasing massive amounts of energy. Fusion reactions take place in a state of matter called plasma, which is a hot, charged gas made of positive ions and free-moving electrons with unique properties distinct from solids, liquids or gases. The sun, along with all other stars, is powered by this reaction. To fuse in our sun, nuclei need to collide

with each other at extremely high temperatures, in the order of tens of million degrees Celsius. The high temperature provides them with enough energy to overcome their mutual electrical repulsion. Once the nuclei come within a very close range of each other, the attractive nuclear force between them will outweigh the electrical repulsion and allow them to fuse: for this to happen, the nuclei must be confined within a small space to increase the chances of collision.

In the sun, the high temperatures alongside the extreme pressure produced by its immense gravity creates the conditions for fusion [11]. On earth, since we cannot have high pressures like those in the sun, even higher temperatures than the solar ones must be reached. Most of the fusion reactor concepts under development, including Eurofusion's ITER, are using a mixture of Deuterium and Tritium isotopes, so hydrogen atoms that contain extra neutrons. The reaction consists in the fusion of Deuterium and Tritium that transform into a neutron and a Helium nucleus [5], as can be seen in Figure 1.1.

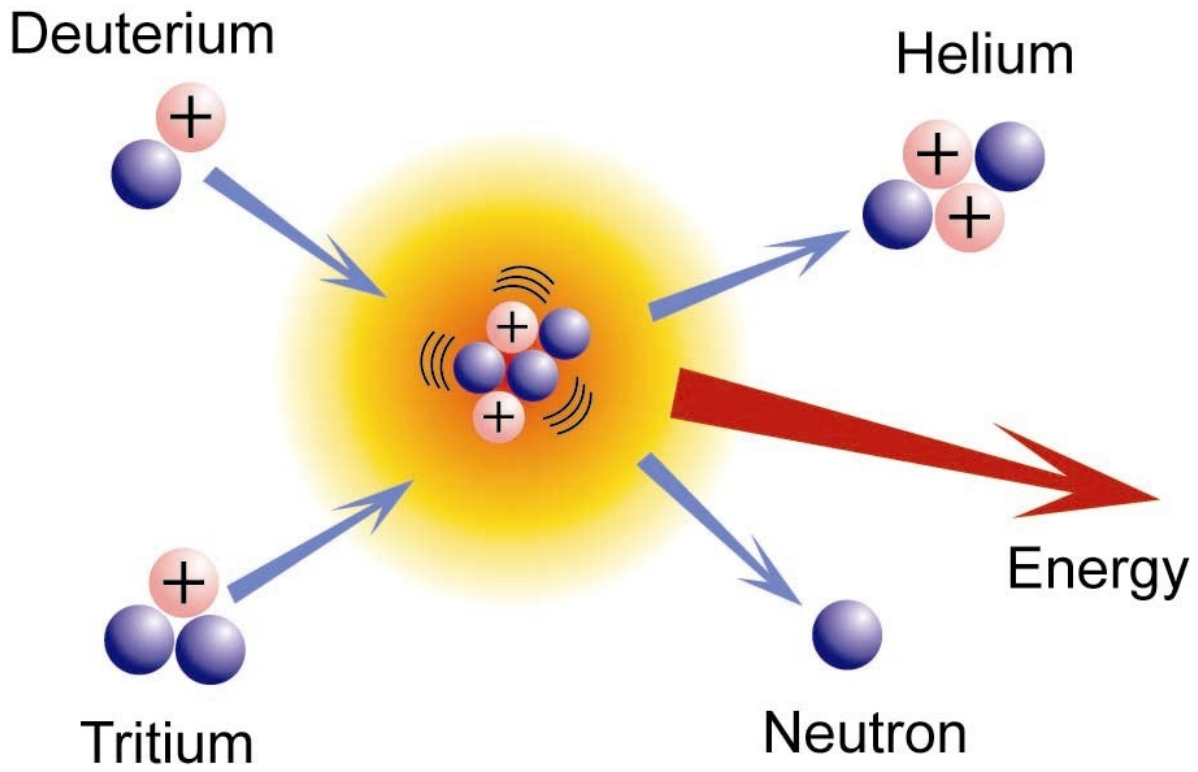

Figure 2.1: *Nuclear fusion reaction of Deuterium and Tritium*

In theory, with just a few grams of these reactants, it is possible to produce a terajoule of energy, which is approximately the energy one person in a developed country needs over sixty years. Furthermore, fusion fuel is plentiful and easily accessible: Deuterium can be extracted inexpensively from seawater, and Tritium can potentially be produced from the reaction of fusion generated neutrons with naturally abundant lithium. These fuel supplies would last for millions of years. Future fusion reactors are also intrinsically safe and are not expected to produce high activity or long-lived nuclear waste. Furthermore, unlike fission, as the fusion process is difficult to start and maintain, there is no risk of a runaway reaction and meltdown; fusion can only occur under strict operational conditions, outside of which (in the case of an accident or system failure, for example), the plasma will naturally terminate, lose its energy very quickly and extinguish before any sustained damage is done to the reactor.

As mentioned before, nuclear fusion, just like fission, does not emit carbon dioxide or other greenhouse gases into the atmosphere [11].

1.3 Aim of the project

As mentioned in the abstract of the thesis, this graduation project finds its place in between two other projects about DEMOfusion network, which will be described in the following chapter.

The first project was a Master of Science thesis work carried out at Technology University of Eindhoven (TU/e), dealing with electric power and energy balance of the DEMOfusion Plant Electrical System, followed by a multi-criteria analysis about several electrical Energy Strorage Systems in order to assess which one could be the most suitable for DEMOfusion operation. As a conclusion of this project it tourned out that, as present, Super Capacitor Energy Storage is the most favourable one, followed by Superconducting Magnetic Energy Storage.

The other project, assigned to a post-doctoral student at TU/e as well, is supposed to model a simplified Plant Electrical System network, including the Energy Storage System (most

likely Supercapacitor), for dynamic simulations of the network. The simulation tool used is MATLAB Simulink, with Specialized Power Systems toolbox.

The aim of this project is thus to make a detailed analysis about Supercapacitors, and try to find a model which best represents their physical and electrical features, in order for the up-coming project to include into simulations a Supercapacitor block which works properly as a black box.

In order to do this, one should figure out what supercapacitors are made of, how they store energy, what are their key parameters, in order to understand how to build a model, *i.e.* an equivalent circuit that behaves as similarly as possible to real experimental results taken from literature about Supercapacitors. Some models can be already found in literature, two of them already exist in Simulink Simscape and Specialized Power Systems, and some have been built from scratch.

2. EUROfusion

Eurofusion is a consortium of European national fusion research institutes, consisting of 26 EU member states, United Kingdom, Switzerland, and Norway, with the aim to pave the way for Fusion Power Reactors [12]. This is done by preparing experiments to be performed at ITER reactor, as well as developing the concept of DEMO, the demonstrative power plant with the aim to connect the energy from the reactor to the electric grid.
It is funded by national budgets of participating countries, and by the European Commission through EURATOM.

2.1 ITER

EUROfusion effort thus far has resulted in the development of several projects. Two prominent projects are the Joint European Torus (JET) and the International Thermonuclear Experimental Reactor (ITER) [13]. JET was a first-of-a-kind tokamak reactor and was considered widely successful. It had shown that it could produce 16 MW of Fusion Power for an input of 24 MW in heating corresponding to a Q factor of 0.67 [14]. The next generation reactor ITER aimed to achieve a Q factor of 10 with a thermal output of 500 MW [14].
ITER is currently under construction in Cadarache, on the southern part of France.
In ITER, fusion will be achieved in a Tokamak device that uses magnetic fields to contain and control the hot plasma. The magnetic fields are generated by several toroidal coils and solenoid systems, and the plasma is contained within the breeding blanket (Figure 2.1).
Plasma in the tokamak will be heated up to around 150 millions degrees Celsius, while conductor materials for magnetic field generation are hold at an extremely low temperature, around -260°C, so ITER system could be the hottest and the coldest place in the world at the same time.
Since the temperatures needed for nuclear fusion would melt down any existing material on earth, the idea is to generate such a magnetic field which is able to confine plasma in its coils, keeping it away from the containing walls.

In ITER, several heating methods will work concurrently to bring the plasma in the core of the machine to those temperatures [15]. Within the tokamak, the changing magnetic fields that are used to control the plasma produce a heating effect. The magnetic fields create a high-intensity electrical current through induction, and as this current travels through the plasma, electrons and ions become energized and collide. Collisions create "resistance" that results in heat, but paradoxically as the temperature of the plasma rises, this resistance, and therefore the heating effect, decreases. Heat transferred through high-intensity current, known as ohmic heating, is limited to a defined level. In order to obtain still higher temperatures and reach the threshold where fusion can occur, heating methods must be applied from outside of the tokamak [15].

Two other external heating methods, neutral beam injection and high-frequency electromagnetic waves, will complement ohmic heating to bring the ITER plasma to temperature.

Neutral beam injection consists in shooting high energy neutral particles from outside the Tokamak into the plasma, transferring their energy to the plasma particles.

Millions of watts of heating power can be delivered to the plasma using this technique, bringing its temperature closer to the level where fusion can occur.

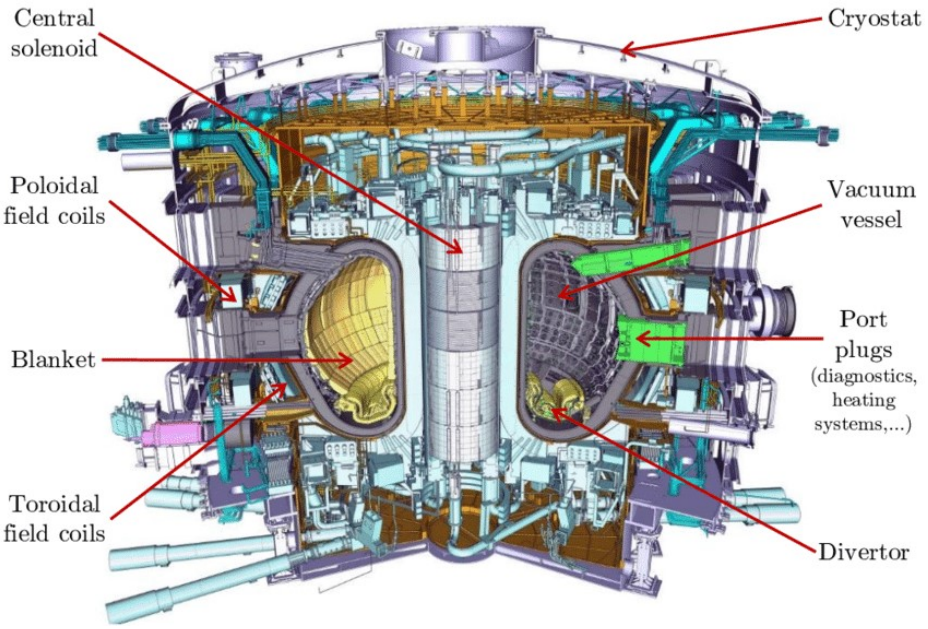

Figure 2.1: *ITER Tokamak Fusion Reactor design, main inner parts*

A third source of heat, high frequency electromagnetic waves, is planned into the design of the ITER Tokamak to boost temperatures to the required 150 million °C.

This principle is similar to how microwaves transfer heat to food in a microwave oven, increasing the velocity of the particles' chaotic motion, as well as the temperature [15].

Therefore, theese three types of waves will be employed in ITER, each matching a frequency of plasma ions and electrons in the interior of the ITER machine to maximize heat transfer.

2.2 DEMOnstration Power Plant

After ITER, the DEMOnstration power plant (DEMO) is next in line to develop fusion technology for a commercial future.

Like the name implies, it has the ambitious goal to be the first demonstrative power plant based on nuclear fusion, and to produce and distribute electrical power throughout Europe, thanks to a connection with the European High Voltage Electrical Grid (typically at 400 kV) [16]. The aim is a Q factor of 25, with a thermal output of 2 GWth [17]. Subtracting conversion losses and self-consumption, the net energy production should be around 300-500 MWe of electricity [12].

DEMO is an extremely complex system, with many subsystems (Figure 2.2).

For the purposes of this graduation project, only the Plant Electrical System (PES) and the Balance of Plant (BoP) are considered, and other systems are regarded as interfaces.

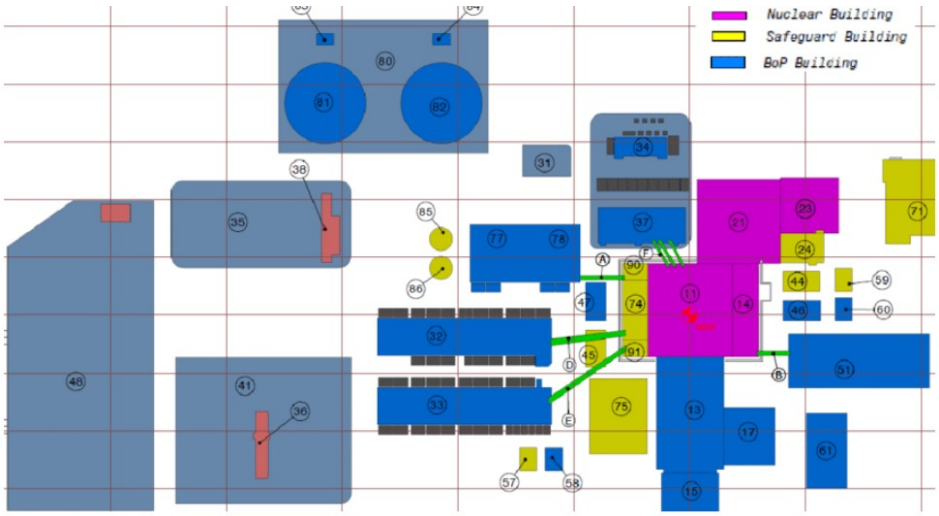

Figure 2.2: *DEMO preliminary plant layout*

The central problem of connecting DEMO to the electricity grid are the intermittent components associated with fusion technology. Due to a limited confinement time, the fusion reaction is not continuous, and reactors have a pulsed thermal production [18].

Besides the pulsed operation on the production side, also consumption of the plant is pulsed. For example, to start DEMO's fusion reaction, a spike in active power is required in the order of 1 GW [19]. To put this figure into perspective, it is in the order of the average consumption of countries such as Estonia, Latvia, and Luxembourg.

In figure 2.3, the EUROfusion foreseen schedule can be checked out.

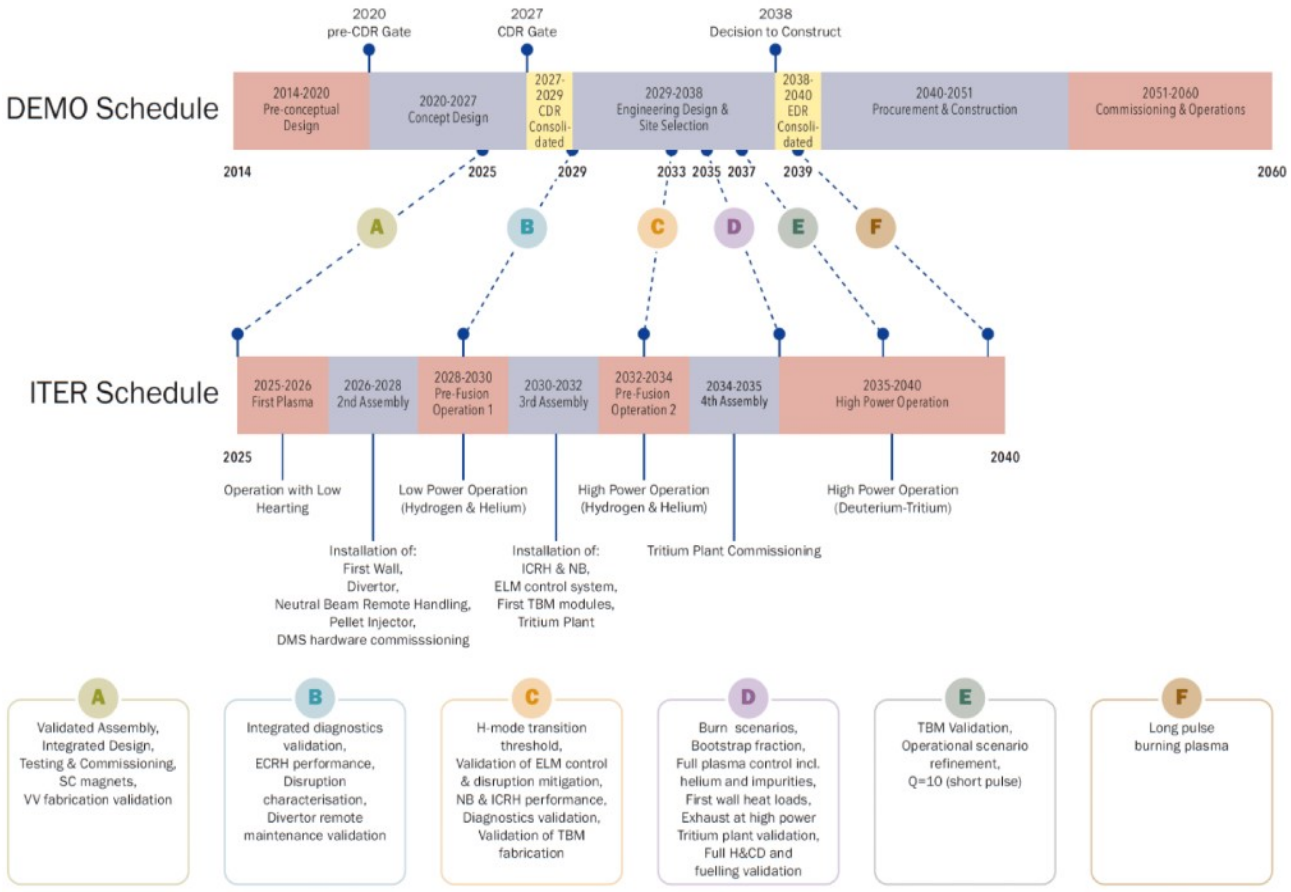

Figure 2.3: *Overview of the European Roadmap to the realization of Fusion Energy. The reported dates are still indicatives [16]*

Moreover, there are several discontinuities thoughout the cycle, so that both the initiation and the control of fusion processes, besides the problems related to the nuclear physics itself, need very complex electrical systems. Also the conversion of the output power is not trivial because of the inherent discontinuity in the DEMO operations [16].

All of the above can disturb the balance of the electricity grid if no mitigation is provided.

Energy Storage System (ESS) are well suited to smooth out variable power production. Application of ESS at DEMO was already envisioned in the form of Thermal Energy Storage (TES) [16]. Although TES is well-suited to smooth out the thermal output of DEMO, the associated response time is too slow to deal with the faster phenomena of the varying self-consumption profile. To this end, Electrical Energy Storage Systems (eESS) could be used [20, 21].

The DEMO operations are strictly related to the physics of the plasma. This also implies a difficulty to achieve very long or steady-state operations that would be preferable for the energy budget. A lot of fusion research is devoted to the possibility of steady-state operations, but presently without relevant practical results. On the other hand, pulsed operations simplify tokamak physics and may be more flexible in an energy market ruled by renewable sources. Presently, the DEMO operations are supposed to be pulsed in basic option but could be steady-state in future advanced ones [16].

In particular, the DEMO operations consist of seven phases:

1. Central Solenoid (CS) pre-magnetization. Some superconductive magnets must be energized to attain a suitable value of magnetic flux into the Vacuum Vessel. The energization current in the DEMO CS modules is expected to be up to 45 kA and to span the range ±45 kA [22]. The duration of the pre-magnetization phase mainly depends on the maximum possible charge rate of the superconductors. The pre-magnetization is typically executed by supplying the superconductors at rather constant voltage, producing an increasing current and resulting in an increasing power demand from the grid. The start of the pre-magnetization phase is conventionally set to a negative value of time and ends at zero.
2. Plasma breakdown. It is the shortest (about 1 s) but also the most critical phase from the power supply point of view. The plasma initiation requires high-power pulses in several superconducting coils (at least in the Central Solenoid). The effective presence of the plasma in the tokamak vessel starts in this phase.
3. Plasma ramp-up. In this phase, the plasma current is progressively increased by the coils and H&CD sources. The ramp-up must be slow in order to keep the plasma under control.

On the other hand, the available CS magnetic flux is consumed by the ramp-up duration, reducing the useful time for the production of electrical energy.

4. Heating flat-top. All the H&CD sources are used to heat up the plasma until fusion temperature and conditions are reached.
5. Burn flat-top. DEMO produces energy thanks to the nuclear fusion reactions. Ideally, during this phase, the fusion reactions taking place at a sustainable rate guarantee the self-sustainment of the plasma. This phase is very long, about 7200 s (2 h).
6. Plasma ramp-down. The plasma is gradually switched off, maintaining its control by coil and H&CD power.
7. Dwell time. It is the time required after the pulse to bring DEMO to a condition stable enough to start a new pulse and to create an adequate vacuum inside the plasma chamber. Of course, it is desirable that the DEMO design will progress towards negligible dwell times. Actually, dwell time conventionally includes also the CS pre-magnetization phase since the CS charging action belongs to those operations necessary to complete a pulse and start the following one. However, since this operation does not last the whole dwell time, in this work they are managed as two different and consecutive phases.

Every DEMO operation and its duration is summarised in Table 2.1, and the sketch is shown in figure 2.4. The duration of the whole cycle is approximately 8240 s (around 2 hours and 17 minutes).

Table 2.1: *Summary of the DEMO operation phases with typical durations*

Phase	Phase Name	Typical Time Duration
1	CS pre-magnetization	500 s
2	Plasma Breakdown	1.4 s
3	Plasma ramp-up	180 s
4	Heating flat-top	10 s
5	Burn flat-top	7200 s
6	Plasma ramp-down	150 s
7	Dwell time	200 s
Total time duration of the DEMO operations		≈8240 s

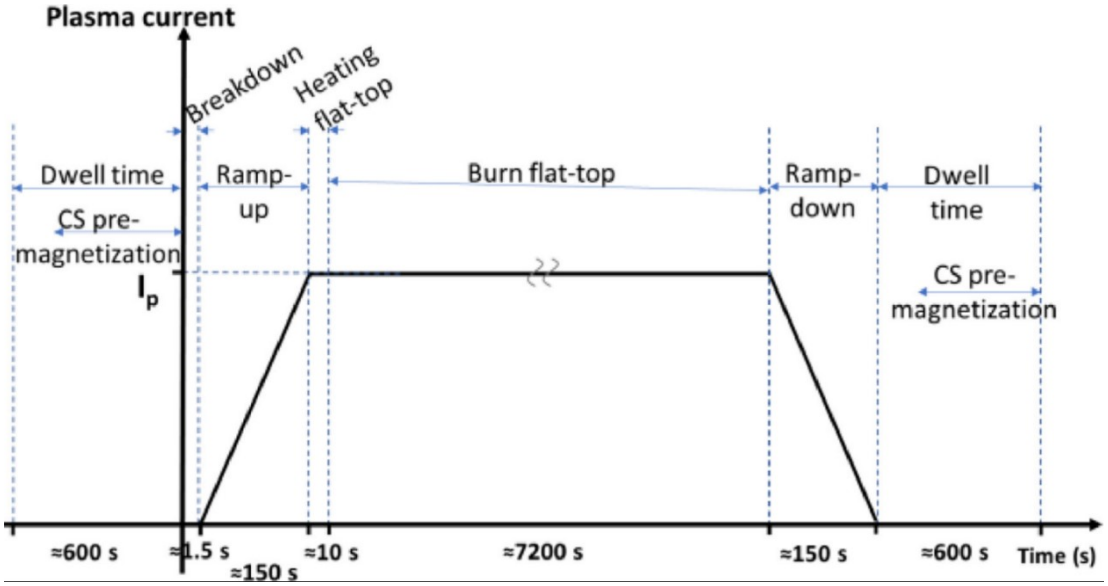

Figure 2.4: *Sketch of plasma pulse indicating the main phases*

2.2.1 Balance of Plant

Although not further considered in this graduation project, an outline of the Balance of Plant is provided in this paragraph.

In DEMO, the Balance of Plant (BoP) transfers thermal energy generated in the reactor to the turbine generator, so anything upstream of the turbine. The BoP can be further characterized by the following subsystems: the Primary Heat Transfer System (PHTS), Intermediate Heat Transfer System (IHTS), and the Power Conversion System (PCS). As the name suggests, the Primary Heat Transfer System is the first interface to transfer thermal energy.

Currently, there are two alternative working fluids that transfer thermal energy from the Breeding Blanket (BB) namely water or helium [23]. The system variant using the former working fluid is referred to as Water Cooled Lithium Lead (WCLL) and the latter is Helium Cooled Pebble Bed (HCPB). The PCS converts this thermal energy into electrical energy using a Rankine cycle [23]. Since the plasma physics are assumed to be pulsed, the thermal production which is transferred will be as well, resulting in a pulsed electrical output [19].

Currently, there are two branches of design in DEMO for transferring the thermal energy to the PCS: directly, or indirectly [23]. In the Direct Coupling Design (DCD), thermal energy from the BB is directly converted into steam which is used in the steam turbine to generate shaft

work. During dwell, depending on subvariant, a small ESS or auxiliary boiler would generate steam for 10% nominal output of the TG to avoid excessive mechanical and thermal stresses [23]. The Indirect Coupling Design (ICD) involves an IHTS.
Thermal output from the BB is transferred to an ESS which outputs a steady steam mass flow rate which is converted into a steady electrical power output of the TG [28].

2.2.2 Plant Electrical System

The Plant Electrical System is one of the largest systems in DEMO.
It is tasked to achieve two main objectives:
• Provide the needed power to the plant electrical loads, for Self-Consumption
• Deliver the generated net electrical power to the Power Transmission Grid
A representation of the PES can be found in Figure 2.5.
It connects to many subsystems at DEMO, which are classified into the following 5 sub categories: Turbine Generator (TG), HV Switchyard & Power Distribution, Heating and Current Drive Power Supply (H&CD PS), Coil Power Supply (CPS), and Steady State Loads.
Here the purpose and characteristics of the subsystems are briefly presented:

Turbine Generator: This subsystem is tasked with converting the mechanical shaft work of the steam turbine into electrical energy. It consists of a synchronous generator.
This system is considered without inclusion of steam generator, which converts thermal power produced by the reactor to mechanical shaft work.

HV Switchyard & Power Distribution: This category of systems forms the connection between the PTG and all loads of the plant. Consists primarily of transformers, busbars and power cables.

Heating and Current Drive Power Supply: This is a pulsed load that is involved with initiating, stabilizing, and switching off plasma. The reference system for this task is the Electron Cyclotron Resonance Heating (ECRH) system.

Coil Power Supply: The CPS is a pulsed load that will supply the voltage and currents to the SC coils. Its main task is to form, sustain and control the plasma during a pulse.

Steady State Loads: This system contains all other electrical loads of the plant. Examples of loads that fall under this category are cooling, cryoplant, tritium extraction, diagnostics, auxiliaries, building and plant site services, emergency power, safety, and investment protection systems.

In the figure, the green box represents the High Voltage electrical Network (HVN), providing the transmission of high voltage (HV, higher than 30 kV) within the plant and the delivery to the external Power Transmission Grid of the net electrical power, resulting from the gross electrical power minus the recirculation power to supply the plant electrical loads. The violet block includes the components of the Medium Voltage and Low Voltage electrical Network (MLVN) to provide the relevant electrical power to the plant electrical loads, according to their classification. The MLVN also includes the emergency power supplies (EmPS) [19].

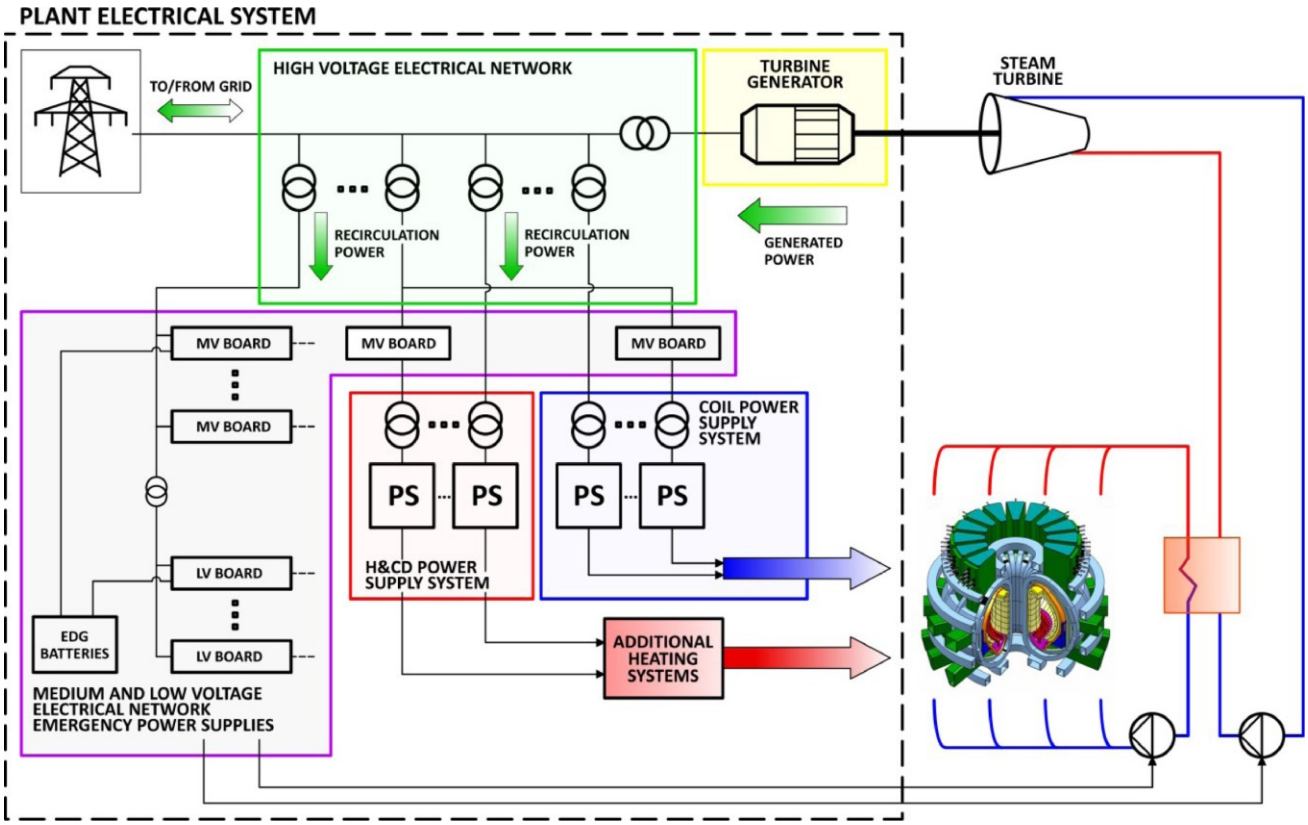

Figure 2.5: *Simplified subsystem representation of PES*

2.2.3 Plant Electrical System power profiles

In this section the power profiles of the before mentioned PES subsystem are outlined in greater detail and their power profiles are shown.

Steady State Loads

The power plant consumes electrical energy to operate. Next to running the building, also systems such as the cryoplant, fueling, and control systems require electricity. This electrical consumption depends in large part on the configuration of the BoP.

The BoP consumes electrical energy to transfer the thermal energy from the reactor to the steam turbine. A major distinction in BoP consumption is a difference in Primary Heat Transfer System (HCPB and WCLL, as seen before).

Since thermal production only occurs during the flat top burn, pumps that move this thermal energy are not required to function at nominal production [16].

In the HCPB PHTS, the dwell consumption of the breeding blanket is 20% of nominal consumption (at a ramprate of 20%/min) [16].

For the WCLL PHTS, there is a limited saving of energy, since pressurizers are used instead of motor pumps, which does not justify additional cycling stresses [16]. Nevertheless, in the WCLL option, there is a difference in dwell consumption because of the small storage and heater in the PCS [24]. Presently, only the BoP has a varying steady state load. The active power consumption of steady state loads for both BoP configurations is shown in Figure 2.6. Note that this is an estimation of the steady-state profile. Not only is the current list incomplete, the profile assumes that steady state loads operate on their installed powers (which in reality is not necessarily requested) [24].

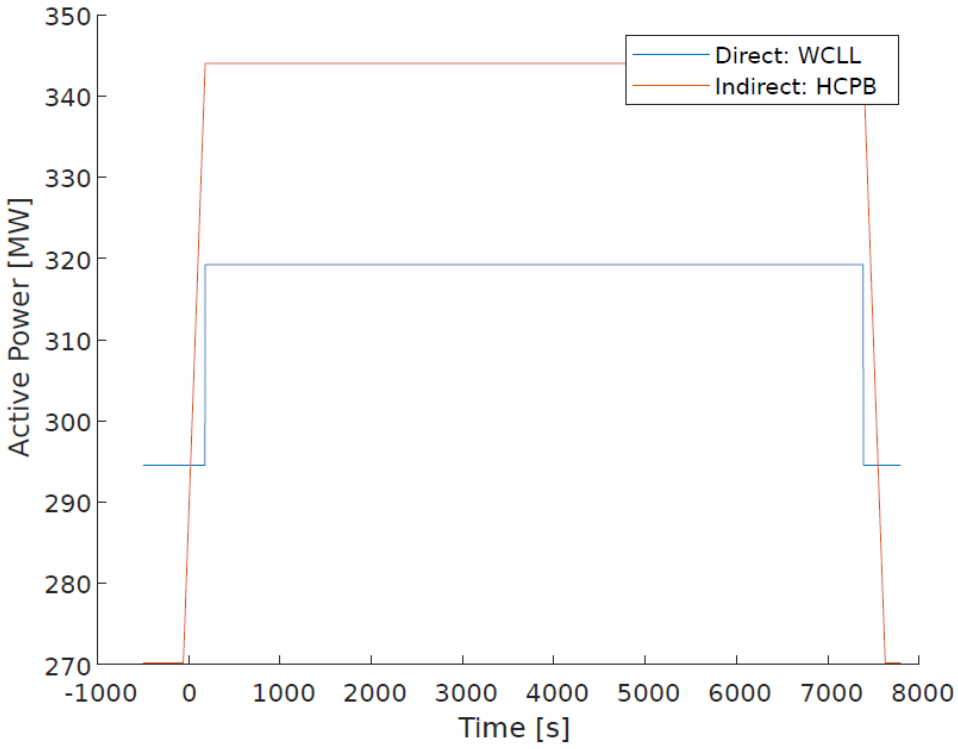

Figure 2.6: *Steady State Loads power profile*

Coil Power Supply

The function of the CPS is to provide the needed voltage and currents to the SC coils, which are used for the formation and control of the plasma. Since the power demands for these operations vary significantly throughout the cycle, the CPS is part of the pulsed power loads. The basic configuration of the modeled CPS is explained on a high-level, and can be found in more detail in [19, 21]. The power profile can be seen in Figure 2.7. A high power demand peak can be seen at breakdown period, followed by high power release after breakdown. During flat-top, the CPS power demand can be considered as negligible.

The ITER-like design for DEMO entails 6 Central Solenoids and 6 Poloidal Field coils [19]. These components are both involved in confining and controlling the plasma.

Active and reactive power profiles are constructed from basic voltage and current profiles using thyristor-based technology. Sequential-control and bypass models are used to minimize reactive power demand [21].

Note that this present estimation of CPS profile is preliminary. The foreseen additional power supply required for Vertical Stabilization is not included. Furthermore, full scenarios

for voltage and current consumption were not yet available. Finally, the converter type will likely be changed from thyristors to IGBT or IGCT as this would significantly decrease the reactive power demand [21].

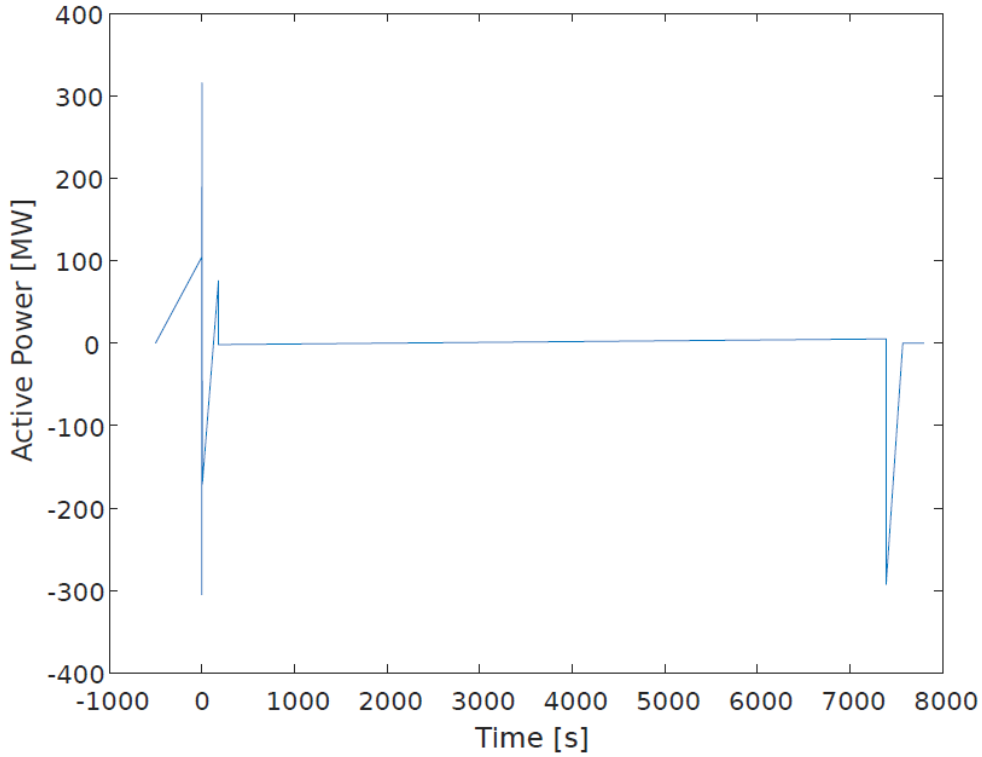

Figure 2.7: *CPS active power demand profile*

Heating and Current Drive Power Supply

The H&CD PS system is tasked with controlling the plasma throughout all stages of an operational cycle: initiation, controlling ramp-up/down, heating to H-mode, controlling instabilities, and switching off the plasma [25, 26]. The system uses controlled pulses of power to heat the plasma, and falls therefore under the category of pulsed power loads. The microwave heating of Electron Cyclotron Resonance Heating (ECRH) system is used as reference H&CD PS system. It should be noted that, next to it, additional heating systems are likely to be used, such as radiofrequency heating using an Ion Cyclotron Resonance Heating (ICRH), or Neutral Beam Injection, as mentioned before. A mix of heating systems will be chosen over next few years. For now, the ECRH system is selected as a reference system as it is deemed closest to implementation and is capable of fulfilling the system's main functions [25]. The reconstruction of the active power demand is taken from [27], and can be seen in Figure 2.8.

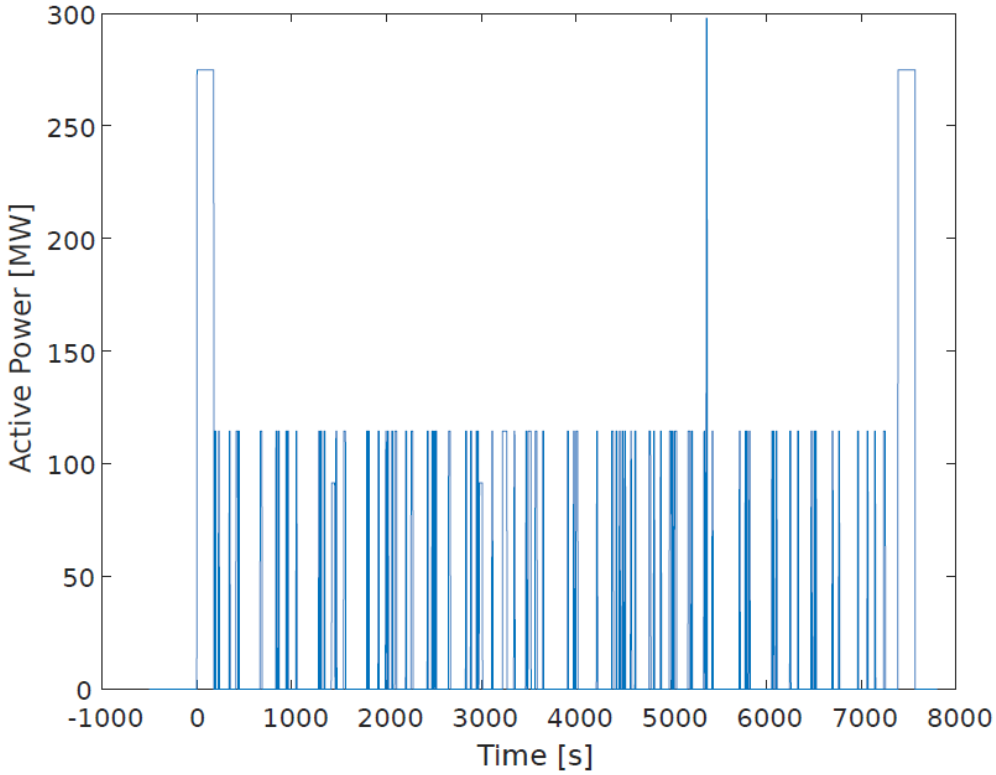

Figure 2.8: *ECRH power profile*

Turbine Generator

The TG is tasked to convert mechanical shaft work from the steam turbine into electrical energy. It produces the gross electrical power, part of which will be recirculated to supply the plant electrical loads.

It is required to be a synchronous machine, which is standard for large power generation. Also, the rotational speed of the machine should be 1500 rpm (for example through a 4 pole configuration) [28]. Besides machine requirements, operation of the active power set point is specified. The machine will be operated between nominal power down to 10% of nominal power, to prevent excessive thermal and mechanical stress [28].

Additionally, precaution is taken with ramping the TG up and down, on the same grounds. The ramp rate is considered to be between 10% per minute, referred to as reference, and the 54% per minute (close to thermal production), referred as optimized.

As mentioned in section 2.2.1, there could be two different coupling methods in the interface between the thermal power production of the reactor and the electric power generation of the Turbine Generator, direct and indirect.

In Figure 2.9, the active power profile generated by the Turbine Generator of both direct and indirect methods is displayed [19].

Note that this is a power generated by the turbine, so it has to be considered of opposite sign respect to the other ones.

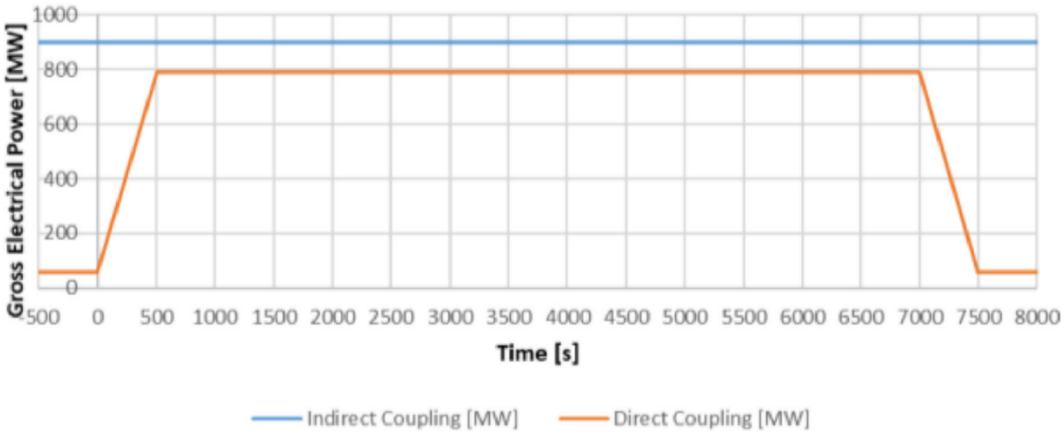

Figure 2.9: *Gross electrical power generated by the TG*

2.2.4 Power Transmission Grid limits

The aim of this section is to explain why an Energy Storage System is needed for DEMO Plant Electrical System network to be connected to the European electricity grid.

In order to do this, the project should satisfy the requirements posed by regulations of the Power Transmission grid (PTG), also referred to as grid code.

Since the location of DEMO is still undetermined, the requirements will be solely based on European-wide requirements, but note that on top of European regulations, the connecting Transmission System Operator (TSO) could pose additional requirements [27].

The requirements for connection differ for location, maximum capacity and type of Power-Generating Module (PGM). Therefore, the DEMO project ought to be classified into these categories defined by [38]. The maximum capacity and location of the project combined determine the type of PGM. The maximum capacity threshold is assumed to be 750 MW and

the location is assumed to be in Continental Europe [33]. In this way, DEMO is classified on the ordinally ranked list of PGM type (A-D) in the last category; type D, as a synchronous Power Generating Module [27].

The applicable requirements for the DEMO project are found in Article 19 of [30]. These should guarantee the following categories:

- Stability
- Admissible Power Reduction
- Frequency Sensitive Mode
- System Restoration
- Load-Frequency Control

A deeper analysis of this requirements is presented in [27]. Based on this, some tentative assumptions are made for connecting DEMO to the Power Transmission Grid. These assumptions are tentative, because the location and strength of the network at the point of connection are unknown. Therefore, they are based on plausible values in a European scenario. These assumptions detail only technical limits of the PTG, and will be refined during the Concept Design phase in collaboration with TSO [19].

The limits can be found in Table 2.2.

For the aim of this project, the focus is placed on the Active Power Peak (600 MW), Active Power Steps (150 MW) and Active Power Derivative (500 MW/s) limits.

Table 2.2: *Tentative assumptions on connecting DEMO to grid*

Characteristic	Values
Voltage Level	400 kV
Short Circuit Level	15 GVA
Voltage Drop in Steady State	1.5%
Voltage Drop during Transient	2.0%
Active Power Peak	600 MW
Active Power Steps	150 MW
Active Power Derivative	500 MW/s
Reactive Power	250 MVAR

2.2.5 Energy Storage System requirements

In this section, the reason why an eESS is needed is presented, and an estimation is made of what will be its requirements in terms of power and energy, followed by a ranking of the Energy Storage Systems that prevailed in a multi-criteria analysis from [27].

In figure 2.10, the Active Power balance of PES is displayed; it is obtained by the sum of the power consumptions of the before mentioned PES subsystems (CPS, H&CD PS, Steady State Loads), subctracted by the Power delivered by the Turbine Generator. The active power limit is visualized with a black horizontal line.

$$Psum = P_{CPS} + P_{HCD} + P_{SS} - P_{TG} \tag{2.1}$$

The Derivative profile and the Step profile are also displayed in figure 5 and 6 respectively. The derivative was calculated over a period of 1 second (MW/s) [27], and the definition of Step was chosen to be the difference between two timesteps, in which the timestep was set to 50 ms for computational reasons [27]. The limits are visualized again as black horizontal lines.

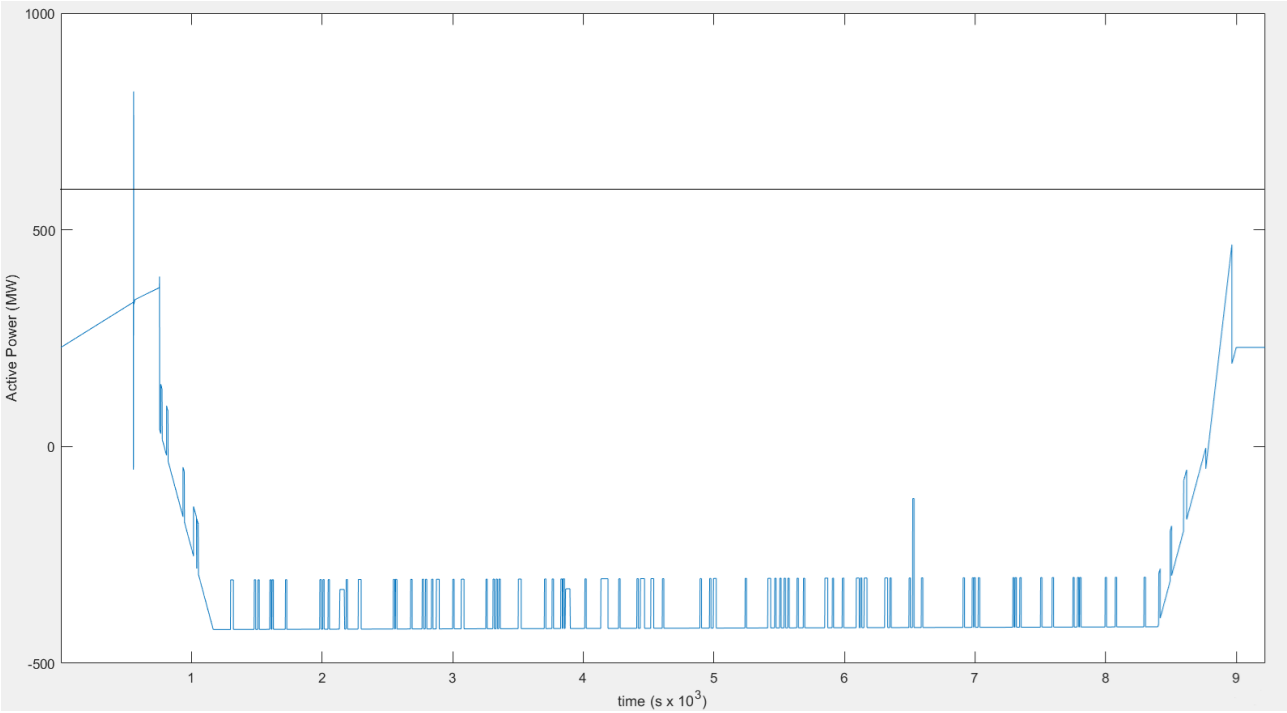

Figure 2.10: *PES Active Power profile*

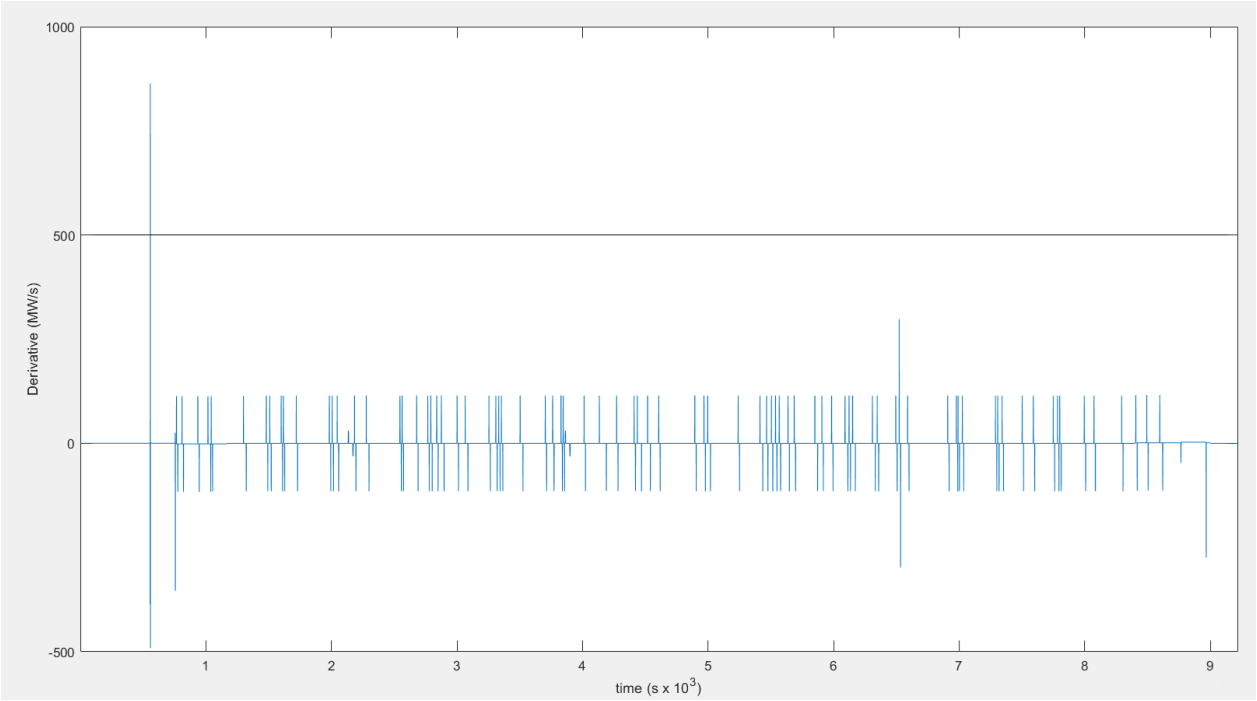

Figure 2.11: *Derivative profile*

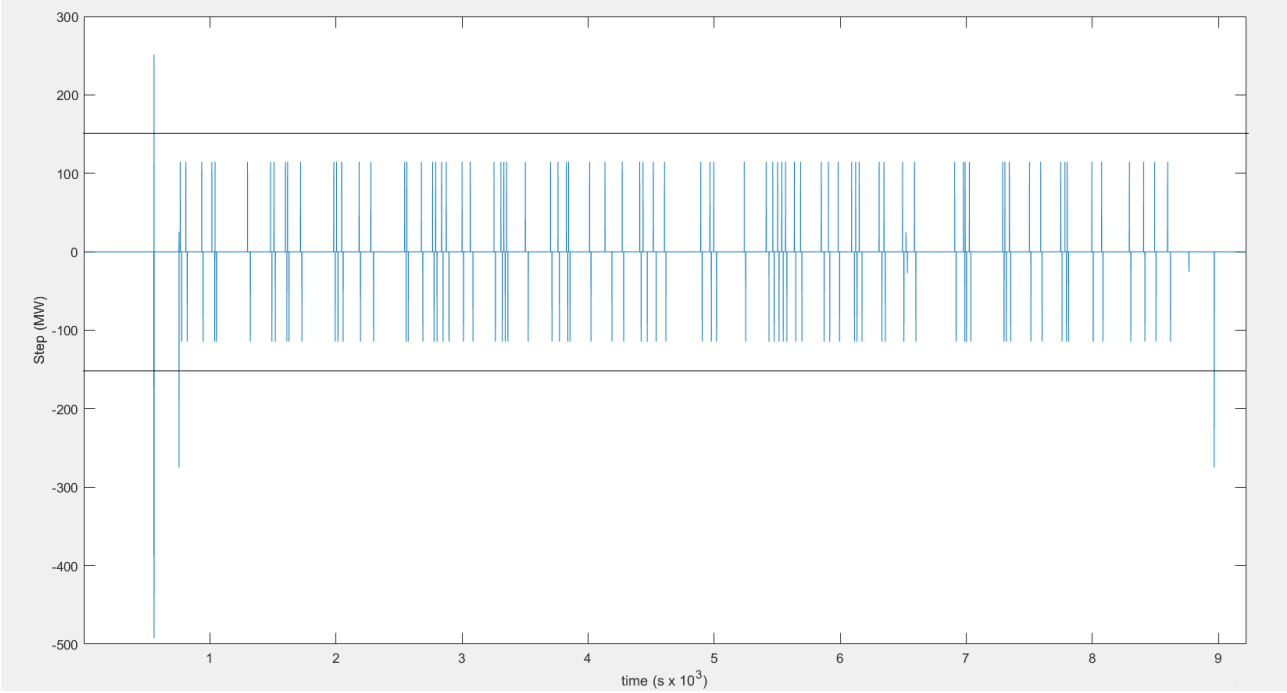

Figure 2.12: *Step profile*

Evidently, all limits are breached since the Active Power, derivative and step profiles exceed the limits at some point during the operational cycle. In the period around t = 0s (breakdown) all three limits are breached. Furthermore, the step limit is breached at the end of ramp-up and ramp-down.

Thus, an eESS is needed to compensate the difference between the profiles and their limits, providing or absorbing enough power to let all profiles stay within the limits.

Note that the only difference between active power peak and active power limit (around 361 MW) is not enough to calculate the power size of the eESS, because if eESS compensates the profile just down to the active power limit, the derivative and step profiles would still breach their limits, so eESS should lower the active power further until all the three profiles are squeezed within the limits.

Obviously, an eESS requires time to respond. It is proved in [27] that the sizing of the eESS depends on this response time, since the further lowering of the active power demand for the derivative requirement as well as the higher and longer power demand for steps increase the size of the energy storage system. Therefore, it was found that systems with slower response times require larger storage sizes. The same holds for discharge and charge ratings, systems with slower response times require more power to achieve a situation within the setup limits.

Based on different time responses, a sizing of the eESS was made in [27]. It resulted to large amounts of power size for the storage system, from 376 to 400 MW of discharge rating (depending on time response), from 161 to 216 MW of charge rating, and an energy size for of orders of magnitude lower: 38 to 50 kWh. This is logical since the longest discharge duration is around 0.6 seconds [27].

Starting from this, a ranking of which Energy Storage Systems would be most suitable for DEMO operation was made in [27], taking into account a set of Storage Systems technologies.

For starters, the maturity of the technology has been presented by EUROfusion as a precondition. Although by the time the project will be realized, improved solutions could be developed. Finding a solution using mature technologies of today, does not exclude the possibility of using a better storage later.

Next to maturity, the selection of eESS should be tailored to specific requirements at DEMO. A list of requirements for storage capabilities has not been composed thus far. Therefore, a start was made by formulating exclusion criteria using general figures that are integral to

the application of DEMO. In this way, the amount of round-trips a storage technology could perform in a lifetime emerged as an important factor.

Since DEMO intends to operate at around 11 cycles a day (with a cycle time of 2 hours and 15 minutes), in a full power year, the number of cycles could go up to around 3 800 cycles [16]. Therefore, the tentative assumption was made that technology should have a lifetime of at least 10.000 cycles. For some technologies, such as Battery Energy Storage (BES), the number of cycles is a bottleneck: Li-ion batteries have a reported range of 1.000 up to 10.000 cycles [31]. Nevertheless, Li-Ion systems typically have a lifetime up to 3500 cycles [32]. The implications of using a technology with such limited lifetime would be frequent maintenance and replacing systems on a yearly basis which in a worst case could impede normal operation.

Here the Energy Storage Systems taken into account are listed:

- Capacitor Energy Storage (CES)
- Super Capacitor Energy Storage (SCES)
- Pumped Hydro Storage (PHS)
- Superconducting Magnetic Energy Storage (SMES)
- Compressed Air Energy Storage (CAES)
- Flywheel Energy Storage (FES)
- Vanadium Redox Battery (VRB)
- Solide Oxide Fuel Cell (SOFC)

Afterwards, a further refinement of this list was made considering technologies with sufficient response time for mitigating violations of the tentative limits. This led to a set of five eESS to be examined in the multi-criteria analysis, namely Capacitor Energy Storage, Super Capacitor Energy Storage, Superconducting Magnetic Energy Storage, Flywheels Energy Storage and Vanadium Redox Battery.

The multi-criteria analysis was based on several weighted parameters. The most important ones are lifetime, efficiency and saftey hazards; then energy size, space requirements and maintenance requirements, followed by capital cost and environmental impact [27].

Obviously Energy Storage Systems have not sharp values for every parameter, but a range of values, which can be either narrow or quite wide. To check the robustness of the results,

different values in the range were used as input. Next to using the middle value, ”optimistic” and ”conservative” inputs were used. Optimistic in this way refers to the best possible value in the range, while the conservative case tested the opposite end of the ranges [27].

As a results of the analysis, SCES came out as the best option for a variety of inputs as well as a wide range of weighting values [27] (that is why SCES was suggested to be further analysed in this thesis project).

SMES is ranked in second place, tieing SCES while using conservative values as input.

Going quite lower, we found FES and CES almost tied for third place, and VRB as lowest ranked, as it scored the worst for most inputs values and weights [27].

3. Super Capacitor Energy Storage systems

3.1 Overview

As mentioned in the previous chapter, Super Capacitor Energy Storage systems (SCES) are chosen as the most suitable Energy Storage System for DEMO application, for diverse reasons.

Supercapacitors (or ultracapacitors) are Energy Storage Systems which store electric energy with a similar principle as normal solid-state capacitors, but with much higher values of capacity and lower voltage limits. Indeed, common capacitors can have a maximum capacity up to 500 microfarads, whereas with Supercapacitors, it is possible to reach values over 5000 Farads, so higher by an order of magnitude of 10^7 [33]. That is why the word “super” is attached to their name.

By contrast, voltage limits for Supercapacitors are quite lower, around 2.7 to 3.0 Volts per cell.

They are one of the favorable candidates for energy storage because of their exceptional electrochemical properties.

Figure 3.1: *Maxwell Supercapacitor*

Supercapacitors are relatively new in the field of energy storage systems. Despite the first experiments with Supercapacitors dating back to 1957 at General Electric laboratories and

the patent released in 1978, it is only in the late 1990s that they became a valuable option for industrial purposes when, thanks to significant progress in the materials used, highly efficient components were achieved at a lower cost, leading to increasing sales.

In performance metrics, a Supercapacitor falls in between a conventional capacitor and a battery, see Figure 3.2.

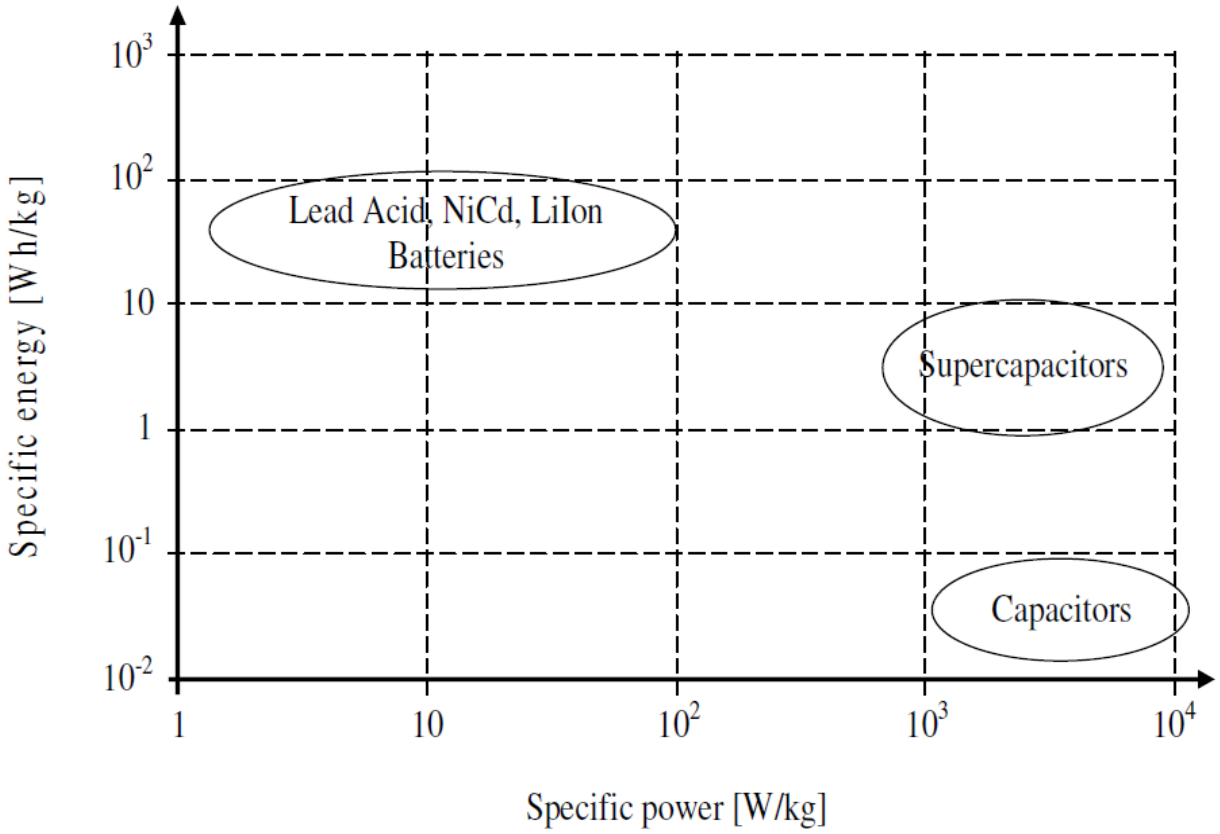

Figure 3.2: *Ragone plot of Supercapacitors, Capacitors and batteries*

They have lower specific energy but much higher specific power compared to a battery, so a low energy to power ratio.

Thanks to their ability to store and release large amounts of energy quickly, they are used in a variety of applications, mainly such as Grid stabilization in the network infrastructure, to balance fluctuating loads and improve power quality; in electric vehicles**,** to provide power during acceleration and recover energy during regenerative braking; in solar and wind energy storage systems, to store produced energy and release it rapidly when needed; in industrial applications such as heavy machinery or wide backup systems, to provide instant

power during peak loads or power outages; in aerospace sector, for satellites and spacecraft, and so on.

As a matter of fact, normal capacitors store energy electrostatically, batteries electrochemically, Supercapacitors fall somewhere in between: although the mechanism of charge/discharge is of electrostatic nature, it involves a chemical reaction, that is however highly reversible and it occurs without any variation of the volume of electrodes, in contrast to what happens in batteries; they store and releases energy by reversible adsorption and desorption of ions at the electrode-electrolyte interface. Furthermore, unlike batteries, it does not have electrochemical limitations due to polarization resistance [33]. This leads to significantly higher number of cycle life respect to batteries.

Besides specific power and longer cycle life, the advantages that Supercapacitor exhibits over other conventional batteries are related also to charge-discharge efficiency, robust thermal operating window and effective handling of fluctuating input–output energy conditions (Table 3.1) [34].

Table 3.1: *Performance comparison of capacitor, supercapacitor and battery*

Performance indicators	Battery	Supercapacitor	Capacitor
Specific power (W/Kg)	<1000	500–10,000	$>10^4$
Specific energy (Wh/Kg)	10–100	1–10	<0.1
Charge/discharge efficiency (%)	70–85	85–98	>98
Charging time	1–5 hrs	Sec–min	10^{-6}–10^{-3}
Discharging time	0.3–3 hrs	Sec–min	10^{-6}–10^{-3}
Cycle life	~1000	~500,000	>500,000

Though the performance of SCES is good, the cost of energy storage, even when compared to other short-duration storage solutions, is high.

The target is to decrease the cost of energy storage down to 600 e/kWh for a 0.5 MWh scale system [59]. Systems are composed of modules which are made up of several supercapacitors. Companies such as Cap-XX (AU), Chemi-Con (JP), Eaton (US), Maxwell Technologies (KR), and Panasonic (JP) produce and sell these in various sizes, for various

applications. Siemens (DE) sells complete systems which can be sized up to 0.5 MWh including converters. With respect to the current performance of these products, it should be noted that the modules have a specific energy of around 1.5-5.5 Wh/kg, and individual cells are available up to 9.1 Wh/kg [87].

Figure 3.3: *SCs configurations*

3.2 Working principle

Supercapacitors are made up of two electrodes, an electrolyte and a porous membrane separator. This specific structure of supercapacitors makes them have the features of conventional capacitors as well as electrochemical batteries.

Nanomaterial-based supercapacitors are used to increase the electrode surface area so as to achieve high performance and enhanced capacitance [35]; theese materials are being further discussed later in this chapter.

A supercapacitor operates by storing electrical energy between two electrostatic double layers created by the formation of thin charge layers on the electrolyte-electrode interface. Because the capacitance value of a capacitor is always exactly proportional to the surface area of its conduction plates, which in this instance is very big, a supercapacitor can store a high quantity of charge value. In addition, the magnitude of capacitance is inversely proportional to the distance between the plates, which is significantly shorter in supercapacitors than in regular capacitors.

Static electricity, also known as electrostatics, is used to store energy in capacitors. Both positively and negatively charged ions are produced in the electrolyte solution between the two plates of the supercapacitor.

When a voltage is supplied across the supercapacitor's plates, one of the plates develops a positive charge, while the other plate develops a negative charge. This attracts the negatively charged ions in the electrolyte to the positively charged plate and the positively charged ions to the negatively charged plate, see Figure 3.4.

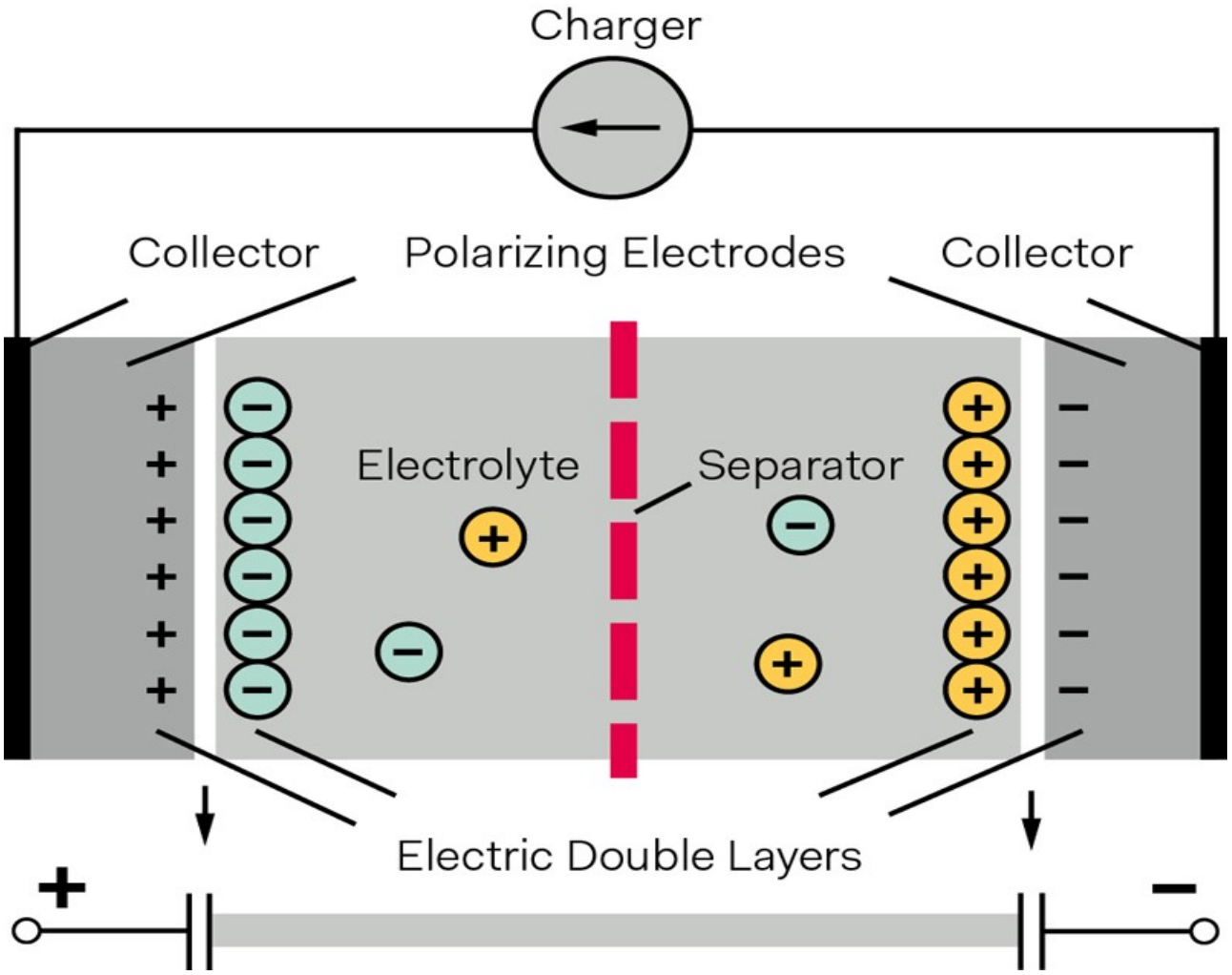

Figure 3.4: *Schematic diagram of a Supercapacitor*

On the inner surface of both plates, a thin coating of ions is deposited. This results in the production of an electrostatic double layer, which is similar to connecting two capacitors in

series. Each charge possesses high capacitance as the distance between both the resultant capacitors is very thin and the area of electrodes is high.

The force at stake is Coulomb's electrostatic force, attractive for opposite charges:

$$F = k \frac{q_1 q_2}{r^2} \tag{3.1}$$

3.3 Classification

Depending on the charge-storage mechanism of SCs, they can be classified into three: electric double-layer capacitors (EDLC), redox electrochemical capacitors (REC), also known as Pseudocapacitors because they involve an electrochemical redox reaction, and hybrid electrochemical capacitors (HEC), which charge electrostatically and electrochemically, combining the advantages of both. Electrodes of supercapacitors can be produced using various forms of carbon [36], metal oxides [37] and conductive polymers [38]. EDLC are majorly focused on the materials based on carbon: activated carbons and graphene, carbon nanotubes, while pseudocapacitors are based on metal oxides, conductive polymers and doped carbon [39], (see Figure 3.5).

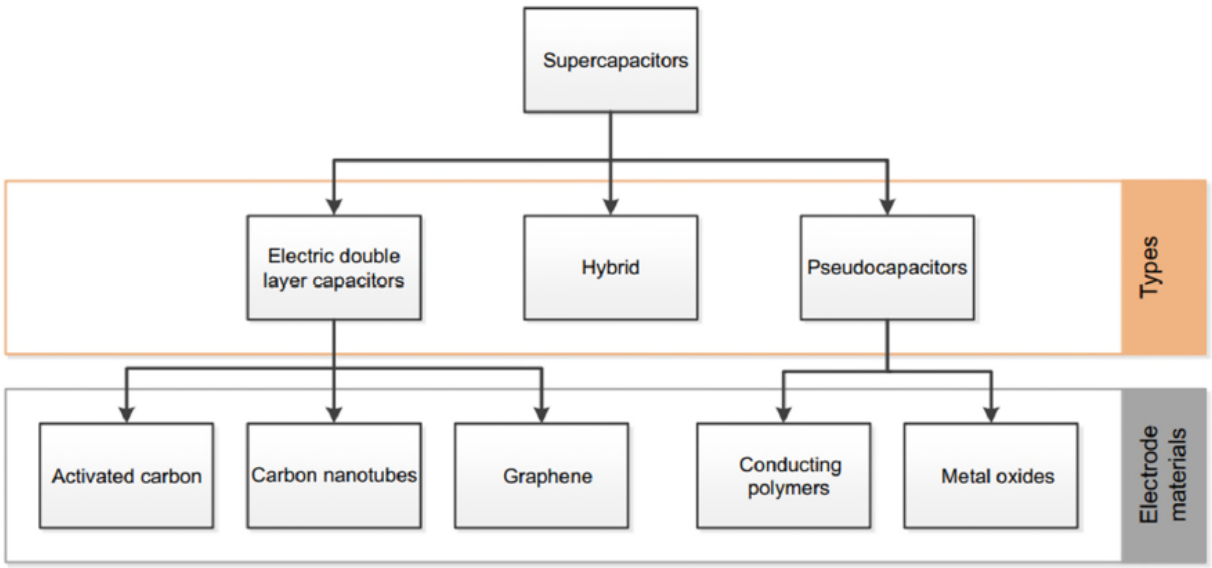

Figure 3.5: *Supercapacitors classification and materials used*

Electrostatic Double-Layer Capacitors (EDLC)

This type of capacitor works on the charge storage mechanism where a charge is physically stored on the surface of the electrodes without causing any irreversible chemical reactions via the formation of an electrical double layer. Usually, carbon-based electrodes are used in supercapacitors which are separated by a dielectric substance that acts as an insulator and possesses electrical properties that eventually affect the performance of the supercapacitor.

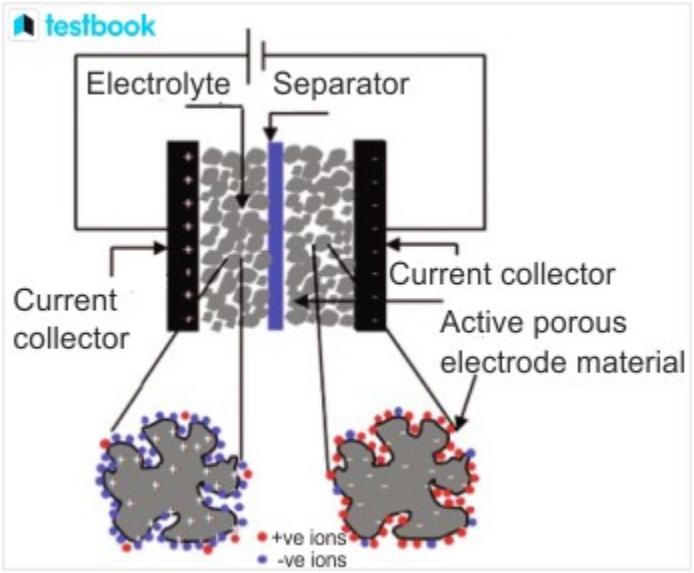

Figure 3.6: *EDLC Supercapacitor*

Charges are electrostatically stored in supercapacitors. An electric field is generated at each electrolyte as soon as the voltage is applied across the terminals which leads to the polarisation of the electrolyte. As a result of which ions diffuse through the dielectric to the porous electrodes of opposite charges. In such a way, the formation of an electric double layer takes place at each electrode. This results in the increased surface area of each electrode and decreased distance between the electrodes, with higher force between charges as a consequence.

Pseudo Capacitors (PC)

Pseudo-capacitors are also called faradaic supercapacitors or Redox Electrochemical Capacitors (REC). They are called “pseudo” because they involve electrochemical reactions.

These devices use electrodes made up of redox-active materials such as metal oxides and conducting polymers and doped-carbon. These electrodes store charge through reversible faradaic reaction mechanisms, near the electrode or at the electrode surface where charges are transferred across the metal-electrolyte interface.

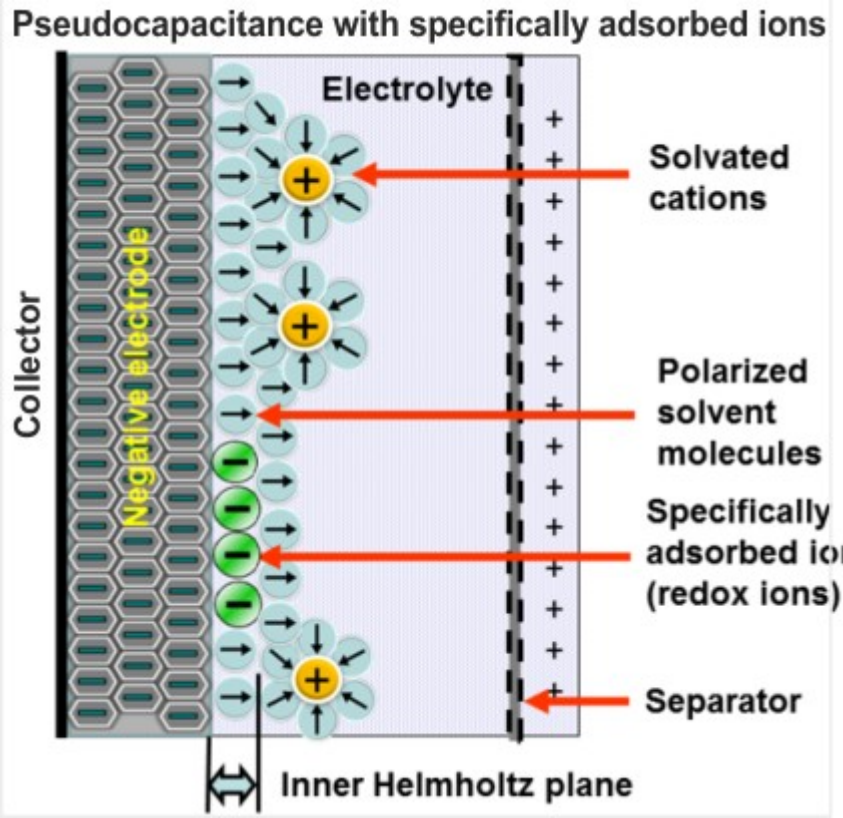

Figure 3.7: *Pseudo Capacitor*

When a voltage is subjected to a Supercapacitor, both reduction and oxidation take place on the electrode material. It involves the passage of charge across the double layer, resulting in faradic current passing through the supercapacitor electrode material. The faradic process employed in pseudocapacitors enhances the electrochemical reactions that result to achieve greater specific capacitance and energy densities compared to EDLCs.

Hybrid Capacitors

These capacitors have adopted both the mechanisms of EDLC and pseudo capacitors. Hybrid capacitors are composed of electrodes with different characteristics based on chemical as well as electrical mechanisms. As a result, one electrode exhibits electrostatic capacitance

and the other provides electrochemical capacitance. The advantage includes higher operating voltage (3.8 V maximum), increased capacitance and energy density.

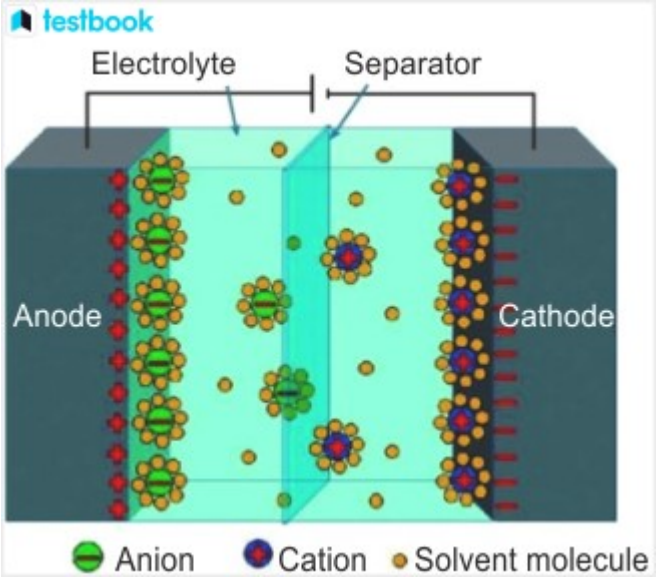

Figura 3.8: *Hybrid Capacitor*

3.4 Structure

Electrodes are the one of the key components and the most important element in SCs.

The electrochemical performance of SCs depends upon the properties of electrode materials used in their development. Plenty of researchers are working on designing low-cost, high-performance electrode materials with high stability, high specific surface area and high electronic conductivity [40].

Carbon-based materials are among the popular electrode materials for SCs, followed by conducting polymers and metal oxides. Theese main materials are described below.

The two electrodes of the supercapacitor can be made of the same material (symmetrical supercapacitors) or different materials (asymmetrical supercapacitors). Asymmetrical systems, usually one activated carbon electrode and one metal electrode, can increase energy density so they could be preferred for large scale applications with troubles of space [49].

Note that the structure of the SC is significant for developing the equivalent circuit to represent the behaviour of the SC itself.

Electrodes:

Carbon-based materials are the most common materials for SC electrodes. Carbon can be transformed in various forms with a very high specific surface area because of its highly porous structure. This is one main reason for using carbon as an electrode material [41].

Among these, Activated carbon is probably the most frequently used. Activated carbons (ACs) have proved applications in energy storage, since it is abundant in the environment, and its activation can be done through physical (thermal) and chemical activation. Hot gasses are used to develop the structure into ACs in physical (thermal) activation. Carbonization is usually done at very temperature (500–1100°C). While chemical activation needs lower temperatures (400–800°C), its pyrolysis and activation are carried out in the presence of dehydrating agents [42].

The structural characters of ACs are close to the structural properties of pure graphite.

ACs have different porous structures, based on different size of the pores [41], see Figure 3.9: micropores, (or nanopores) with a diameter of less than 2 nanometers; mesopores, with a diameter between 2 and 50 nanometers; and macropores, with a diameter of more than 50 nanometers. These pores are important in the kinetics of adsorption and do not increase the adsorption capacity. Changing the factors during carbonization and activation can lead to ACs with different porous structure areas. Large pore sizes result in higher power densities while smaller pore sizes relate to higher energy densities.

Graphene is an other common carbon-based material. It is basically a monolayer of carbon atoms packed into a honeycomb lattice (Figure 3.10). It has excellent mechanical properties and a large surface area with great electronic transportability and thermal conductivity.

The chemical vapor deposition (CVD) method, as well as as hummer's method, dispersion method, microwave method can be used for the synthesis of graphene [43]. To enhance the capacitance performance of graphene that is synthesized by the methods mentioned above, researchers switched to doping graphene, conductive polymer composites or oxide materials to enhance the electrochemical behavior of the materials [44].

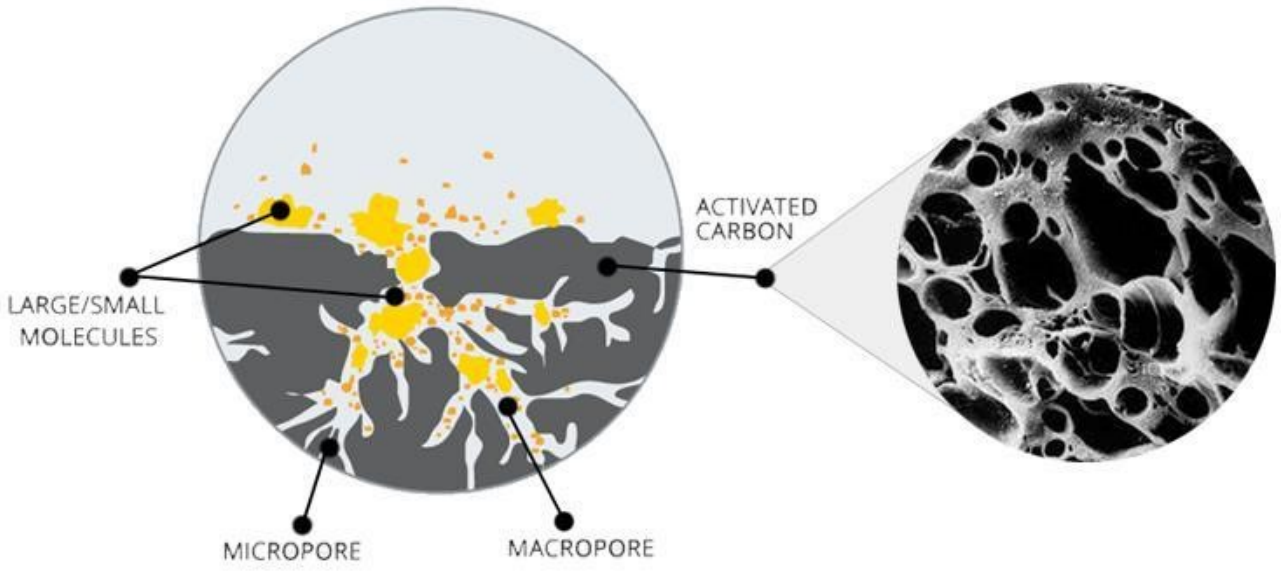

Figure 3.9: *Activated carbon porous structure*

Carbon nanotubes are another allotrope of carbon. They are chemically and thermally resilient and have the highest strength to weight ratios. CNTs can be produced by various techniques, including arc discharge, laser ablation, high-pressure carbon monoxide disproportionation and, most commonly, CVD [45]. Carbon nanotubes are still in the experimental phase and have a very high production cost, mainly due to the carbon purification process. Another type of electrode widely used today is aerogel, which appears as a highly porous solid foam, making it very suitable for adsorption. There are many types of aerogels, and so far, this technology has been a leader in the production of supercapacitors. For example, Maxwell supercapacitors use carbon aerogel as the electrode coating [46].

Electrolyte

An electrolyte is a chemical compound when dissolved in a solvent and dissociated in ions. These ions provide ionic conductivity between the positive and negative electrodes of the device, thus helps in electric charge transportation.

The electrolyte plays a vital role in the supercapacitor performance, life cycle, and safety of the device. Chiefly the electrolytes used in supercapacitors are classified into three types,

aqueous electrolytes, organic electrolytes, and ionic liquid. Each class has its distinct features related to voltage window and ionic resistance [47].

In order to obtain supercapacitors with high energy storage capacity, it is advisable to use aqueous solution electrolytes, although the choice between electrolyte and solvent is crucial as it determines both the capacity and energy of the electric double-layer capacitor. Therefore, it is important to select both the electrode and its properties, as well as the electrolyte, which must allow proper adsorption at the electrode-electrolyte interface.

Separator

The separator must allow the transit of ions through the electrolyte but must not allow the occurrence of currents between the two electrodes, which would result in a loss of accumulated charge energy. It stands between the two positive and negative electrodes to prevent electrical shorting by physical contact of electrodes.

There are essentially two types of separators: polymer and cellulose fiber separators, used for organic electrolytes, and fiberglass or ceramic separators, used for aqueous solution electrolytes. It should be noted that many materials are currently being studied in this field to achieve increasingly suitable characteristics for the role of the separator [48]. Often, the separators used in supercapacitors are the same as those used in electrolytic batteries because their industrial production makes them economical, but most importantly, they have reliable characteristics and existing usage data feedback.

Separators should be an inert element, just permeable for the electrolyte ions [48].

3.5 Test modes for Supercapacitors

Various instruments and test modes have been developed and applied to characterize the electrochemical performance of SCs. The constant current charge/discharge (CCCD), then Cyclic voltammetric (CV), and electrochemical impedance spectroscopic (EIS) tests are the commonly used ones. In essence, all such instruments can be used to measure, besides voltage, current and time obviously, the main key parameters we will see later such as the capacitance, equivalent series resistance, operating voltage and subsequently time constant, energy and power performance of SCs, can be derived from them. However, each

of the instruments has its own focus and the targeted parameters by design, and their applications and limits are hence discussed below.

In addition, the three test modes can all be used to examine not only SC materials, i.e. the electricity storage media including electrode materials and electrolyte materials, but also SC devices, i.e. the whole package of SCs [50].

CCCD Test

CCCD (Constant Current Charge/Discharge) test is the most widely used method for characterization of SCs under direct current [51]. It is conducted by repetitive charging and discharging the SC device or the working electrode at a constant current level with or without a dwelling period (a time period between charging and discharging while the peak voltage *Vo* remains constant), and normally a plot of potential (*E*) *vs*. time (s) is the output, see Figure 3a for linear voltage change, and Figure 3b for non-linear voltage change (remember that current is constant in this test).

Choosing a proper level of the constant current is critical to produce consistent and comparable data from a CCCD test.

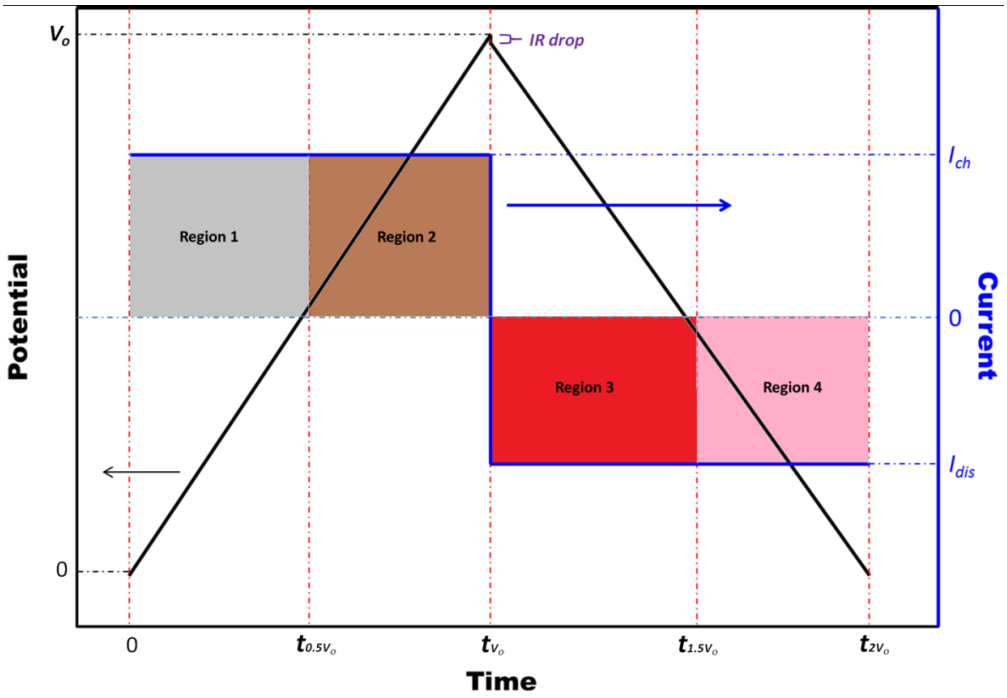

Figure 3.10: *A CCCD test result with linear potential change over time*

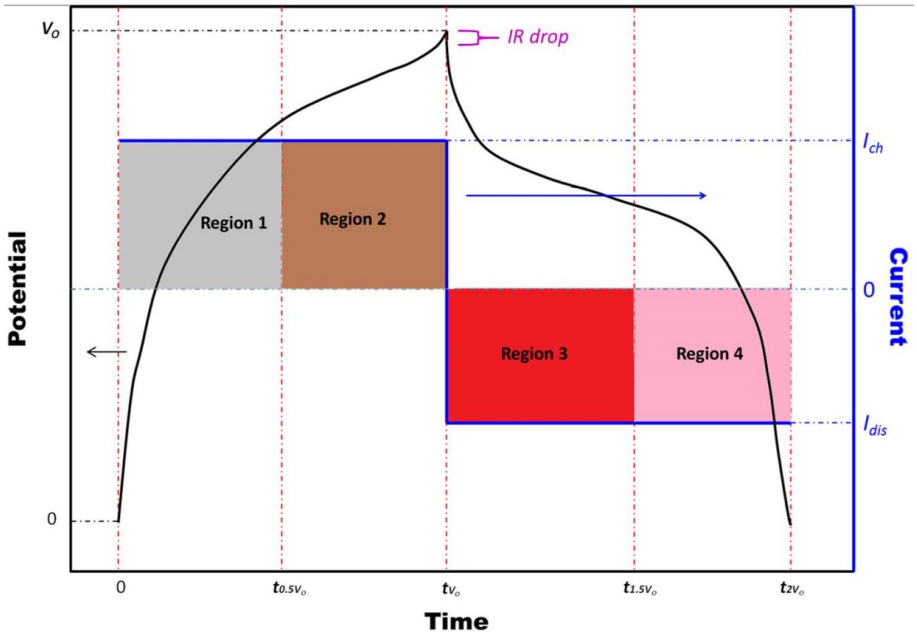

Figure 3.11: *A CCCD test result with non-linear potential change over time*

CCCD test is regarded as the most versatile and accurate approach in characterizing SC devices. All three core parameters of SC devices, Capacitance, Equivalent Series Resistance and operating voltage, can be tested from it and subsequently used to derive most of the other properties, such as the time constant, power and energy densities, and leakage and peak current. It can also be conveniently used to study the cycling stability of SC devices. Moreover, by using a three-electrode setup, the specific capacitance, reversibility and potential window for SC materials can also be obtained via CCCD test.

CV Test

CV (Cyclic Voltammetric) test applies a linearly changed electric potential between positive and negative electrodes for two-electrode systems, or between reference and working electrodes for three-electrode configurations. The speed of potential change in mV/s is termed as the sweep rate or scan rate, and the range of potential change is called potential window or operating potential. The instantaneous current during the cathodic and anodic sweeps is recorded to characterize the electrochemical reactions involved. The data are plotted as current (*A*) *vs*. potential (*V*), or sometimes, current or potential *vs*. time (Figure 3.12).

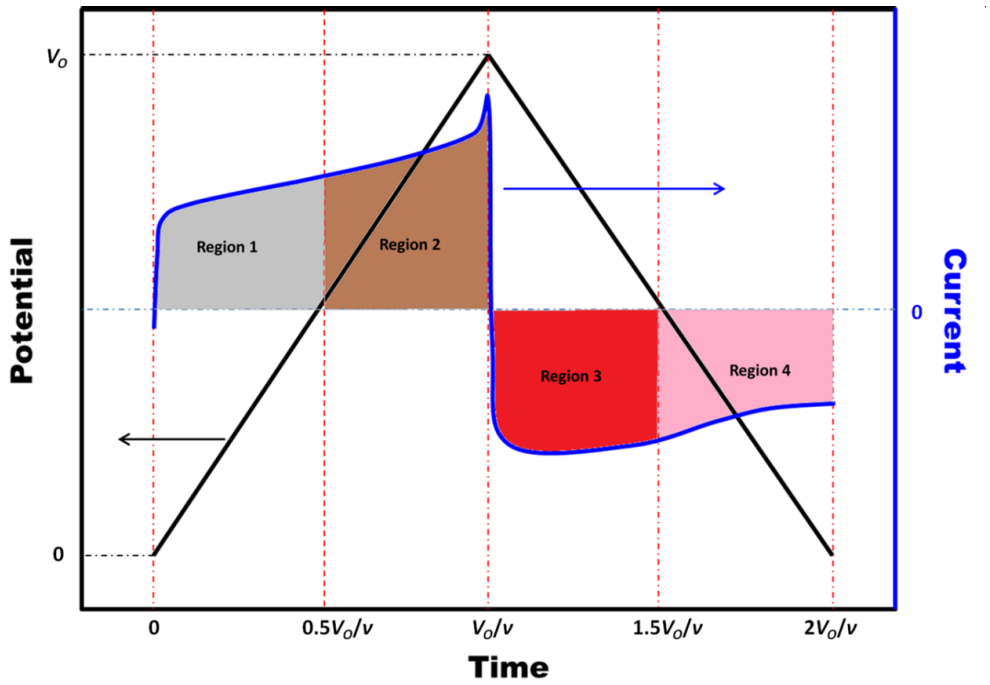

Figure 3.12: *A typical CV test result*

To examine the charge storage mechanisms of SC materials where EDLC and PC types are separate, CV test with the three-electrode setup is regarded as the most suitable approach [52].

The test results can first be analyzed by examining the shape of the CV curves, as for EDLC materials, the resulting CV curve shape is rather rectangular, whereas for most PC materials, a sudden current surge appears to skew the curve. However, a complication in this is that there a few PC materials whose CV curves also appeared rectangular.

To add a further twist, the shape of the CV curves can be affected by the experimental setup so that some PC materials, which ordinarily would generate skewed CV curves, can produce rectangular curves as well. Caution is hence required in the process.

Another more quantitative and reliable method in interpreting the data from a SC cell tested is to extract the contributions from EDL and PC mechanisms separately by utilizing the knowledge that the instantaneous current induced by EDL mechanism is proportional to the scan rate, while the diffusion controlled ion-intercalation by PC mechanism is to the square root of scan rate [52, 53]. However, this approach is limited to detect the contribution from the surface-redox mechanism. Therefore, more experimental and theoretical studies are demanded to address this issue.

CV test is also particularly suitable in practice to determining the potential window (operating voltage) for SC materials by successive adjustment of the reversal potential in a three-electrode system, and the reversibility of the charge and discharge processes can also be studied at the same time [53]. In addition, the specific capacitance and energy performance of the SC materials can be obtained via integration of the CV curves as discussed in detail later. Similar process can also be conducted for SC devices to obtain their total cell capacitance and hence the amount of electricity stored.

EIS Test

EIS test, also known as the dielectric spectroscopic test, measures the impedance of a power cell as a function of frequency by applying a low-amplitude alternative voltage (normally 5 mV) superimposed on a steady-state potential. The resulting data is normally expressed graphically in Bode plot to demonstrate the cell response between phase angle and frequency, and in Nyquist plot to show the imaginary and real parts of the cell impedances on a complex plane [54, 55].

Besides the frequency response and impedance, EIS has also been employed to characterize the charge transfer, mass transport and charge storage mechanism, as well as to estimate the capacitance, energy and power properties [56, 57]. Different equivalent circuits and models have been developed to distinguish the contribution of individual structure component in a cell system to the total impedance. When SC devices are tested, the real parts of the complex impedance at selected frequencies are used in literature to represent *RES*. However, one needs to keep in mind that this Equivalent Series Resistance from EIS test is often much smaller than that derived from the CCCD test [58], and therefore is limited in describing the power performance of SC devices.

For SC materials, EIS test can be deployed to study the impedance, specific capacitance, charge transfer, mass transport and charge storage mechanisms involved by executing similar analysis in a three-electrode system.

In conclusion, for SC materials, all three techniques, i.e. CV, EIS and CCCD tests, can be employed with different emphases. However, for SC devices, the most effective and accurate approach is CCCD test for measuring the cell capacitance, equivalent series

resistance and operating voltage [59]. Subsequently, the time constant, energy and power densities, and leakage and maximum current of SC devices can be derived based on these three core parameters.

3.6 Key Parameters

In this section, the most rilevant parameters of SCs for our case, DEMOfusion power plant, will be discussed and analysed.

The main three parameters for SCs are the capacitance (C), Equivalent Series Resistance (ESR) and rated voltage, or operating voltage (V_o) [50]. Next, there are specific power, specific energy, specific capacitance, specific cost, energy efficiency, number of life cycles, operating temperature range, and others.

Some assumptions should be made before starting dealing with the parameters, in order to understand which ones are to be analysed in detail, and which one we could consider as negligible.

Since there shoudn't be issues of space in DEMOfusion network, due to the vast size of the operational site, in our analysis less attention will be paid to all the parameters with regard of space, so specific energy, specific power and so on.

The cost of the Energy Storage System also, compared to the dimension of the whole project, is definitely negligible, and so are all the parameters concerning it such as cost per kWh, cost per kW, or cost per volume size of the ESS.

Here , the main three seen before are described:

Capacitance

The capacitance of a SC is tied to the ability of its electrodes to store charge in an electric field. It is defined as the ratio between the electrical charge stored under a given voltage change:

$$C = \frac{\Delta Q}{\Delta V} \tag{3.2}$$

A further definition of capacitance is given by equation (3.3)

$$C = \in_0 \in_r \frac{A}{d} \tag{3.3}$$

where:

• $\in_0$ is the permittivity of free space (approximately 8.854 x 10^{12} F/m)

• $\in_r$ is the relative permittivity (dielectric constant) of the material.

• A is the surface (in normal capacitors it is the surface of one of the two plates)

• d is the distance between electrodes

Note that, though this formula is valid for both normal solid-state capacitors and supercapacitors, it results to be more suitable for normal capacitors, as it is harder to find the values of the surface and distance between electrodes in supecapacitors.

The unity of measurement of capacitance is Farad (F), from the english physicist Michael Faraday (1791-1867). One Farad is equivalent to one Coulomb per Volt.

As mentioned before, the capacitance in SCs can reach values up to 5000 Farad, several orders of magnitude higher respect to normal capacitors.

There are several methods to calculate the capacitance of a SC; here the calculations done with the CCCD test seen before is outlined, as it is the most widely used one for supercapacitors.

Since constant current is used in a CCCD test, Eq. 3.4 can be converted to:

$$C = \frac{I * \Delta t}{\Delta V} \tag{3.4}$$

where *I* is the constant current, *Δt* is the charging or discharging time corresponding to the specified potential change *ΔV*. So the key issue now is that the correct time *Δt* and *ΔV* are used in calculation. Often the entire discharging curve is used:

$$C = \frac{I_{dis} * \Delta t_{V_0 - 2V_0}}{V_0} \tag{3.5}$$

In the next section about Equivalent Series Resistance we will see that in CCCD test, an IR voltage drop will occur while discharging the supercapacitor.

Since this *IR* drop is inevitable, one can adjust *ΔV* so as to exclude the *IR* drop for more accurate result, so:

$$C = \frac{I_{dis} * \Delta t_{V_0 - 2V_0}}{V_0 - V_{IR\ drop}} \tag{3.6}$$

With linear curve results, as shown in Figure 3.10, identical capacitance value is obtained regardless of the segment used, since the voltage changes linearly with time.

Whereas, for PCs or hybrid SCs with nonlinear curves as seen in 3.11, the selection of different regions from the curve can make a great difference in determining *ΔV*, and hence the value of C.

In such cases, the use of a proper or fixed region or selection of suitable potential window becomes critical and needs to be standardized. Based on Burke [59], Region 3 or a potential window from *Vo* to the shoulder voltage is recommended.

Equivalent Series Resistance

A SC is not an ideal electrical component in the sense that it has its own internal resistance, thus dissipating the energy stored. This resistance is usually termed as the Equivalent Series Resistance (ESR), and is essential in reflecting the power performance and energy efficiency of SCs. In general, a small ESR is preferred for better electrochemical performance.

Note that in actual measurement, only calculations made for a packed cell can give an accurate ESR value, it results to be hard to estimate it a priori just by knowing the materials used for the device [50].

In a CCCD test, ESR is responsible for the voltage drop when a SC is discharged at a constant current. This voltage is also known as IR drop, and is proportional to the current passing through the SC, see Figure 3.13.

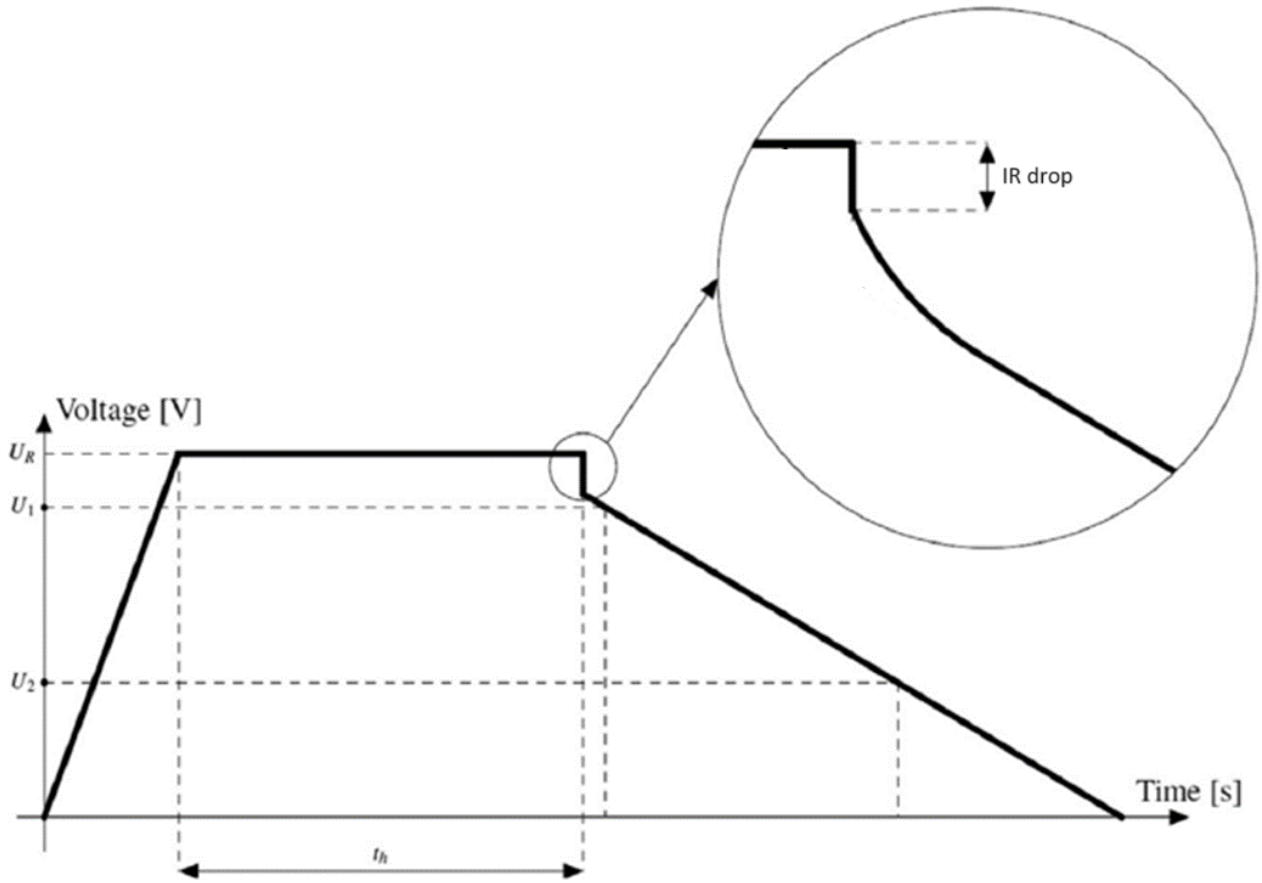

Figure 3.13: *Voltage drop in a CCCD test*

The most widely accepted method to evaluate ESR is through the analysis of this IR drop at the initial stage of the discharging curve from CCCD tests. By applying Ohm's law to the IR drop, *RES* can be acquired readily:

$$ESR = \frac{\Delta V_{drop}}{\Delta I} \tag{3.7}$$

Another less common approach is based on the voltage recovery behavior after a current interruption during a discharge process [60]. This method is fundamentally the same as the *IR* drop method and yields matching results.

There are two major factors that affect the accuracy of ESR from CCCD test: the dwelling time and the size of SC.

Normally, CCCD tests are usually carried out without dwelling at peak potential, that is, the discharging starts once the peak potential is reached. However, the practice of non-zero

dwelling time is widely adopted in tests (Figure 3.14a), which can greatly influence the final value of ESR.

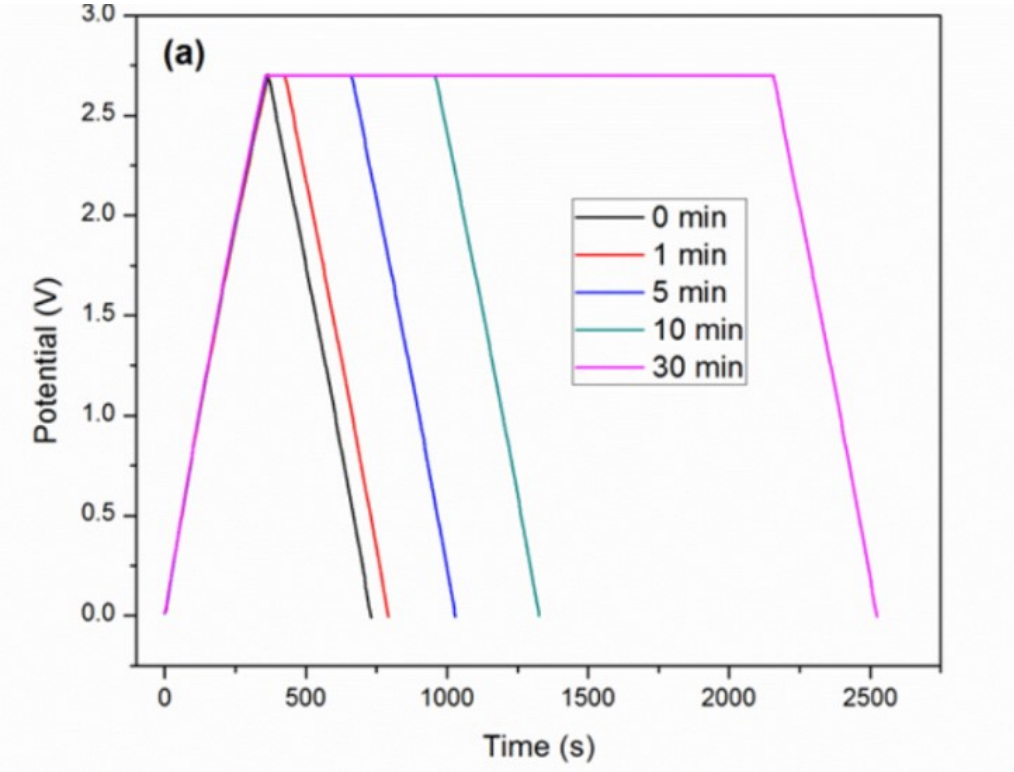

Figure 3.14a: *Different dwelling times in CCCD test*

From simulations carried out in [50], ESR resulted to be a bit higher for CCCD tests with longer dwelling time, a bit smaller for shorter dwelling time, and visibly smaller for zero dwelling time, see Figure 3.14b.

The explanation for the ESR to be much smaller for the latter case, is that we have a charge-discharge transition in which the delta of current must be taken into account, so that ΔI is larger than the discharging current for every other cases.

According to [61], in order to prove that to obtain reliable ESR values the voltage drop must be normalized by a factor of two (ESR = $\Delta V / 2\Delta I$).

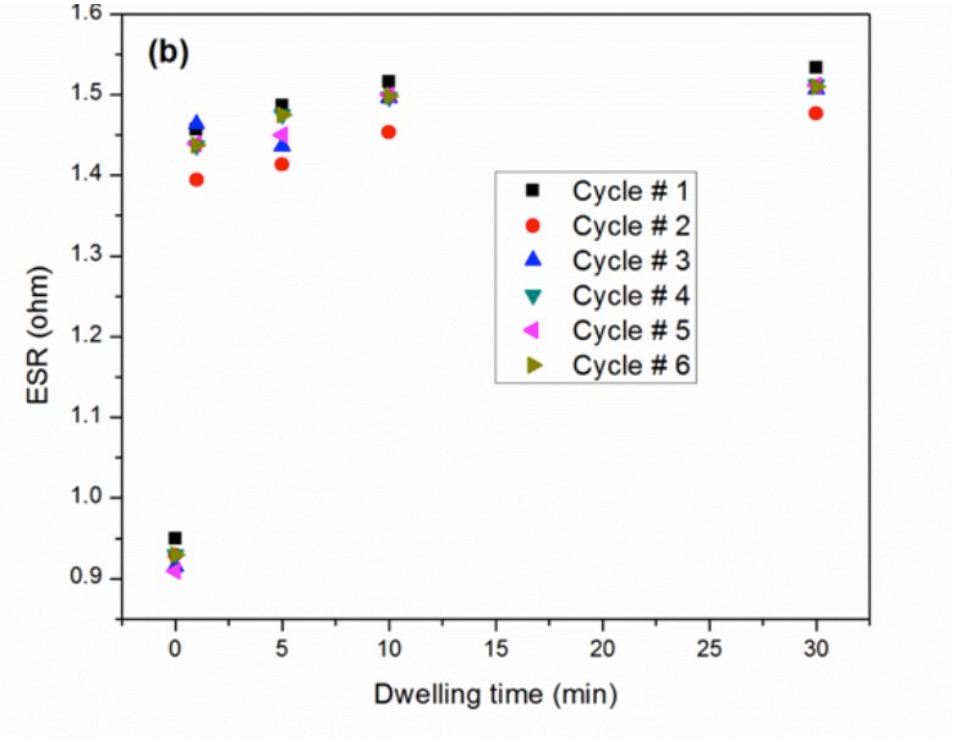

Figure 3.14b: *Different ESR values*

As far as found in literature papers, there is no study carried out to examine the reasons for the influence of dwelling time on ESR, as well as it is still not clearly understood how the cell size affects the CCCD results. But regarding the cells size, it is generally accepted that the *IR* drop method works fine only for small SCs, and a steady-state voltage drop method should be used for large SCs [50].

As shown in Fig. 3.15a, the steady-state voltage drop *ΔV2*, rather than the *IR* drop *ΔV1*, is obtained through the back extrapolation of the potential trace; it is larger than *ΔV1* by almost 50%, thus leading to a nearly 50% increase in ESR. An actual example is provide in Fig. 3.15b reported in [59].

Studies have been conducted and the results demonstrated that more accurate power performance can be estimated using *ΔV2* for large cells, and it is therefore recommended [59, 62].

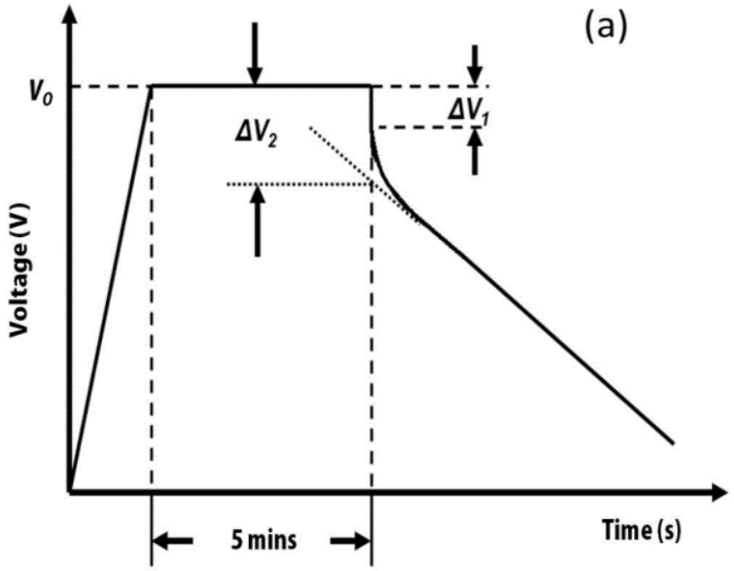

Figure 3.15a: *Steady-state voltage drop in CCCD test*

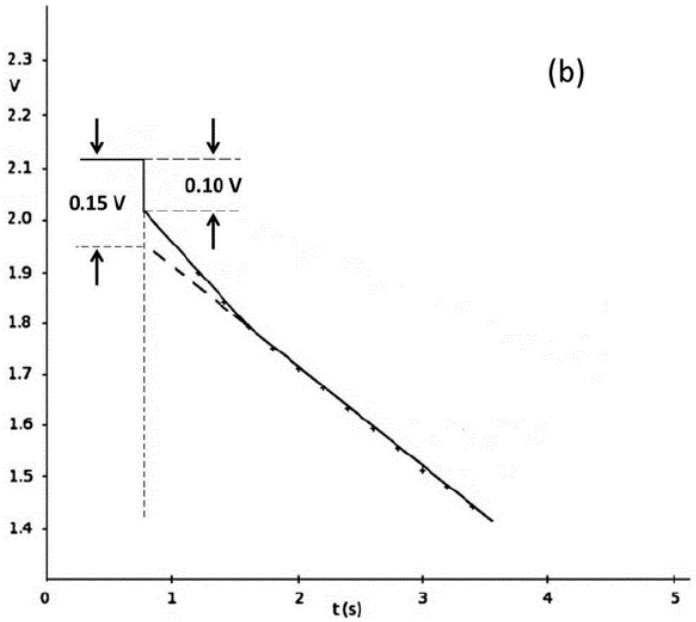

Figure 3.15b: *Experimental results for IR drop and steady-state drop in CCCD test*

An other parameter normally appearing in the specifications for commercial SCs is the 10ms DC ESR. The procedure for this includes again a dwelling time, usually 10 minutes, after which the SC is discharged with a constant discharging current [70]. 10 ms DC ESR is calculated from the measured voltage drop at 10 ms into a discharge divided by discharge current.

ΔV_{10ms} is the difference between voltage measured just prior to discharge and the voltage measured at the device terminals at 10±5 ms into a discharge. *Id* is the nominal current

during the first 10±5 ms of discharge. The 10 ms DC ESR measurement can be taken by equipment which is designed to supply a short burst of dc current pulses and measure & average the voltage drops at the end of 10 ms pulses [70].

$$DC\ ESR_{10ms} = \frac{\Delta V_{10ms}}{I_d} \tag{3.8}$$

Measuring the ESR at 10 ms provides a wider and more applicable view of supercapacitors performance under real operating conditions. In fact, practical applications often involve discharges that occur over milliseconds rather than instantaneously. Additionally, while the instantaneous ESR may be primarily influenced by purely ohmic resistance, the measurement at 10 ms allows for the observation of resistance characteristics that take into account the electrochemical reactions and charge transfer processes occurring at this time scale.

Operating voltage

Strictly speaking, the operating voltage V_0 refers to the potential applied to the system or the suitable potential window within which a cell normally operates. The term is sometimes interchangeable to cell voltage or rated voltage/potential, which represents the maximum voltage a cell can endure.

As said before, for SC the rated voltage is quite low, normally 2.7 V, 3V at most.

Both CV and CCCD tests can be used to determine *Vo* of either the SC materials or the devices. However actual test of this maximum potential can be risky of destroying the cell. Two major factors affecting *Vo* for SC devices include the solvent in electrolytes and the cell configuration.

Normally, in aqueous systems, a cell can be charged to 1.0 V, limited by the thermodynamic decomposition potential of water at room temperature. V_0 in organic solvent electrolyte varies between 2.3 – 2.7 V [63], as both energy and power densities are proportional to V_0. Much effort has been dedicated to develop novel electrolyte that can endure high voltage, so more than 3 V: room temperature ionic liquid (RTIL) is considered to be the most promising candidate by which high V_0 values between 3.0 – 6.0 V have been achieved in research labs [64]. In addition, various mixtures of different RTILs, or RTIL and organic solvents, also appear to be attractive [65].

By the time for the DEMO to be operative, the development of new materials to enhance operating voltage on SCs is likely to happen.

The other factor influencing V_0 is the cell configuration. In an asymmetric system, *Vo* can be increased by using different SC materials so as to introduce additional electrochemical potential difference. This way, even in aqueous systems, *Vo* can reach 2.0 – 2.3 V [66].

Following this, the other parameters derived from these main three are described.

Note that the considerations about energy and power are kept away from weight-related or other specific parameters as explained before.

Time constant

Time constant τ is defined as the product of capacitance C and Equivalent Series Resistance ESR, as shown in Eq. 3.9:

$$\tau = C * R_{ESR} \tag{3.9}$$

Normally τ is fixed around a certain value for SCs produced using the same technology, for example 0.55 s from Maxwell Technologies, 1.1 s from NessCap and 3.8 s from JSR Micro, as reported in [67]. Consequently, *C* and ESR for the same type of SCs are inversely proportional to each other when τ is fixed.

A smaller τ reflects a better responsiveness of the device; in fact the voltage of SC device changes by 36.8% at time $t = \tau$, and by 98% at time $t = 4\tau$, during the charge/discharge processes.

As mentioned in section 2.2.5 (“Energy Storage Systems requirements”), the responsiveness of the eESS has influence on his size, since the slower the response, the higher become the peaks it has to compensate. So, a small time constant will be a paramount factor while choosing the eESS for DEMOfusion network.

It could be preferable not to choose a SC with extremely high capacitance, since that leads to a bigger time constant for a given ESR. On the other hand, a lower capacitance is related to a lower energy storable in the SC, but it should be reminded that we don’t need exceptionally high values of energy size for the storage system (in the order of tens of kWh), we rather need high values of power (hundreds of MW), and capacitance doesn’t appear in the expression of power for SCs, as we will see in the next lines.

Energy expression

Although not being inherent parameters of a SC, the expressions for Energy and Power of SCs are illustrated and explained in this paragraph and the next one.

Given a working diagram of a complete charge/discharge process of a SC (Figure 3.16a fo EDLC, 3.16b for PC), which means a charging from a completely discharged device up to rated voltage, and same for discharging with opposite direction, the electricity stored in or released from a SC can be evaluated through the integration of the working diagrams corresponding to ECLCs and PCs, where the difference in shape is caused again by their distinct charge storage mechanisms.

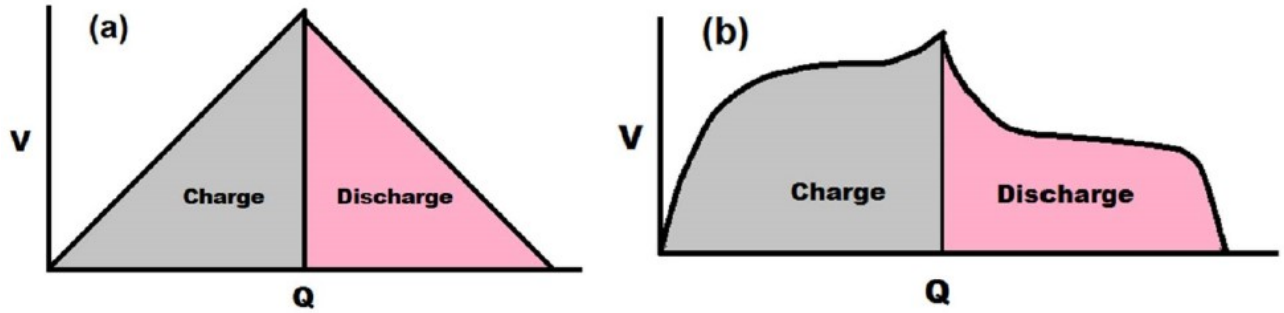

Figure 3.16: *Representative working diagram from CCCD test for EDLCs (a), and PCs (b)*

In either case, the stored electric energy can be obtained from the charging curve, and the deliverable energy from the discharging curve. The ratio of the two is termed the *energy efficiency* of the cell, an indicator of the difference between the two parts of the curve. Calculations for the stored energy are illustrated below.

For EDLCs or any other SCs with linear charge/discharge curves, the integration of the working diagram turns into the calculation of triangle area as shown in Fig. 3.16a, therefore:

$$E = \int_0^Q V_0 dq = \frac{1}{2} V_0 Q \tag{3.10}$$

From the definition of capacitance (Eq. 3.2), yields:

$$E = \frac{1}{2} C V_0^2 \tag{3.11}$$

Dividing by 3600 converts the Energy from Joule (J) to Watt hour (Wh):

$$E = \frac{\frac{1}{2} C V_0^2}{3600} \tag{3.12}$$

However, for PCs or hybrid SCs with nonlinear charge/discharge curves as shown in Fig. 3.16b, the integration of the diagram has no simple solution, depending on the specific shape of the curve, so that:

$$E = \int_0^Q V\, dq = \int_0^{t_Q} V\, I dt \tag{3.13}$$

Power expression

The outstanding power performance of SC devices is one of their major merits. The maximum electric power that can be delivered by a SC is given by:

$$P_{max} = \frac{V_0^2}{4R_{ES}} \tag{3.14}$$

In order to understand why the presence of number four at the denominator, we should consider first the the maximum power transfer theorem, also known as Jacobi's law [68]. It states that, to obtain maximum external power from a power source with internal resistance (see Figure 3.17), the resistance of the load must equal the resistance of the source as viewed from its output terminals.

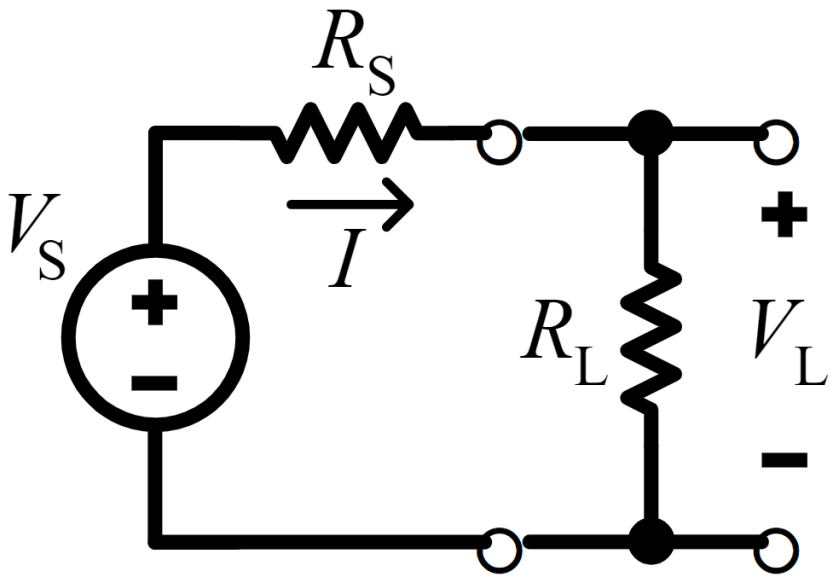

Figure 3.17: *Simplified model for powering a load R_L by a voltage source (V_S) with a series resistor R_S*

In the simplified model of powering a load with resistance R_L by a source with voltage V and source resistance R_S, then by Ohm's law the resulting current I is simply the source voltage divided by the total circuit resistance:

$$I = \frac{V}{R_S + R_L} \tag{3.15}$$

The power P_L dissipated in the load is the square of the current multiplied by the resistance:

$$P_L = I^2 R_L = \left(\frac{V}{R_S + R_L}\right)^2 R_L = \frac{V^2}{\frac{R_S^2}{R_L} + 2R_S + R_L} \tag{3.16}$$

The value of R_L for which this expression is a maximum could be calculated by differentiating it, but it is easier to calculate the value of R_L for which the denominator:

$$\frac{R_S^2}{R_L} + 2R_S + R_L$$

is a minimum. The result will be the same in either case. Differentiating the denominator with respect to R_L:

$$\frac{d}{dR_L}\left(\frac{R_S^2}{R_L} + 2R_S + R_L\right) = -\frac{R_S^2}{R_L^2} + 1 \tag{3.17}$$

For a maximum or minimum, the first derivative is zero, so:

$$\frac{R_S^2}{R_L^2} = 1$$

or

$$R_S = \pm R_L$$

In practical resistive circuits, R_S and R_L are both positive, so the positive sign in the above is the correct solution. So, in order to have maximum power transfer from the power source to the load, it should be:

$$R_L = R_S$$

The theorem results in maximum power transfer from the power source to the load, but not maximum efficiency of useful power out of total power consumed. If the load resistance is made larger than the source resistance, then efficiency increases (since a higher percentage of the source power is transferred to the load), but the magnitude of the load power decreases (since the total circuit resistance increases). If the load resistance is made smaller than the source resistance, then efficiency decreases (since most of the power ends up being dissipated in the source). Although the total power dissipated increases (due to a lower total resistance), the amount dissipated in the load decreases.

For SCs, let R_S be the R_{ES} (or ESR) of the supercapacitor, and let the load be called just *R*. Similarly to before, the power dissipated in the load is:

$$P = I^2R = \left(\frac{V}{R_{ES}+R}\right)^2 R \tag{3.18}$$

R_{ES} and R must have the same value to maximise the power, so:

$$P = \left(\frac{V}{2R_{ES}}\right)^2 R_{ES} = \frac{V^2}{4R_{ES}^2}\ R_{ES} = \frac{V^2}{4R_{ES}} \tag{3.19}$$

Obviously, in order to have maximum power, the voltage should be the maximum voltage (rated voltage) and the Eq. 3.19 is obtained.

Leakage and maximum peak currents

For SC devices, an additional yet useful parameter is the leakage current, widely used in industry to evaluate the capability of SCs to maintain the rated potential when not in use. Normally, it is recorded as the compensating current that applied to hold a fully charged SC after 72 hours. The leakage current will be further discussed later in section about self-discharge.

Another similar device parameter is the maximum peak current, normally appearing in the specifications for commercial SCs. It can be evaluated in two ways [69]: as the instantaneous maximum current possible in a short circuit event, given by:

$$I_{SS} = \frac{V_0}{R_{ES}} \tag{3.20}$$

Or, as the calculated maximum nominal current that could be delivered over a 1 second interval, evaluated by discharging a fully charged SC device from V_0 to 1/2 V_0 in 1 s, and calculated as:

$$I_{max@1s} = \frac{\frac{1}{2}CV_0}{CR_{ES}+1} \tag{3.21}$$

3.7 Aging effects

As mentioned before, activated carbon is the electrode material of supercapacitors widely used in industry at present, which mainly uses biomass resources to obtain porous activated carbon materials through physical activation or chemical activation treatment with an activator. Because of its simple preparation process and low price, it is widely used in industrial manufacturing of SCs. In the process of chemical activation treatment, corrosive activated materials will be used to make the porous electrode materials. After the activation treatment is completed, the electrode material will be cleaned to remove the activated substances remaining on the surface of the material. While cleaning, some residues will still be adsorbed on the electrode surface. The impurities left in the electrode during electrode manufacturing are the main source of aging and failure [71].

During the normal use of the supercapacitor, the residues on the electrode surface will react reversibly with the electrolyte to form solid and gaseous products, as shown in Figure 3.18. The gradual deposition of solid products on the electrode surface (as illustrated in area 1) can obstruct the porous structure and lead to a reduction in the contact area between the electrode and electrolyte. This phenomenon is commonly referred to as electrode fouling. Gaseous products may diffuse to multiple areas inside the supercapacitor. For example, when the gaseous products reach the free zone (shown in area 2), the air pressure inside the capacitor will rise; when gaseous products are adsorbed on the electrode surface (as shown in area 3), the contact area between the electrode and electrolyte will be reduced.

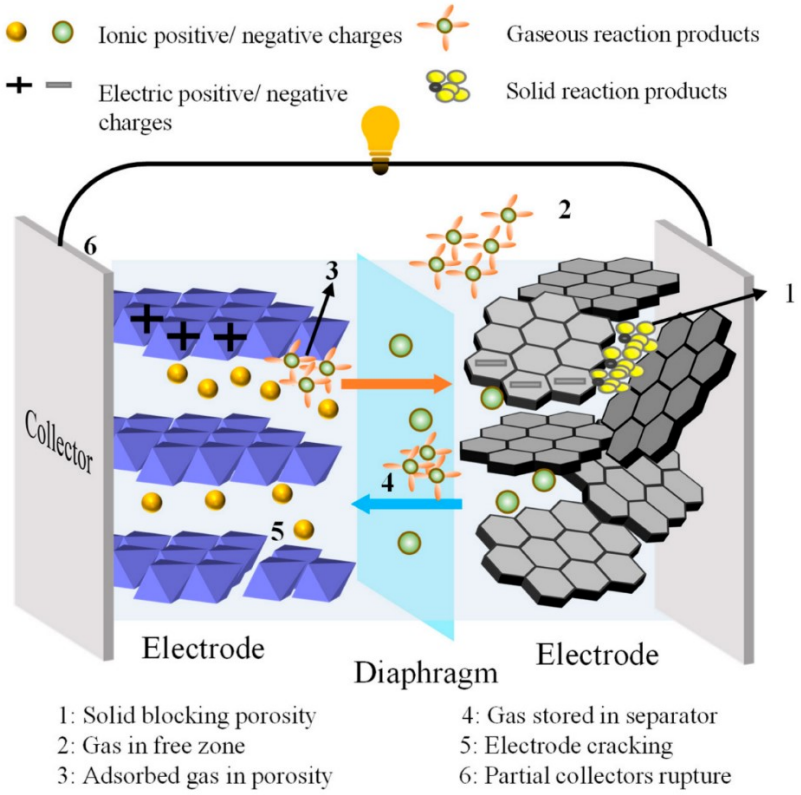

Figure 3.18: *SC aging principle*

Gaseous products may also be adsorbed on the membrane, thus blocking the path of ionic charge (shown in area 4). These products lead to an increase in the internal air pressure of the SC, which may cause electrode cracking (as shown in area 5) or shell deformation to damage the collector (as shown in area 6). The above series of reactions will lead to aging of the supercapacitor.

Taking the influence of temperature as an example, in reference [72], the SCs were cyclically tested in 40–50 °C, 40–60 °C, and 50–60 °C, and the results showed that the degradation rate of the supercapacitor was significantly accelerated with the increase in temperature. The high temperature stimulates the chemical activity of each component of the supercapacitor and accelerates the aging speed. In addition, the high temperature accelerates the decomposition of electrolyte, which leads to the decrease in ion concentration. Simultaneously, the impurities generated from its decomposition block the pores of the diaphragm and electrode materials, reducing the ion mobility, reducing the accessibility of the ion to the porous structure on the electrode surface, thus causing the decrease in capacitance and the increase in ESR.

Voltage can also accelerate the attenuation rate of a supercapacitor. The authors of [73] draw a conclusion through experiments that 10 K temperature rise and a voltage increase of 100 mV have virtually the same effect on the aging behavior of a supercapacitor. The maximum working voltage of a supercapacitor is subject to the decomposition voltage of electrolyte solution; in contrast, the working voltage affects parameters such as current density and temperature, which are closely related to the stability of electrolyte.

In technical terms, the cycle life of a supercapacitor is impacted by its charge and discharge power. Higher charge and discharge power levels result in a more rapid decay of the supercapacitor's lifespan. This is due to the fact that increased power levels generate more Joule heat, which, in turn, accelerates the degradation of the supercapacitor's internal materials, increases its internal resistance, and accelerates the aging process [74].

The aging process of supercapacitors is accompanied by self-acceleration, which is specifically shown as follows: when supercapacitors are used in modules, due to the complexity and diversity of the application environment and uneven temperature distribution, individuals close to the heat source have a higher initial temperature, which will accelerate their aging speed and cause the ESR to rise faster, and the rise of ESR, in turn, will cause their own temperature to rise faster, thus forming a positive feedback effect [75];

due to the difference in individual parameters of supercapacitors, there is a voltage imbalance between each individual in the module during charging. Specifically, the single supercapacitor with the smallest capacity has the highest charging voltage, which is most prone to overvoltage and has the most serious aging occurring during use. The more serious the aging is, the further the capacity is reduced and the charging voltage is further increased, which also forms a positive feedback effect.

Different materials and manufacturing processes also affect the service life of supercapacitors. On the one hand, the polymer that plays a bonding role in the electrode preparation process contains a large number of functional groups. During the preparation of the porous electrode, physical or chemical activation is carried out and water residues are inevitably introduced. During the normal use of the supercapacitor, the surface functional groups are decomposed by redox reaction; on the other hand, the impurity atoms on the surface of the carbon electrode that cause electrochemical phenomena also appear during

the preparation of the electrode. In addition, different capacitor packaging methods will lead to significantly different life.

However, in our model, aging effects will be not taken into account, as well as temperature effects. SCs' lifecycle is extremely long, over half a million cycles up to one million cycles [33] on average: if we assume that the Storage System in DEMOfusion PES network runs one charging/discharging cycle every two hours, it could be something like tens of years any appreciable aging effect can be observed. Nonetheless, further analysis should be carried out about this topic, especially for systems with a huge number of cells in series.

If we would add aging effects in our model, they can be modelled with an extremely slow-trend logarithmic decrease of capacitance, or similar increase of ESR [71].

4. Supercapacitor modeling

A number of equivalent circuit models of various complexity have been proposed over these years to predict or describe SC behaviour models under numerous conditions in power storage applications [76].

In general, the SC models for EDLCs classify into numerical models and electrical models. Numerical or mathematical models consist of a set of partial di_erential-algebraic equations with many parameters; circuit-based or electrical models are able to reproduce the electrical behavior of supercapacitors with equivalent circuits [77].

In this chapter, mainly two of them are described and discussed. Note that the focus is put on Electric Double Layer Capacitors (EDLC), since they are the most widely used at present, and literature most commonly refers to them.

From now on, Supercapacitor (SC) and Electric Double Layer Capacitors (EDLC) abbreviations are considered as interchangeable.

The aim is to provide a SC model that best represents and describes the dynamic behaviour of a real SC, in order for it to be later connected to a simplified network model of DEMOfusion Plant Electrical System during next-in-line work, for the progression of the DEMO project yielded by Technology University of Eindhoven.

The future simulations are likely to be developed in MATLAB Simulink, so that is why this environment was used also for this thesis project. Precisely, Simscape Electrical and Specialized Power Systems libraries were used in Simulink.

The working principle of a SC is similar to a normal solid-state capacitor; then, the first question that comes up to mind is, can a SC be modelled like a normal capacitor?

The easiest combination of electric components one can figure out to model a SC, is a capacitor with a really high value of capacitance, with a resistance in series, representing the internal resistance or, as it is called for SCs, Equivalent Series Resistance (ESR), see Figure 4.1.

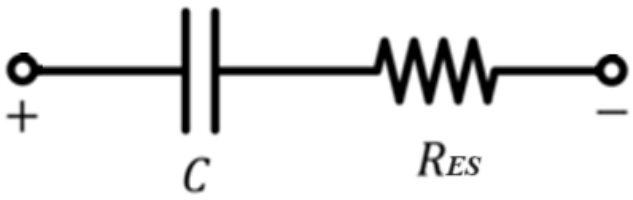

Figure 4.1: *Equivalent circuit of a normal capacitor*

This simple circuit, however, does not correctly describe the behaviour of a Sc. The reasons why a more complex model is needed are explained throughout this chapter.

4.1 Physical processes at the solid-liquid interface

Before moving on to the models, a deeper inside of what happens alongside the interface between solid electrodes and liquid electrolyte solution of an EDLC is necessary to develop further equivalent circuits.

A double-layer charge distribution is formed when two different phases, solid/liquid in the EDLC's case, are in contact, and charge separation occurs at the boundary. The formation of the double-layer can be explained in the following way: when two phases are brought into contact, ions, which are assumed to be positively charged, migrate from one phase, in which the escaping tendency is larger, to the other phase. Because of this ionic migration, one phase becomes positively charged and the other negatively charged, producing a double-layer charge distribution structure [78].

The reason for this chemical process, in which ions migrate from one phase to the other, is the difference in the inner potential between the two phases. When the superficial contact is established, the inner potential difference produces a force which transfers the particles across the interface [79].

The double-layer charge distribution generates an electric field, and subsequently an interface potential. That electric field will hinder further migration of the ions as it compensates for the inner potential difference between the phases. Therefore, after a certain number of ions have migrated, a state of equilibrium is reached.

The double-layer effect behaves like an electric capacitor in that it is capable of storing energy. If a comparison with a parallel plate capacitor is done, the charge is stored in the double-layer formed across the interface. However, in this case, the distance between the plates (phases) is very small, producing a device with high specific capacitance [80].

This layer is known as the “Helmhotz double layer”, “Stern layer” or simply “compact layer”, and its width is of atomic dimensions.

On electrodes side, as the solid structure does not allow much of a charge distribution, the charge produced in the solid phase is a surface charge. The surface charge at the solid phase generates a dipole orientation which produces another effect called "bound" double-layer. This bound double-layer is extremely thin, probably one molecule thick, and can be said to form a molecular capacitor. In the bound double-layer, the charges neither move nor separate from the surface. The capacitances of the two kinds of double-layer mentioned can be assumed to be in series, and they will produce the capacitor effect used in the double-layer capacitors.

Moving away from the solid electrodes, towards the inner part of the electrolyte solution of the EDLC, the electric charges distribute themselves throughout one single phase, liquid, an other layer occurs, the ‘‘diffuse layer’’ or ‘‘Gouy–Chapman layer’’ (Figure 4.2); this layer thickness depends on the ions concentration in the electrolyte solution [81], as it contains anions and cations distributed unequally in obedience to the laws of Poisson and Boltzmann.

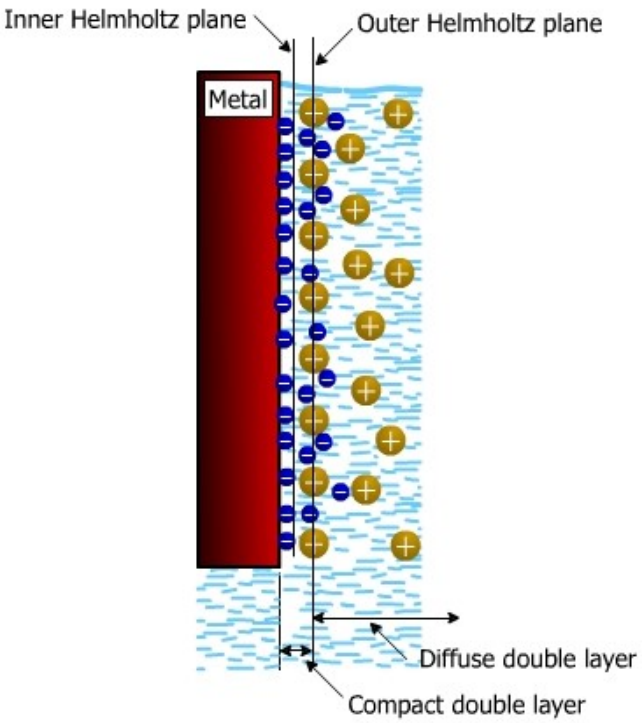

***Figure 4.2**: Double-layer effect in the EDLC interface between solid electrode and liquid electrolyte*

4.1.1 Voltage-dependent capacitance

From the situation displayed in Figure 4.2, if an external voltage is applied to the EDLC, the potential difference between the phases is increased or decreased depending on the sign of the applied voltage, which modifies the number of charges needed to establish equilibrium [79]. The relationship between the charge stored in the double-layer and the external voltage will define the capacitance for the double-layer interface.

Figure 4.3 presents the potential curve at the interface, illustrating the effect of the externally applied potential on the charge stored at the double-layer.

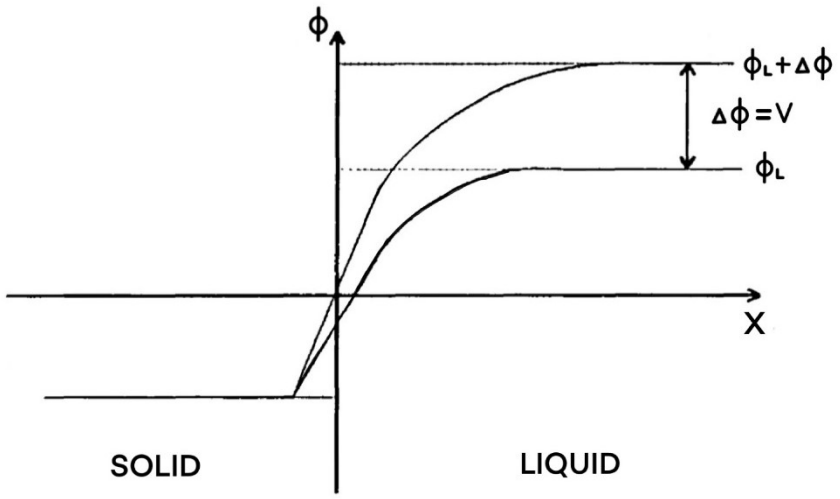

Figure 4.3: *Potential of the double-layer charge distribution*

In the figure, "ϕ_S" is the inner potential at the solid, "ϕ_L" is the inner potential at the liquid, "x" is the position, and "V" is the external voltage applied. A positive external voltage increases the space charge at the interface. Also noted in the right section of Figure 4.3 is the effect of the diffused double-layer that produces a curve in the potential characteristic. Previous studies in interfacial electrochemistry reported that the interface can never be represented simply by a parallel plate capacitor. The more complex representation of the double-layer capacitor is mainly due to the following factors:

First, the charge held by the capacitor is not a linear function of the potential across it. Second, all double-layer capacitors can be self-discharged by electrochemical reactions taking place across the interface.

Third, the double-layer capacitance was found to depend not only on the composition of the solution but also on the concentration of the electrolyte in a given system [77].

The first factor establishes that the total charge stored in the two layers is not linearly related to the potential difference between the layers; therefore, the capacitance of the double-layer is not a constant but depends on the potential difference.

Capacitance is generally defined as the ratio between charge and voltage, as seen in section 3.6; but, because of the non-constant capacitance in the double-layer distribution, the previous definition is now insufficient to appropriately represent the double-layer capacitance. Therefore, a differential capacitance needs to be introduced for EDLCs. The

differential capacitance is defined as the derivative of the charge with respect to the potential difference between the phases:

$$C_{diff} = \frac{dQ}{dV} \tag{4.1}$$

The double-layer charge distribution is physically studied through the so-called interfacial tension. The interfacial tension is developed at the contact surface between phases and is given by the force per unit of length at the interface; this quantity is also a function of the potential difference. Based on the interfacial tension definition, the curve of interfacial tension vs potential difference has been measured using different solutes and electrolytes in the formation of the double-layer [79]. This curve is called the electrocapillarity curve, and the results have been concordant with the fact that the capillarity curve can be modeled, at least for potential differences close to zero volts, as a third-order function.

Based on the capillarity curve, the so-called capillarity equation is developed:

$$\frac{d\gamma}{dV} = -\sigma \tag{4.2}$$

Where:

- γ is the interfacial tension
- *V* is the potential difference across the phases
- σ is the surface charge

Using the defined differential capacitance presented in equation 4.1 and the capillarity equation 4.2, the capacitance of the double-layer is related to the interfacial tension through the following equation:

$$C_{diff} = \frac{\mathrm{d}}{\mathrm{d}V}\left(K\,\frac{d\gamma}{\mathrm{d}V}\right) = K\,\frac{\mathrm{d}}{\mathrm{d}V}\left(\frac{d\gamma}{\mathrm{d}V}\right) \tag{4.3}$$

As the capillarity curve can be represented by a third-order equation in the region close to zero volts, the differential capacitance expected in this region results in a linear function of the potential difference after the double differentiation indicated in equation 4.3.

Figure 4.4 presents the double-layer charge and double-layer capacitance calculated from Figure 4.3. The region of interest for the double-layer capacitors is again indicated (from around -2V to around 3V).

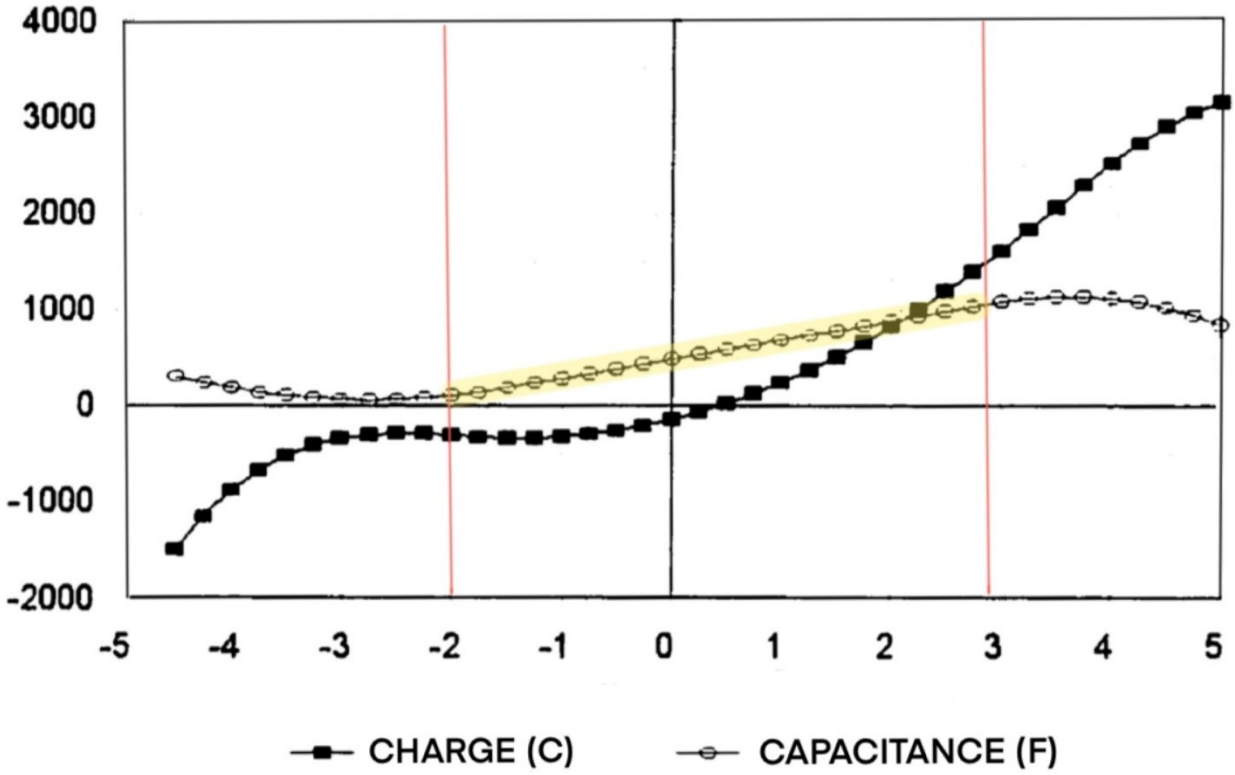

Figure 4.4: *Typical double-layer charge and capacitance curve*

4.1.2 Charge redistribution

The previous paragraph presented the fact that electrical charge is stored in the double-layer when external voltage is applied.

However, the flow of charges across the interface is not an instantaneous process. It depends on the ion mobility, environmental conditions, and several other factors.

Furthermore, crossing of electrical charges is followed by a series of charge redistribution processes and dipole orientations, which take a considerably long time [79].

In effect, when a material is charged (or discharged), the outer surface of the material responds quickly, but material in the bulk may lag significantly [83]: the potential of the active layer increases faster than that of the bulk, causing a potential gradient through the material; to equalize this gradient, charge will move alongside the porous interface, as shown in Figure 4.5. This process is called charge redistribution.

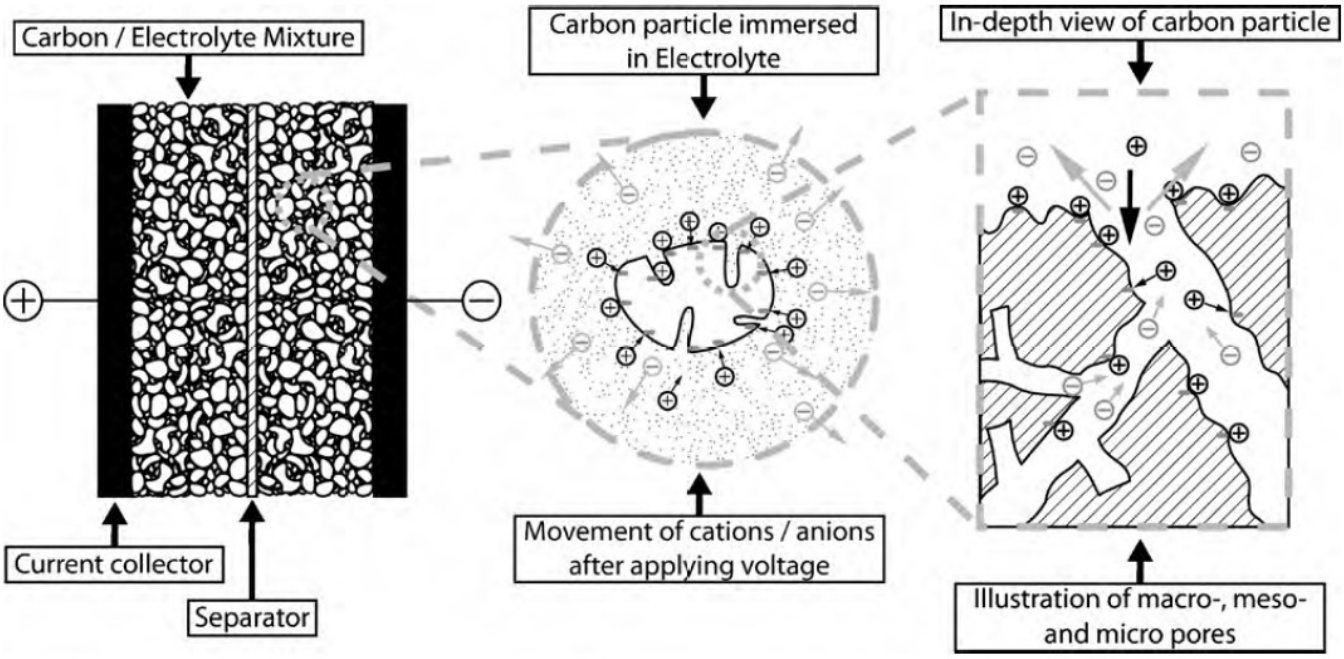

Figure 4.5: *Charge redistribution process alongside the porous electrode structure*

Whereas the time constant of charging the electrodes is of the order of seconds, there are charge redistribution phenomena with time constants of the order of seconds, minutes and hours, which constantly establish situations of dynamic equilibrium between forces.

For instance, a completely discharged supercapacitor can be charged to the nominal voltage in a few seconds, but then the voltage at the SC terminals drops due to charge redistribution [76].

Similarly, and contrarily, a recovery voltage appears in SCs after they are discharged (Figure 4.6a), due to redistribution of charges from the electrolyte to the electrodes when the discharge is stopped [76].

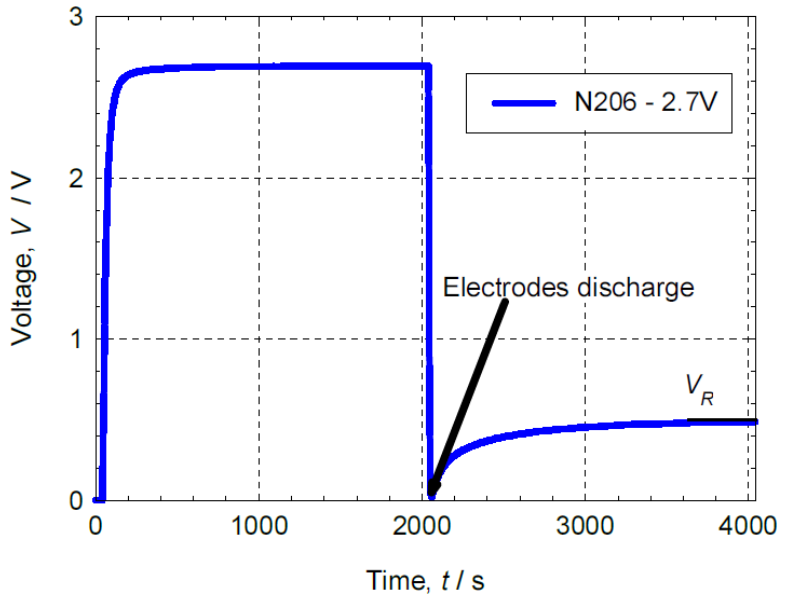

Figure 4.6a: *Recovery voltage phenomenon*

The recovery voltage value seems to be linearly proportional to the initial bias voltage value (Figure 4.6b) [76].

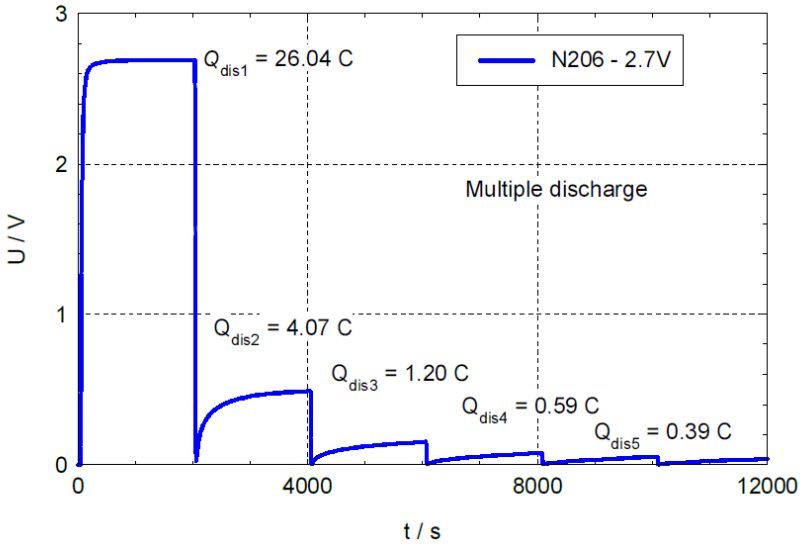

Figure 4.6b: *Recovery voltage for multiple discharge of electrodes*

Apparently, such these behaviours differ from those that occur in conventional types of capacitors [84]. Again, the traditional models used to describe the capacitor behaviour are inadequate to the electrochemical capacitors.

4.2 Zubieta model

The before mentioned physical processes happening in the inner structure of a EDLC were the starting point for further development carried out by L. Zubieta and R. Bonert for their SC equivalent circuit, known as “Zubieta-Bonert model” or simply “Zubieta model”.

In an initial draft of the equivalent circuit of a SC, the charge redistribution processes can be seen as capacitors, namely RC circuits, each one with a different time constant, to represent the slower and faster charge redistribution phenomena, as shown in Figure 4.6.

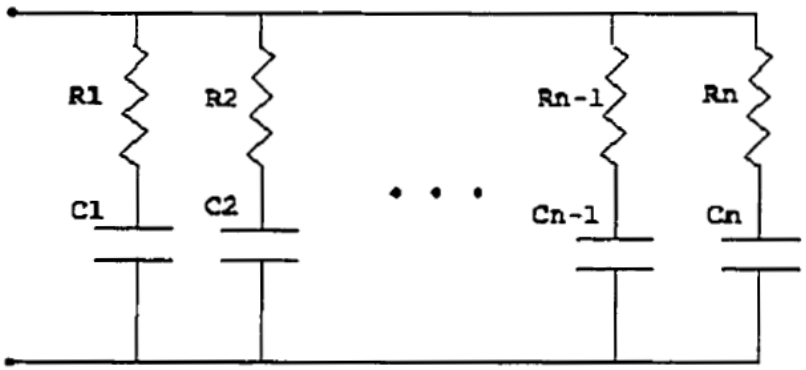

Fig. 4.7: *Equivalent circuit of a SC considering charge redistribution processes*

The circuit in Figure 4.7 contains infinite RC branches as, theoretically, the charge redistribution processes go on indefinitely.

In this circuit:

$$R_1C_1 < R_2C_2 < \cdots < R_{n-1}C_{n-1} < R_nC_n$$

Unfortunately, this representation is not adequate for characterization due to the following reasons:

- The presence of an infinite number, or even a very large number, of branches makes the model too complex for practical use and requires excessive effort to represent the model mathematically.
- The parameter calculation of so many branches based on current and voltage measurements is difficult, arbitrary, and inaccurate. In addition, physical data for the parameter values of the above equivalent model is not available.

Based on these considerations, the Zubieta model will use the RC structure of the model in Figure 4.5 but with a finite number of branches. The number of branches should be the smallest number possible while maintaining a good level of accuracy when simulating the SC performance.

The branch with the fastest response can be assumed to have a very short time constant compared to the subsequent branches. Selecting a much larger time constant for one branch relative to the previous one simplifies the identification and calculation of the parameters [79].

In conclusion, the best tradeoff for the number of branches in Zubieta model was chosen to be three:

- First branch (immediate branch), with a time constant of seconds
- Second branch (delayed branch), with a time constant of few minutes
- Third branch (long-term branch), with a time constant of tens of minutes

As explained in chapter 4.1, the capacitance of the double-layer is not constant but depends on the potential difference. Specifically, the differential capacitance is linearly dependent on the potential. This must be included in the equivalent model to achieve accurate results. Therefore, the model should include a fixed capacitor in parallel with a variable capacitor, linearly dependent on the voltage.

Since the presence of three voltage-dependent capacitances, one for each branch, would increase the complexity of parameter identification, the voltage-dependent capacitance is neglected for the second and third branch, as it does not introduce an appreciable error for longer charge distribution effects [79].

Another characteristic of SCs mentioned in chapter 3.6 is the leakage current, flowing within the SC as a result of electrochemical reactions occurring across the interface when charge separation is present. This means that part of the charge stored in the double-layer is lost internally and may not be recovered.

The leakage effect is represented in the Zubieta model by a resistance in parallel with the RC branches.

As a result, the model proposed by Zubieta is shown in Figure 4.8.

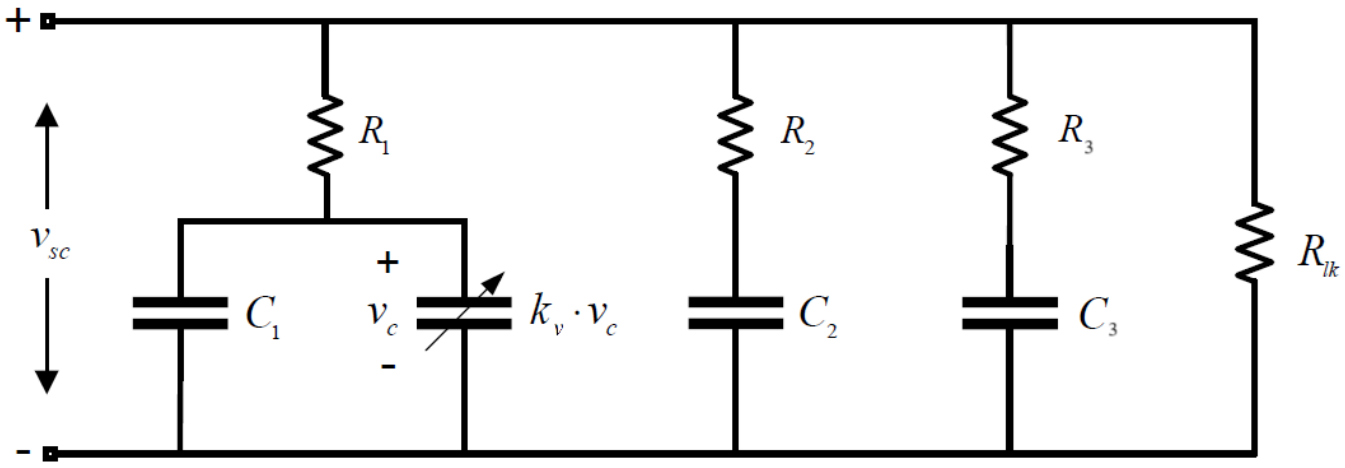

Figure 4.8: *Zubieta model*

The first branch (immediate branch) has the shortest time constant, determined by the capacitor's response to rapid charge processes, such as high-current charging. Based on manufacturer-rated values, the expected time constant for this branch is on the order of a few seconds. The capacitance of this branch is the sum of a fixed capacitance, representing the high-value constant capacitance of the Helmotz layer, and a variable voltage-dependent capacitance, as a result of the diffused layer. Their relation is linear by the constant k_v, so that the equivalent capacitance of the first branch is:

$$C_{eq_{first\ branch}} = C_1 + k_v * v_c \tag{4.4}$$

The second branch (delayed branch) features a medium time constant. The chosen time constant for this branch ranges between one and five minutes. This indicates that the time constant of the second branch is at least ten times greater than that of the immediate branch.

The third branch (delayed branch) possesses a time constant exceeding 10 minutes, making it significantly slower compared to the delayed branch.

Note that this is the equivalent circuit of one cell of a EDLC. More cells can be connected in series or parallel. This model already exists in Simulink Simscape as “Electrochemical double-layer capacitor” block.

4.3 Stern model

A different model of SC is proposed using the "Stern model" or "Stern-Gouy model" to describe the nonlinear capacitance. Stern model combined the Helmhotz model with the Gouy-Chapman model: the Helmhotz model included only the compact layer alongside the interface (Figure 4.9a), while the Gouy-Chapman model features only the diffuse layer, with increasing presence of charges of opposite sign moving towards the electrode (Figure 4.9b). Stern model combines the two layers, giving a better overview of the nonlinear diffusion dynamics (Figure 4.9c).

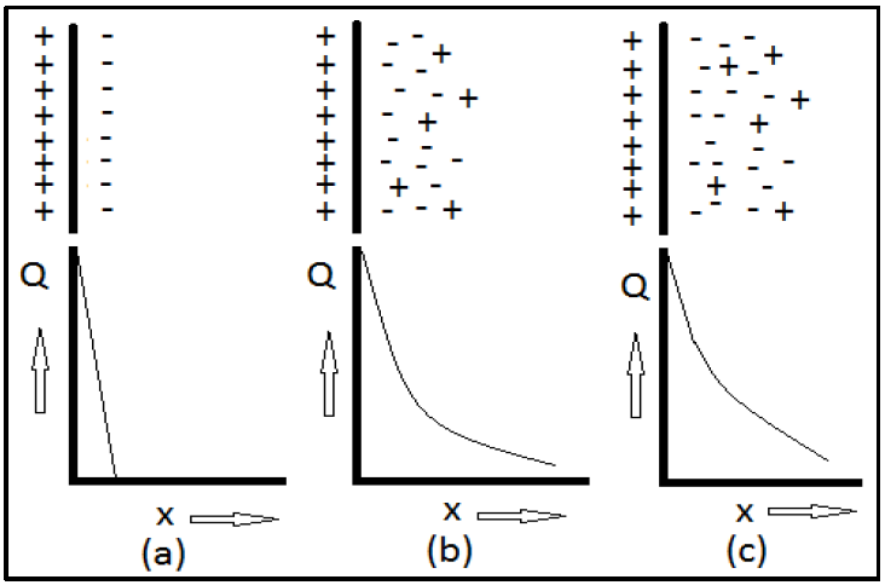

Figure 4.9: *Helmhotz model (a), Gouy-Chapman model (b), and Stern model (c)*

To do this, the supercapacitor model combines both the Helmholtz's capacitance (C_H) and Gouy-Chapman's capacitance (C_{GC}).

Helmhotz's capacitance is given by the equation [81]:

$$C_H = \frac{N_e \varepsilon \varepsilon_0 A_i}{d} \tag{4.5}$$

Where N_e is number of layers of the electrode, d is the molecular radius (m), ε is the relative permittivity of the electrolyte material (F/m), and ε_0 is the free space permittivity (F/m).

Gouy-Chapman capacitance is given by the equation [87]:

$$C_{GC} = \frac{FQ_T}{2N_e RT} \sinh\left(\frac{Q_T}{N_e^2 A_i \sqrt{8RT\varepsilon\varepsilon_0 c}}\right) \tag{4.6}$$

Where Q_T is the electric charge (C), R is the ideal gas constant (J/(K mol)), T is the operating temperature (K), c is the molar concentration (mol m^{-3}).

Then, the Stern capacitance is:

$$C_S = \frac{N_P}{N_S}\left(\frac{1}{C_H} + \frac{1}{C_{GC}}\right)^{-1} \tag{4.7}$$

Where *Np* is the number of parallel SC cells and *Ns* is the number of series SC cells.

From the definition of capacitance, the total voltage of the SC cell is calculated as the ratio between the total charge Q_T and the capacitance C_S, and the model is implemented as shown in Figure 4.10.

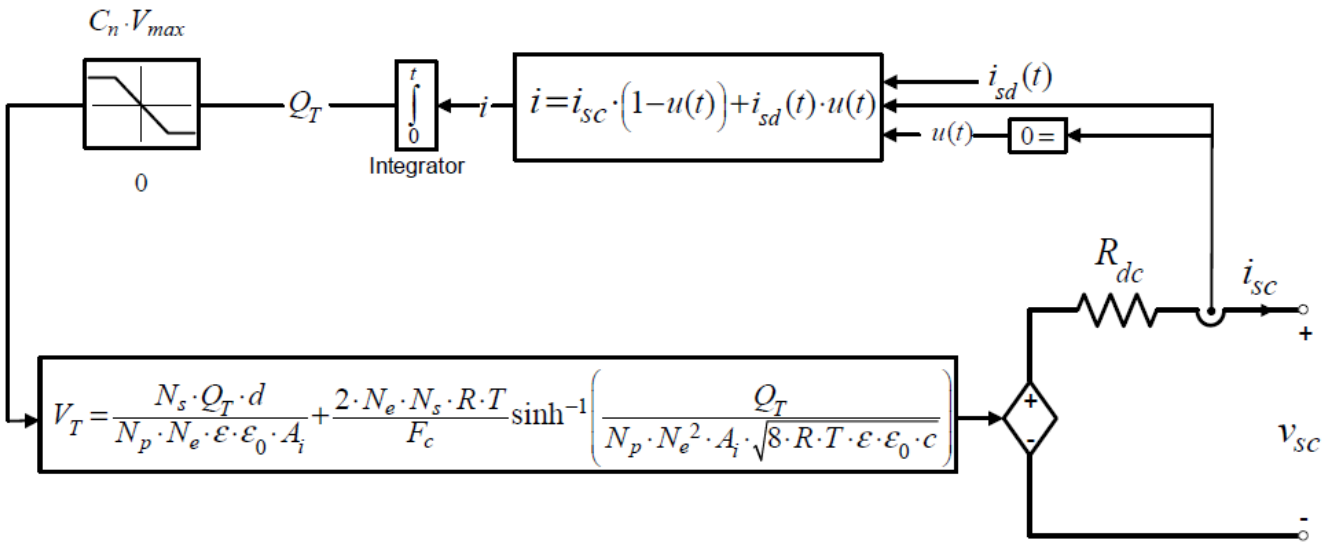

Figure 4.10: *Stern model*

As is visible in the figure, there is the Stern equation (the long equation at the bottom) to calculate the total voltage inside the SC cell, which is diminished by the resistor on the right, representing the Equivalent Series Resistance, which leads to the voltage across the SC cell, V_{SC}.

Furthermore, there is a loop for the current, passing through a block for the usage time of the SC (on top): the leakage current (i_{sd}) plays a role only in dwelling time for the SC, represented by the term *u(t)*, and for the rest of the time (1- *u(t)*), which means when the SC is charged/discharged, the i_{SC} flows in the SC.

Thanks to an integrator block, the current is transformed to electric charge Q_T, which is used, as well as the capacitance C_S, to calculate the total voltage V_T.

This model is already implemented in Simulink library: Specialized Power Systems; its implementation is shown in Figure 4.11:

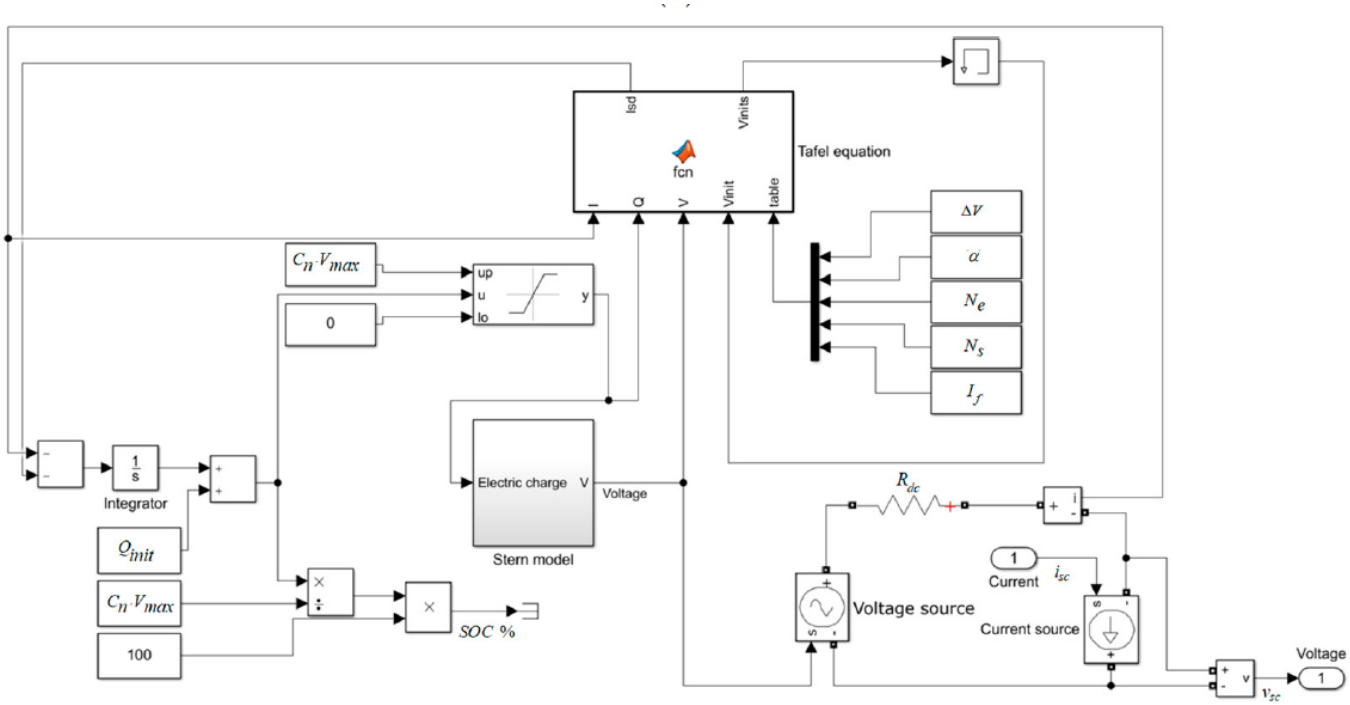

Figure 4.11: *Simulink implementation of Stern model*

4.4 Parameterization

From the analysis of these two models in MATLAB Simulink, substantial differences regarding the input of the two blocks can immediately be noticed.

The advantage of the Stern model, whose block is located within the Specialized Power Systems library, is that we can directly give as input the datas from a real SC datasheet, such as rated capacitance, ESR, rated voltage, number of series/parallel cells, initial voltage and operating temperature, as visible in the block parameters shown in Figure 4.12. The values in Figure 4.12 are the values of default.

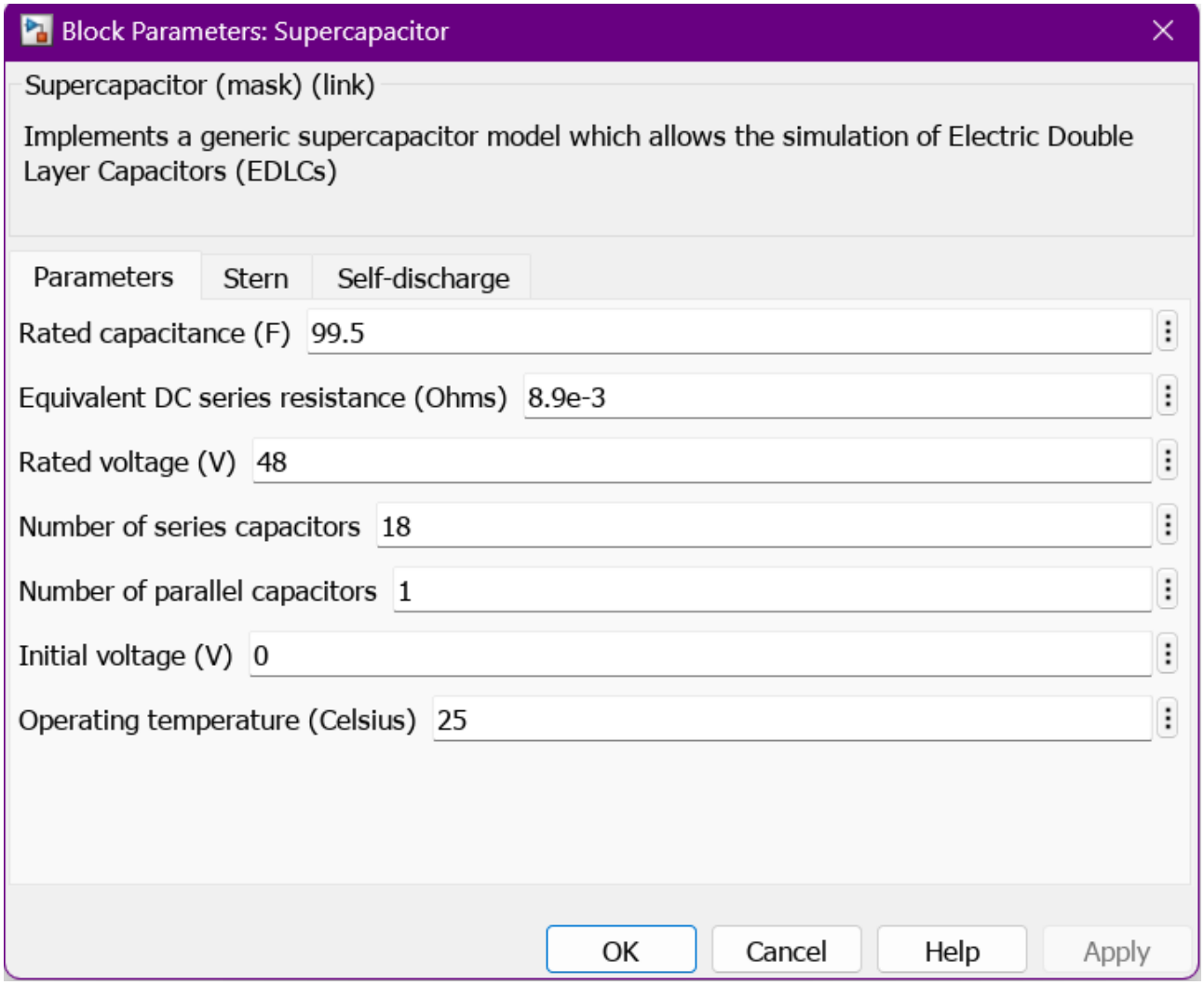

Figure 4.12: *Simulink Stern model, input block parameters*

Furthermore, under "Stern" window, there is the possibility to set some detailed parameters of Stern's capacity equation seen in paragraph 4.3, such as the molecular radius, the number of layers of the electrode (usually equal to one), and the permittivity of electrolyte material. Either, one can directly input experimental CCCD test data, if available, in the section below. The datas consist in the charging current of the test, and the voltage increase after 0 seconds (initial voltage), 20 seconds and 60 seconds.

Besides resulting greatly convenient if test datas are known, this possibility makes the model strongly reliable in a time-span of one minute if the datas are put in correctly. Similarly, one can input the self-discharge test datas, as will be discussed in the next chapter.

On the contrary, for the Zubieta model, within the Simscape Electrical library, it is not possible to input known parameters from datasheet, neither known test datas.

As visible in Figure 4.13, the only nominal values we can input are the number of series/parallel cells, and the nominal values of current and voltage, as well as their initial targets. Every other parameter, included two key parameters such as rated capacitance and ESR, do not appear in the block parameters window.

By constrast, there are the values of the equivalent circuit explained in the paragraph 4.2 (Figure 4.8), that is the three resistances of the three branches (R1, R2, R3), the three capacitances (C1, C2, C3), the voltage-dependent capacitor gain (Kv) and the self-discharge resistance.

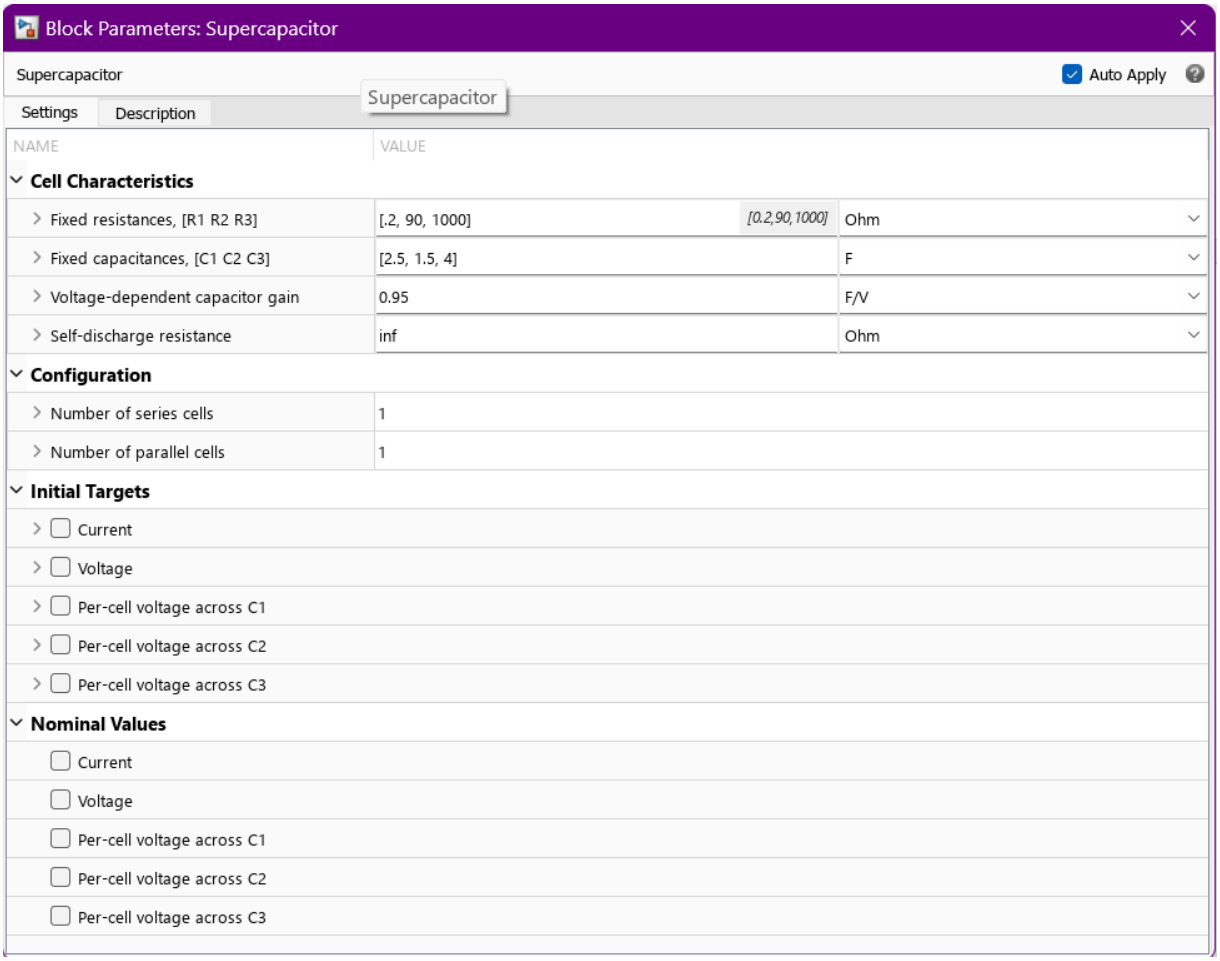

Figure 4.13: *Simulink Zubieta model, block parameters*

However, they don't appear in any SC datasheet, neither they are findable in any repository. Hence, a parameterization of the model is necessarily needed.

Below, the metodology for parameters calculation found in [79] is outlined.

During this Msc thesis project, this metodology has been implemented step by step in a MATLAB script, in order to automathically find out the proper parameters for a given Supercapacitor.

The parameterization is based on results of a CCCD test previously carried out on a real SC.

As mentioned before, the Stern model is supposed to be suitable at least for a short time-span, which means for fast charging/discharging processes, and with test data at hand. Hence, the idea is to run first simulations with Stern model of a given real SC, with experimental data taken from literature ([88], [89], [90]), and use the voltage waveforms as starting point for the parameterization of Zubieta model.

The CCCD simulation consists of three different phases:

- Charging phase, with a constant current of 32 Amperes for 60 seconds
- Dwelling phase, for around half an hour (1840 s)
- Discharging phase, with a constant current of 25 Amperes for 17 seconds

The charging current needs to be high in order to charge the SC as fast as the second and third branch (the two with longer time constants) can be considered as negligible within the charging phase [79].

Identification of immediate branch parameters

The resistance of the immediate branch (R1) is determined by observing the voltage drop across the terminals when the charging current is applied to the SC, initially fully discharged (at t0).

At a subsequent time (t1) after turning on the current source, corresponding to the maximum rise time of the current source, the terminal voltage (V1) is measured again. At this point, the current has reached its desired value, but the stored energy in the equivalent capacitance is minimal. The measured voltage step (ΔV) is therefore attributed to the equivalent resistance of the immediate branch, and the resistance value (R1) is calculated using this equation, where I is the controlled current, R1 is the immediate branch resistance, and ΔV is the difference between the voltage measured at t1 and V_0:

$$R_1 = \frac{\Delta V_{t1-t0}}{I_{ch}} \tag{4.8}$$

The voltage measured at time t1 serves as the starting point for capacitance calculation. The fixed part of the immediate capacitance (C1) is determined based on the defined differential capacitance at the start of the charge action, using the equation:

$$C_1 = \frac{dQ}{dV} = \frac{Idt}{dV} = \frac{I}{dV/dt} \tag{4.9}$$

Calculated at V_{t1}.

As the current magnitude is constant, the voltage drop across the immediate resistance is constant, therefore, the dV/dt of the terminal voltage curve over time is equal to the dv/dt of the voltage curve at the immediate branch capacitance. The slope of the terminal voltage versus time curve is measured immediately after the current is stabilized. This value is used in conjunction with the known current value and *C1* is determined.

The slope of the curve (dV/dt) is measured as follows: when the terminal voltage has increased by a value *ΔV* with respect to the voltage measured at *t1*, the time *t2* is recorded. The time difference *Δt* corresponding to this *ΔV* is equal to t2 - t1. This *ΔV* is used to measure the dV/dt of the terminal voltage curve over time, and its value is used in last equation. The size of the voltage step *ΔV* is chosen to be 0.05 Volts, as in [91].

The voltage-dependent capacitance can be calculated from the equivalent total capacitance of the first branch C_{T1}:

$$C_{T1} = \frac{Q_{TOT}}{\Delta V} = I\frac{t_3 - t_1}{V_{t3} - V_{t1}} \tag{4.10}$$

Where t1 is the time at the start of the charge already mentioned in the calculations of R1 and C1, and V_n represents the terminal voltage at the time t_n.

The voltage-dependent capacitor gain is calculated as [74]:

$$k_V = \frac{2(C_{T1} - C_1)}{V_{t3} - V_{t1}} \tag{4.11}$$

Figure 4.12 presents a typical curve of voltage vs time for a simple charge action with constant current.

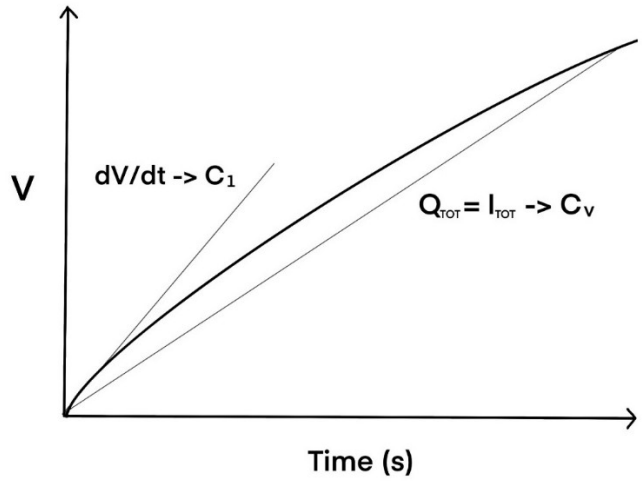

Figure 4.14: *Calculation of fixed and variable immediate branch capacitances*

Identification of delayed branch parameters

When the terminal voltage reaches the rated value, the current source is turned off and the redistribution of charge between the immediate and the delayed branch is the predominant action inside the SC. At this point the calculation of the delayed branch parameters begins. The assumption made for the calculation is that the voltage at the delayed branch is zero volts when the current is removed; in other words, the time constant of the delayed branch is much higher than the charge time of the immediate branch. The equivalent circuit in Figure 4.15 represents the SC during that redistribution process.

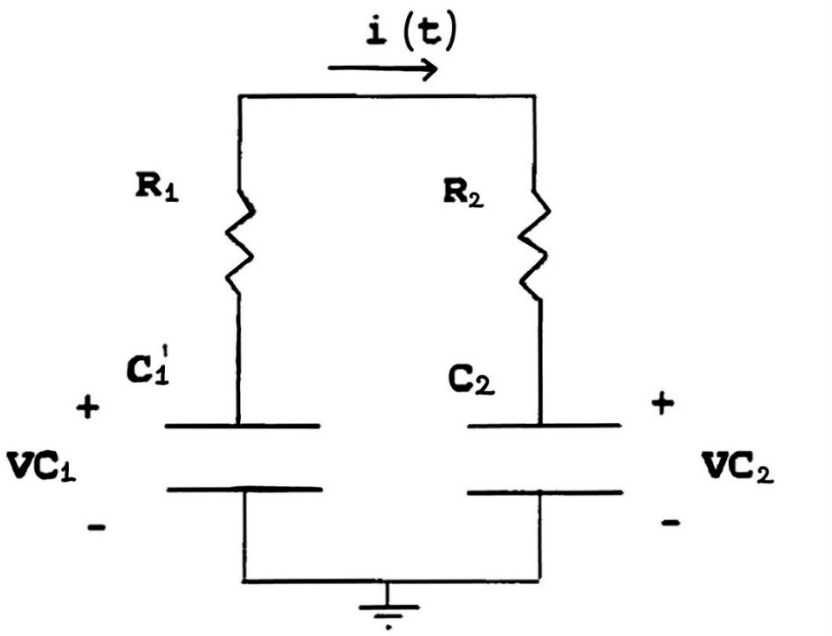

Figure 4.15: *Charge redistribution equivalent circuit*

In this figure 4.15, *C1'* is the value of the immediate branch capacitance at the corresponding voltage, and *R1* is the immediate branch resistance.

The initial current flowing through the circuit when the current falls to zero and Vcd is zero (t4), is given by:

$$i_{t4} = \frac{V_{C1}}{R_1 + R_2} \tag{4.12}$$

In addition, the following relation between the SC current and its voltage is valid at this istant:

$$i_{t4} = C' \frac{dV_{C1}}{dt} \tag{4.13}$$

The time t4 is equal to the time during which the current sourrce was turned off plus the maximum fall time of the current. The terminal voltage at t4 is measured, and then the voltage is continuously measured until it has dropped a fixed value ΔV, considered of 0.05 V again. This point determines the intant t5.

With these two points of time and voltage the value of dV/dt = ΔV / Δt is determined.

Assuming R2 >> R1 , V_{Ci} is approximately equal to the terminal voltage.

Therefore, measuring the terminal voltage and dVci/dt, R2 can be calculated through the following equation:

$$R_2 = \frac{V_{C1}}{C' * dV_{C1}/dt} \tag{4.14}$$

The value of Vc_1 and C' used in the calculation of R2 is the terminal voltage and the immediate branch capacitance at the medium point of the dV/dt calculation. (See figure 4.16).

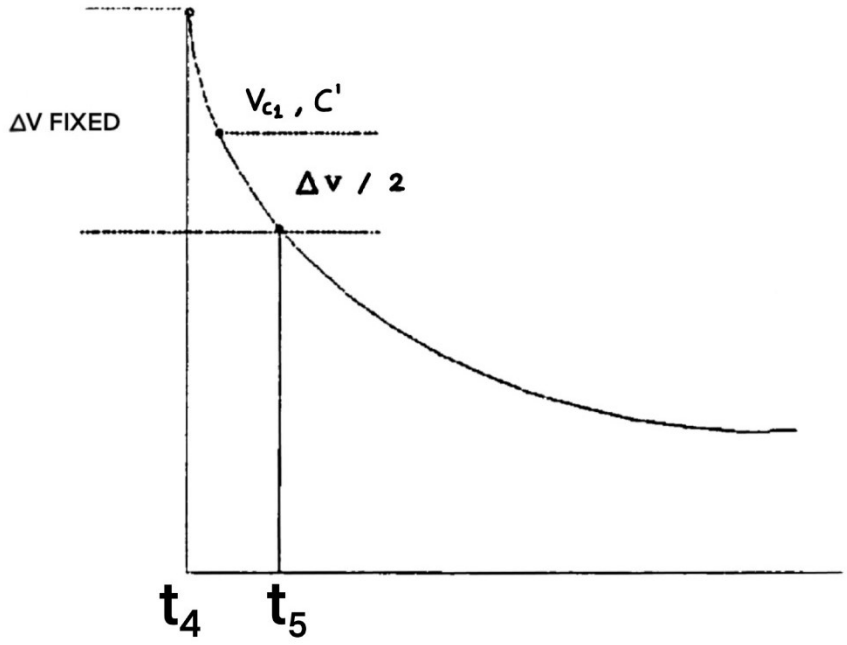

Figure 4.16: *dV/dt calculation*

The delayed branch capacitance (C2) can be calculated based on the charge equilibrium. For this identification, the time constant for the delayed branch is previously assumed to be 100 s [86]. After three-time constants of the delayed branch, the voltages across the immediate and delayed branches are practically equal, and for the charge equilibrium [79]:

$$C_2 = \frac{Q_{TOT}}{V_{t6}} - (C_1 + \frac{k_V}{2} * V_{t6}) \quad (4.15)$$

Identification of long-term branch parameters

The long-term branch parameters' calculation follows similar steps to those for the delayed branch. In this case, the delayed capacitance is assumed with equal voltage to the immediate branch and the long-term capacitance is assumed fully discharged. To make these assumptions valid, the start time for the calculation of the long term branch should be at least three times the delayed branch time constant. This criterion assures that the delayed voltage is within 95% of the immediate branch voltage.

The equivalent circuit for the charge transfer to the long term branch is shown in Figure 4.17:

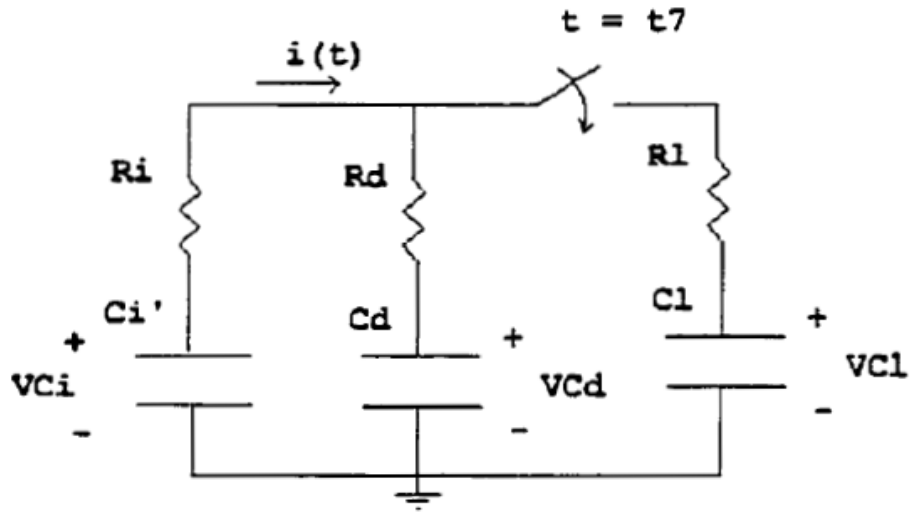

Figure 4.17: *Equivalent circuit for charge distribution to C3*

The switch is closed at the instant t7 in which the voltages at the immediate and delayed branches are almost equal. In this instant most of the charge transference occurs between the immediate branch and the long-term branch because the value of R1 is much lower than R2. Therefore, R3 is calculated the same as R2 three delayed branch time constants after the instant at which the current was turned off. The calculation of the dV/dt is done in the same form explained for the delayed branch.

The capacitance C3 is calculated using the same procedure explained for the delayed branch, but now the capacitance C' is equal to the capacitance of the immediate branch in parallel with the capacitance of the delayed branch. The instant of calculation for C3 is thirty minutes after the termination of the current source.

5. Results and comments

In this chapter, the results of varied simulations using different SC models are presented and discussed.

First, the results of the MATLAB code simulation about parameterization described in the previous paragraph are shown. The time-span is in the order of minutes.

Then, the different models are compared for time-span of seconds and hours, as the DEMOfusion PES network requires accuracy for up to two hours of cycle.

For time-span of seconds, constant current charge/discharge (CCCD) tests are provided, assessing the responsiveness of the two models. The slope of the two phases is an indicator of the accuracy of the capacitance value.

Greater emphasis was put on the time-span of hours, which means self-discharge processes, and an additional model is proposed for this aim.

5.1 Parameterization results

As previously mentioned, a MATLAB script was executed about the parameterization of Zubieta model. The SC taken into account was a IOXUS X-SERIES 129V Supercapacitor, with 48 cells in series each one with a rated voltage of 2.7 V, for a total nominal voltage of 129.6 V. The datasheet was taken from [88].

Just as a reminder, the simulation consists of a charging phase with a constant current of 32A for 60 seconds, then a dwelling time of aroud half an hour, finally a discharging phase with a constant current of 25A for 17 seconds.

The time-span for the parameterization is thus in the order of minutes.

First, the simulation was run with the Stern model, taking advantage of the possibility of giving experimental data as input to the SC block.

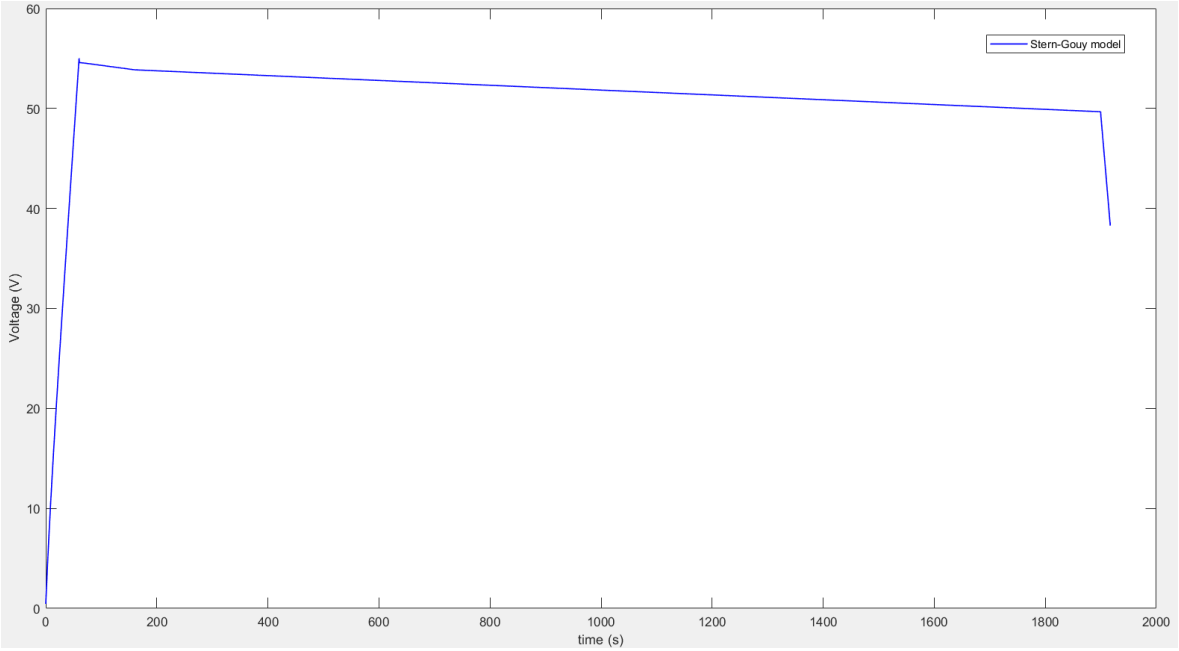

Figure 5.1: *Stern model simulation*

Subsequently, the parameter calculation was developed following the steps described in paragraph 4.4.

In the end, the same simulation, with the same input currents, was run for the Zubieta model with the parameters found, in order to compare the voltage vs time waveform of the parameterized model with the starting waveform, as displayed in Figure 5.2.

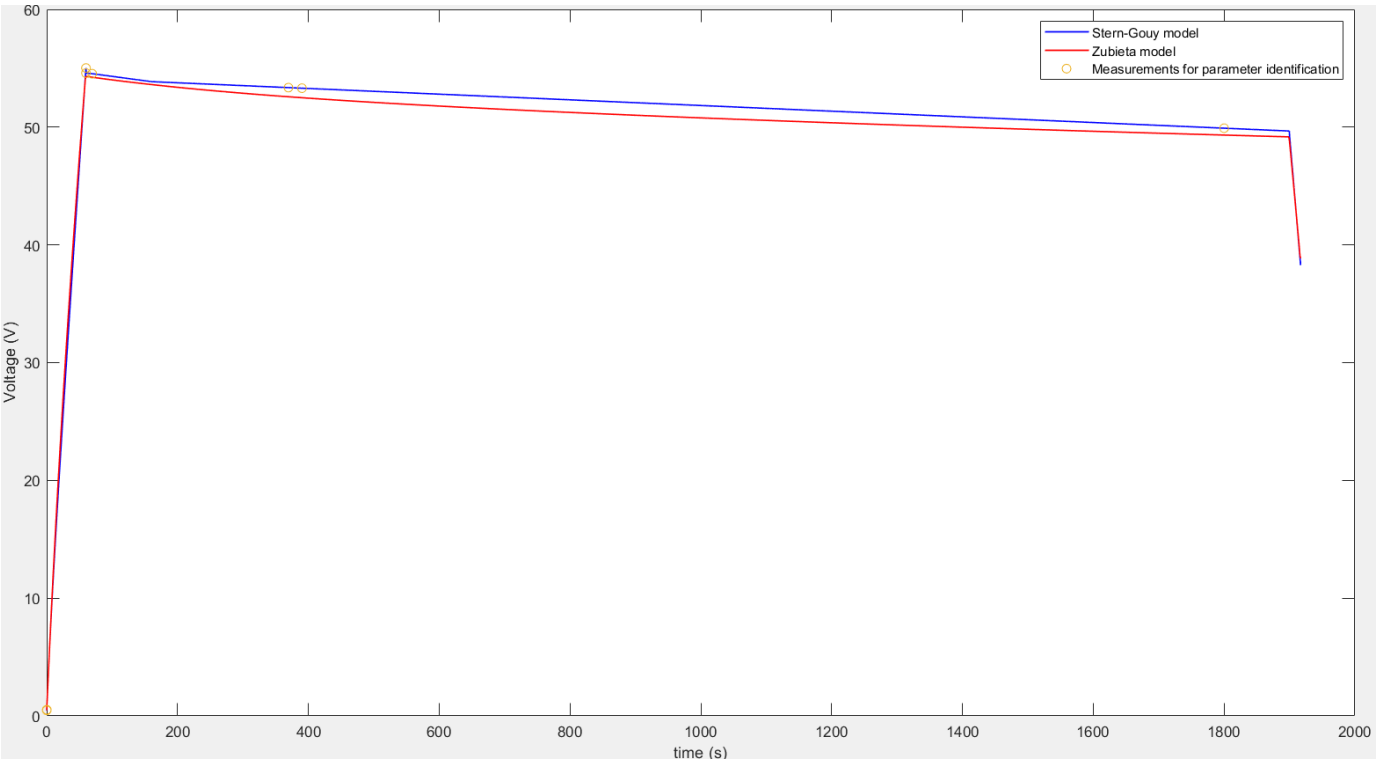

Figure 5.2: *Zubieta model parameterization results, overview*

The yellow spots are representative of the parameter identification events, namely *t1, t2,.., t8,* outlined in paragraph 4.4.

The results seem to confirm an acceptable precision of the parameterization, although the Zubieta model tends to slightly undervalue the voltage during the dwelling time.

Figure 5.3 zooms in on the charging phase, not clearly visible in Figure 5.2, i.e. on the first minute of the simulation.

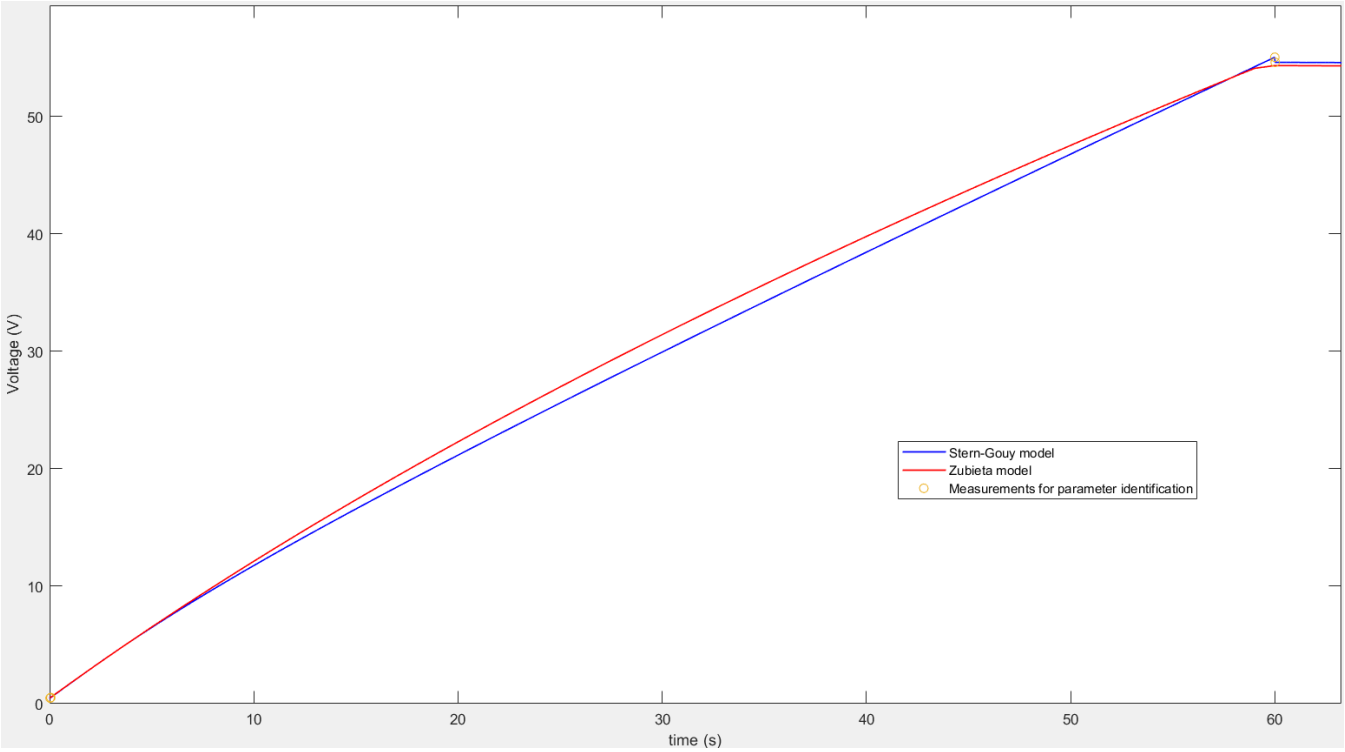

Figure 5.3: *Zubieta model parameterization results, charging phase*

It is visible from the Figure that the Zubieta model charges the SC with a smoother and curve trend respect to Stern model. It can be caused by the (low) influence of the second and third branch in the charging phase.

Indeed, in a further analysis about the charging phase, the currents flowing in the three branches were examinated. The chargin current profile corresponds to a step of 32 A at a step time of 60 seconds (Figure 5.4a)

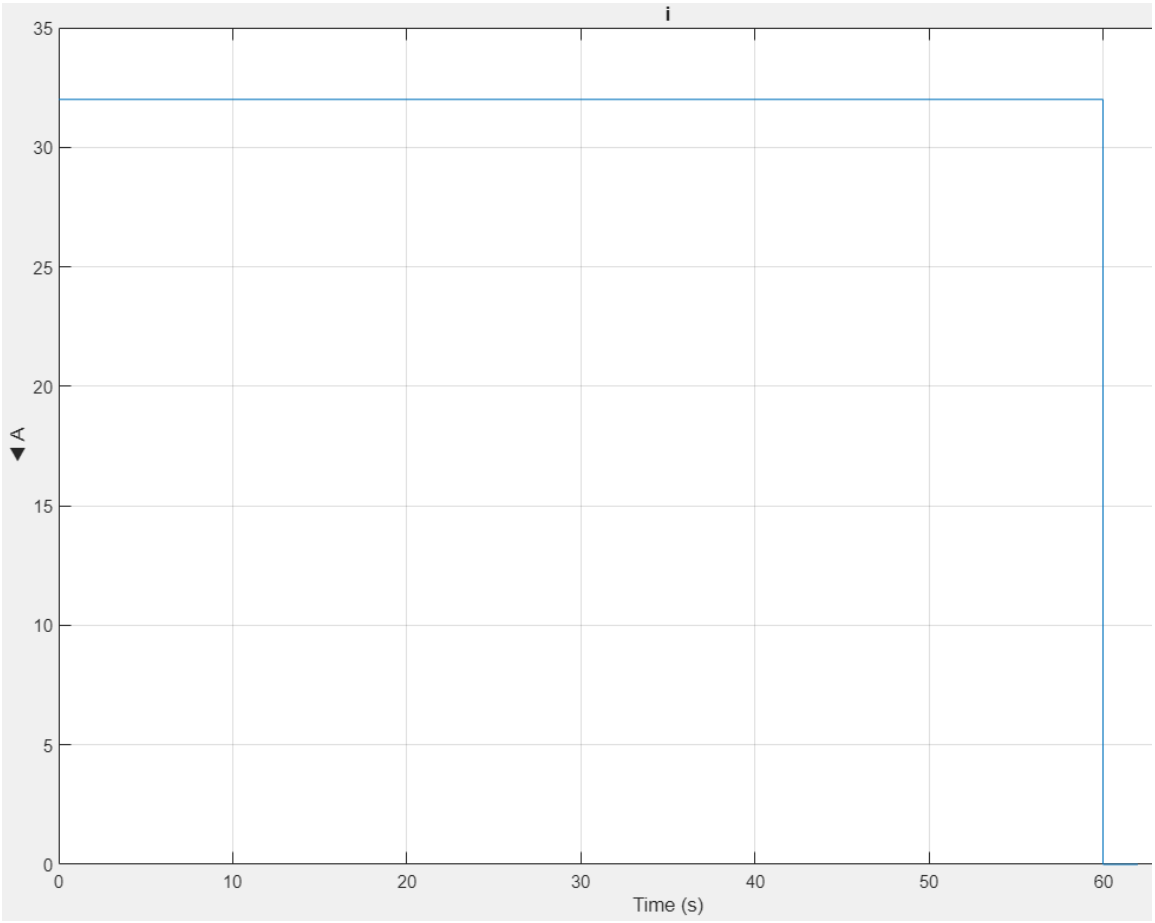

Figure 5.4a: *32 A charging current profile*

This amount of current is partitioned into the three branches, in unequal way (Figures 5.5a, b, c). At the beginning, all the current flows in the first branch; then, some current starts to flow in the other two branches: it is a small amount of current for the second branch, and even smaller for the third one, due to the longer time constants.

After 60 seconds, the value of the current in the second branch (i_2) is around 2.4 A (Figure 5.5b) and i_3 is around 0.38 A (Figure 5.5c), which means that they correspond to 7.5% and 1.2% of the total current respectively.

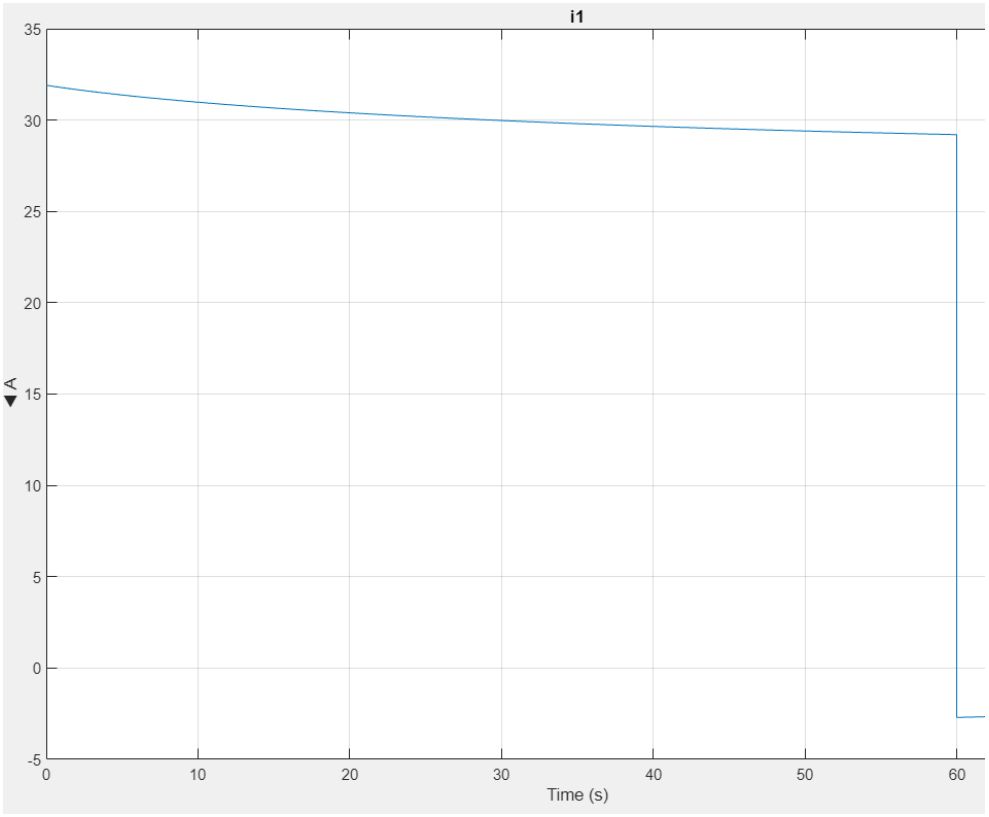

Figure 5.5a: *Current flowing in the first branch, i1*

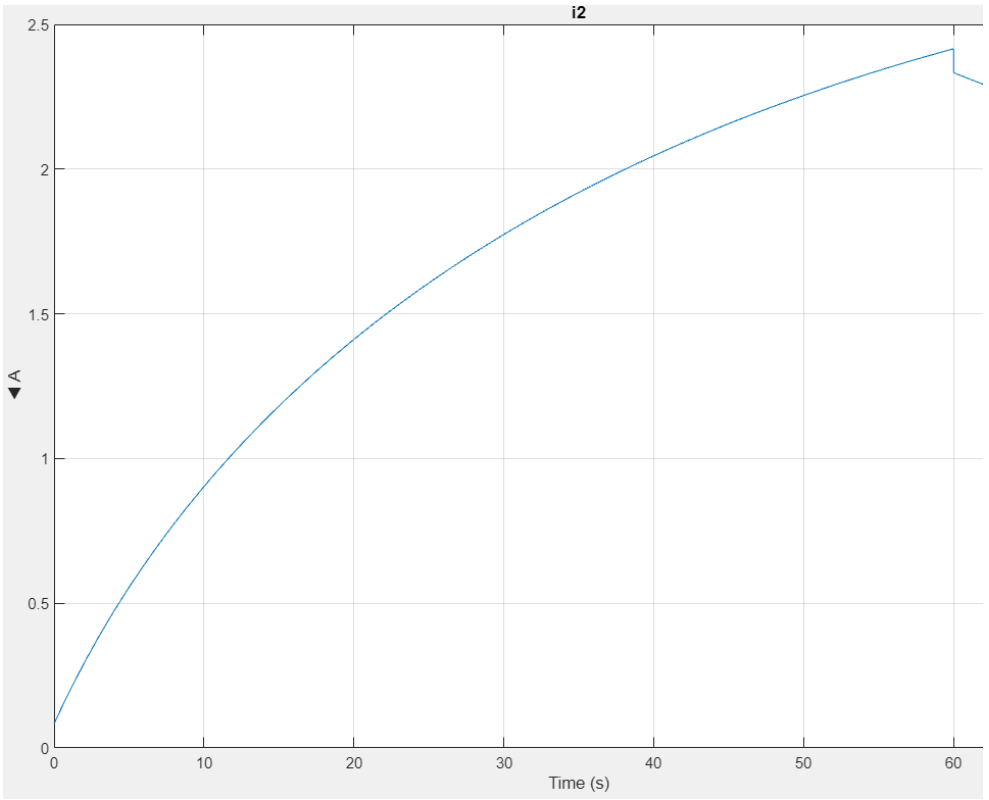

Figure 5.5b: *Current flowing in the second branch, i2*

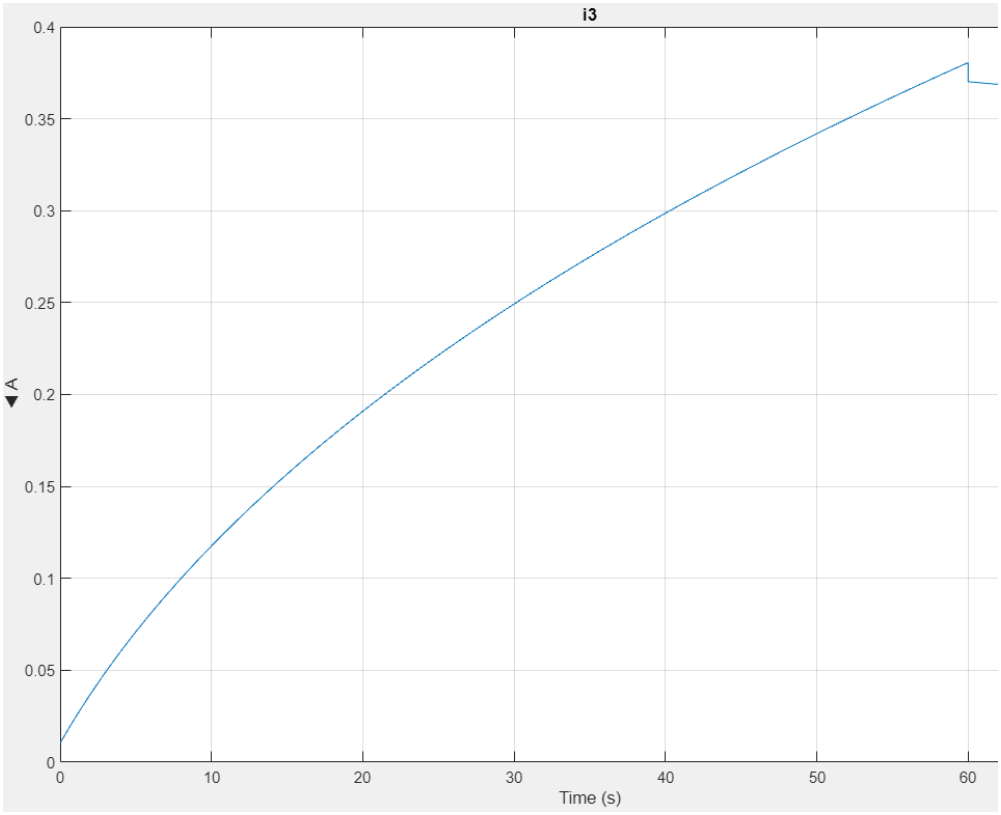

Figure 5.5c: *Current flowing in the third branch, i3*

An other charging test was executed with a smaller charging current, 1 A. It resulted in a larger percentage of current flowing in the second and third branch after 60 seconds. Then, with a larger charging current, 200 A: it resulted obviously in a smaller percentage of i_2 and i_3. The results of the test can be seen in Table 5.1.

It can be stated that the higher the charging current, the larger the quantity of that current flowing in the first branch.

Table 5.1: *Percentage of currents flowing in the three branches after 60s charging*

i charge	i1 (%)	i2 (%)	i3 (%)
1 A	82.8	15	2.2
32 A	91.3	7.5	1.2
200 A	95.7	3.7	0.6

Moreover, extending the simulation time to see what happens after the discharging phase, an interesting point of the Zubieta model is that it is able to simulate the recovery voltage effect mentioned in paragraph 4.1.2, while Stern model seems to be not. Since the recovery voltage value is larger for bigger voltage drops, the discharging current has been increased to make it more visible: it is immediately noticeable in Figure 5.6, where the discharging current was set to 32 A for 40 seconds.

In Zubieta model, this happens because the fast discharging current discharged the first branch capacitor mainly, while the second and third branch capacitors remained partially charged, having a longer time constant. The residual charge in second and third capacitors is then released in the circuit until a new charge equilibrium is reached, thus partially restoring the SC.

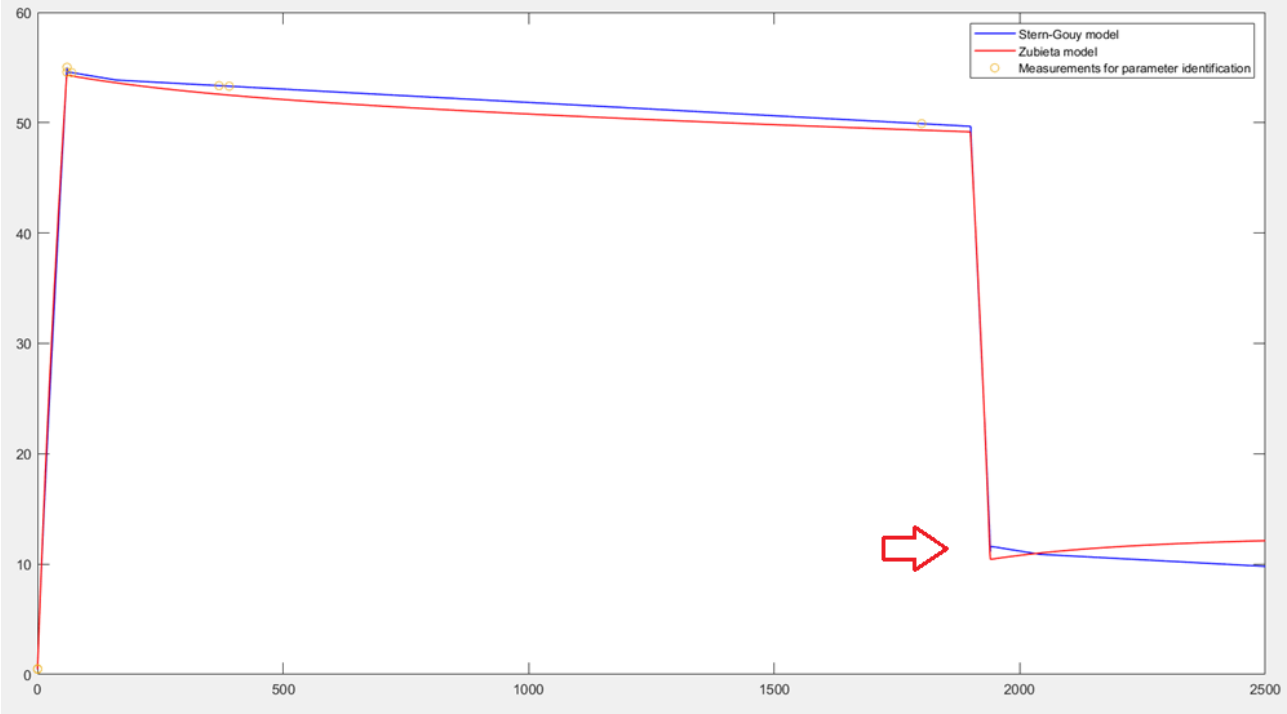

Figure 5.6: *Recovery voltage effect visible in Zubieta model after discharging*

In order to check a further validation of the parameterization of Zubieta model, a standardized CCCD test called “IEC 62391 test” was implemented in MATLAB. This test is mainly used to calculate the capacitance and the ESR of a supercapacitor during the constant

current discharging phase, thus it can be seen as a litmus test for the Zubieta model parameterization.
The parameters are calculated as depicted in paragraph 3.6 (“Capacitance” and “Equivalent Series Resistance” subparagraphs).
The Zubieta block was modelled basing on a IOXUS X-SERIES SC with the following key parameters from datasheet [88]:

• Rated capacitance (min, normal) = 39 / 41 F
• DC ESR (normal, max) = 13.9 / 16.8 mΩ

Therefore, The test results on Zubieta model should be as close as possible to the initial SC parameters. After running the test simulation, in which the SC was initially fully charged, and a discharging current of 1A was set after 10 seconds of dwelling time, the script calculated the capacitance and the ESR.
Keeping in mind that these values can slighty change depending on the boundary conditions of the test, (see paragraph 3.6), and that the capacitance is calculated assuming the slope of the discharging phase to be constant (which is a simplification), it resulted in:

• Rated capacitance test value = 37.8 F
• DC ESR test value = 13.9 mΩ

An acceptable error was committed about the rated capacitance, considering the variability of the parameter, and an accurate value was found about the ESR, corresponding to the minimal value in the datasheet.

5.2 Time-span of seconds

An different CCCD test, taken from [83], is used to assess the accuracy of the charging and discharging phase in the time-span of tens/hundreds of seconds, depending on the value of the charging/discharging current.

For this case, a MAXWELL 48V SERIES BMOD0140-E048 Supercapacitor was used. It is composed by 18 cells in series, each one of 2.7 V rated voltage for a total rated voltage of 48.6 V, a maximum voltage of 51.8 V, and a capacitance of 140 F, and an ESR of 6,67 mΩ.

Three charge/discharge tests with three different values of charging/discharging currents are reviewed: 20 A, 40 A and 60 A.

From simulation results carried out in [83] for charging phase test, it turned out that the SC, initially fully discharged, took the following time values to be charged up to maximum voltage (Figure 5.7):

- 135 seconds with a charging current of 60 A
- 202 seconds with a charging current of 40 A
- 405 seconds with a charging current of 20 A

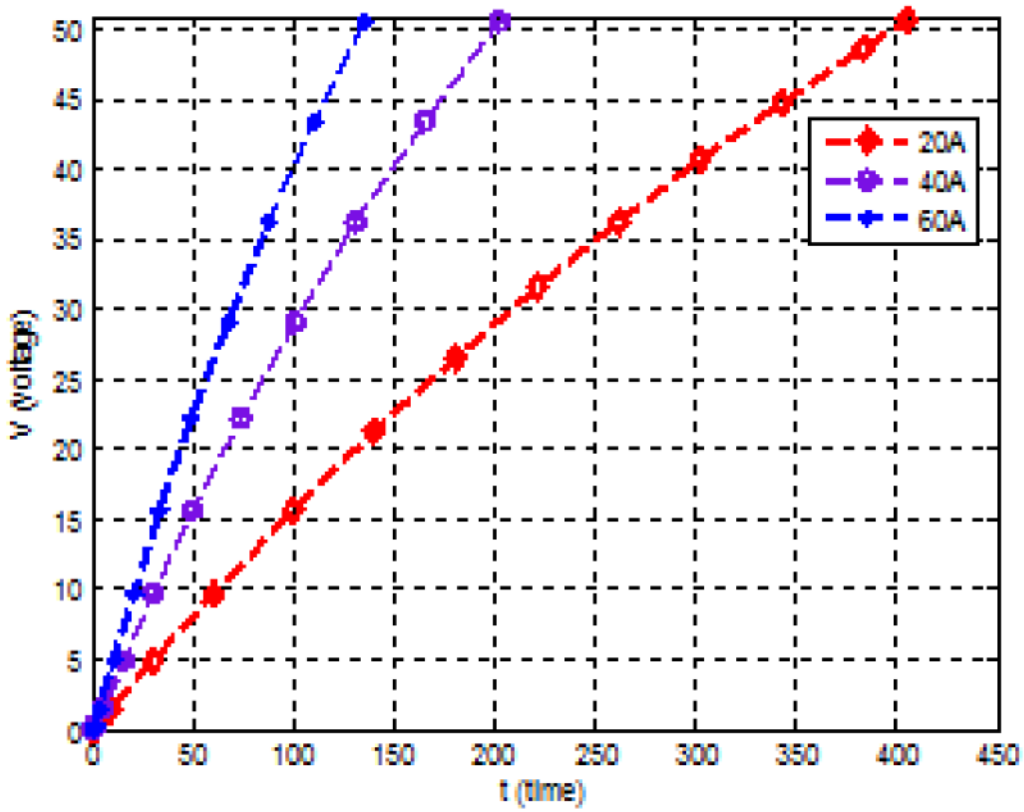

Figure 5.7: *Results of CCCD test with three different charging currents [83]*

This simulation was recreated in MATLAB Simulink, for both Zubieta and Stern model. As noted earlier, the Zubieta SC block is located in Simscape Electrical library, while the Stern

SC block in Specialized Power Systems toolbox; anyway, they are both from Simulink environment. Figures 5.8 displays the Simulink model of the simulation with the Zubieta SC block.

It should be pointed out that, from now on, every Zubieta SC model was parameterized with the metodology described in 4.4 before being used for simulations.

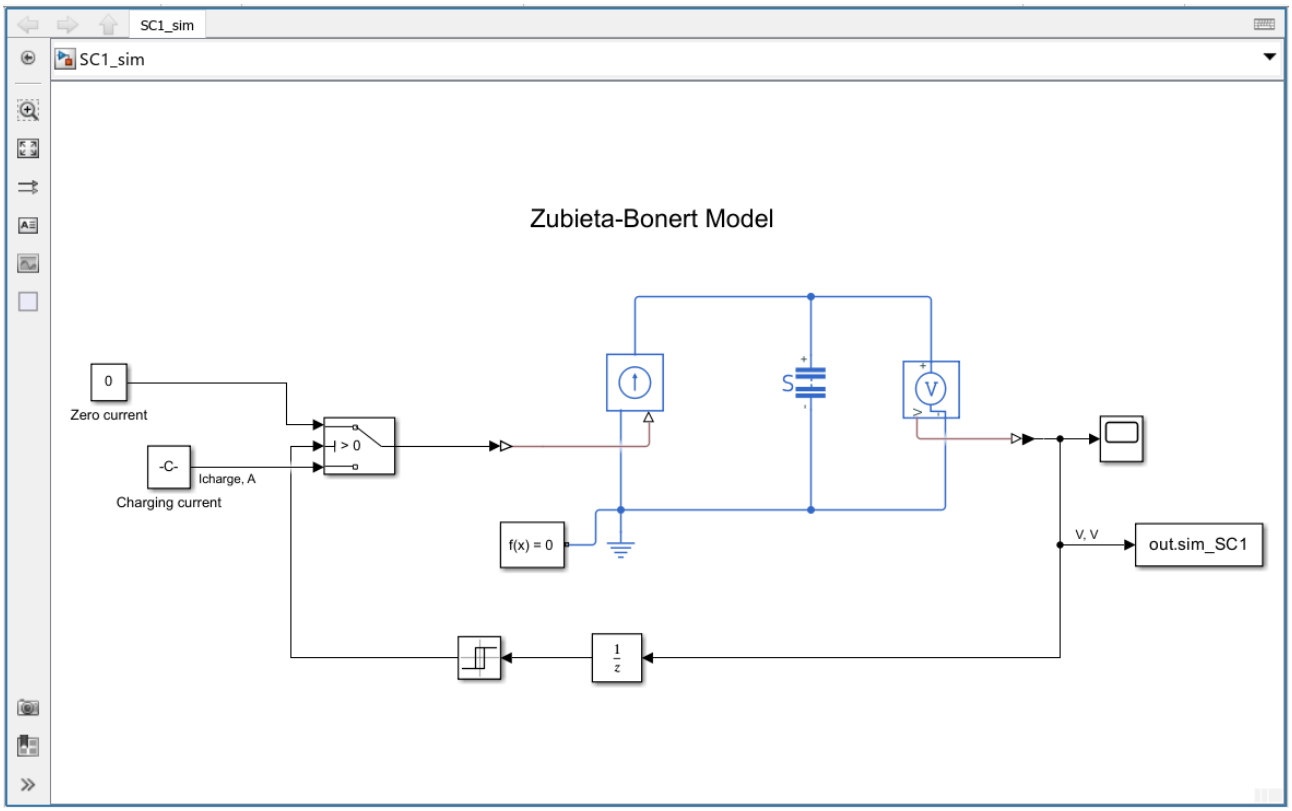

Figure 5.8: *Simulink model of CCCD simulation with Zubieta SC block*

The charging current, set in respective MATLAB code, is provided until the maximum voltage of the SC (51.8 V for this Maxwell SC) is reached. This was regulated by a control loop; the Voltage Sensor (the blue "V" block in Figure 5.8) continuously measures the voltage of the SC. This signal passes through a Unit Delay block (1/z), and then a Relay block, whose output output is "0" when the signal is within a threshold, set to the maximum voltage, and "1" when the signal overcomes that threshold. In this way, the switch block turns into "Zero current" when the maximum voltage of the SC is reached. A Simulink-PS converter is needed to interface Simulink blocks (in black) with Simscape system (in blue).

Similarly, Figure 5.9 shows the Simulink Specialized Power System simulation model with Stern SC block.

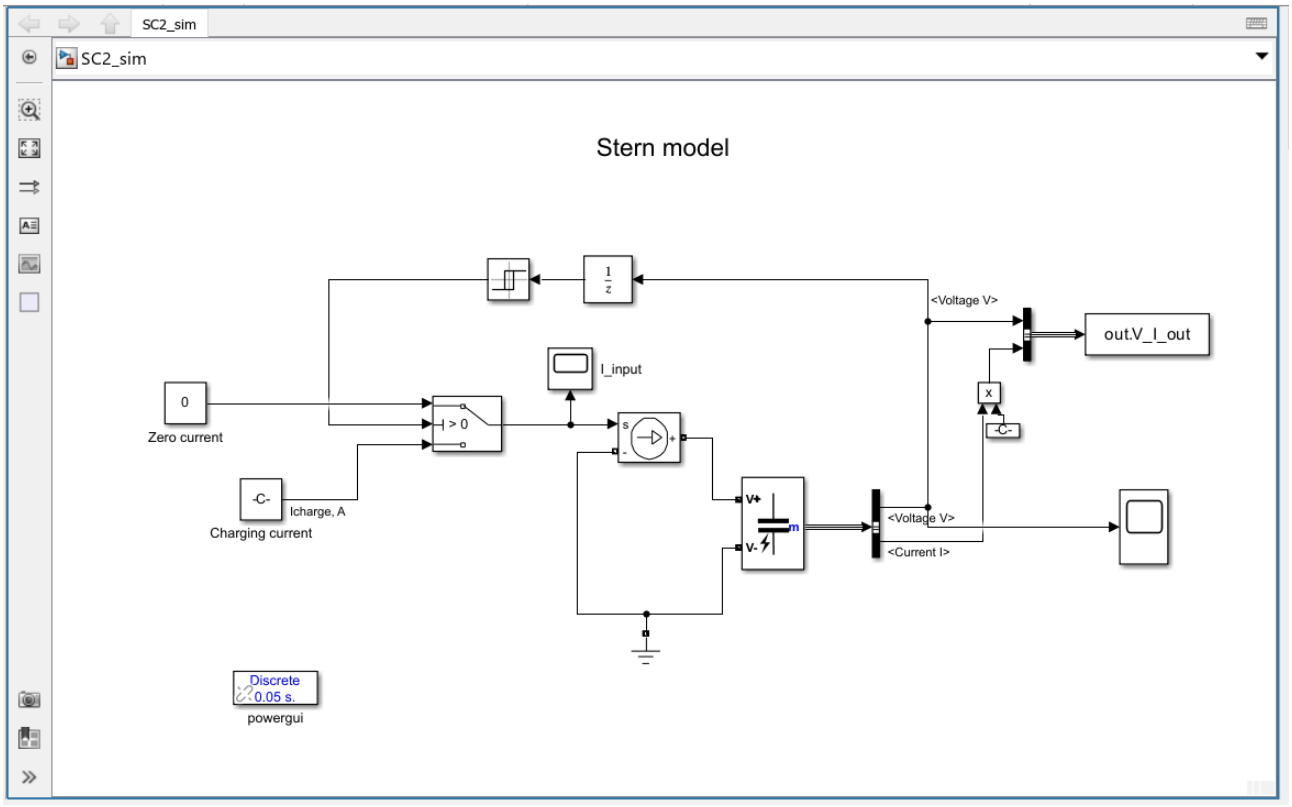

Figure 5.9: *Simulink SPS model of CCCD simulation with Stern SC block*

This model is analogous to the previous one, with some exceptions like it does not need a Simulink-PS converter as the Specialized Power System toolbox interfaces directly with Simulink blocks, and this SC model authomatically calculates the SC voltage and current so that a voltage sensor is not needed. Moreover, Specialized Power Systems models always require a powergui block (in bottom-left corner), in which one can set the simulation to be continuous or discrete, and decide the type of solver. In this case, the simulation is discrete with a sample time of 0.05 s, same thing for the previous model.

The results of the simulations with the three different charging currents are shown in Figure 5.10.

Again, it can be noticed that the Zubieta model displays a curved voltage waveform during the charging phase respect to the flatter one of Stern model. In these terms, Zubieta's charging profile results to be more similar to the experimental profile of Figure 5.7.

With regard to the time for the SCs to be fully charged, the following values emerged: with a charging current of 60 A, both models took around 130 seconds to charge, 5 seconds less than simulation results in [88].

With a charging current of 40 A, the Zubieta model took around 196 seconds to charge, a few seconds less for the Stern model, while in simulation results of [88], it was 202 seconds.

Finally, with a charging current of 20 A, a noticeable difference can be seen between the two models: due to the curved trend of the Zubieta model, the gap between the two charge durations increases for longer time values, so that Zubieta model took 405 seconds to charge, around 40 seconds more than Stern model. In simulation results of [88], the time was exactly 405 seconds, that is in accordance with Zubieta model.

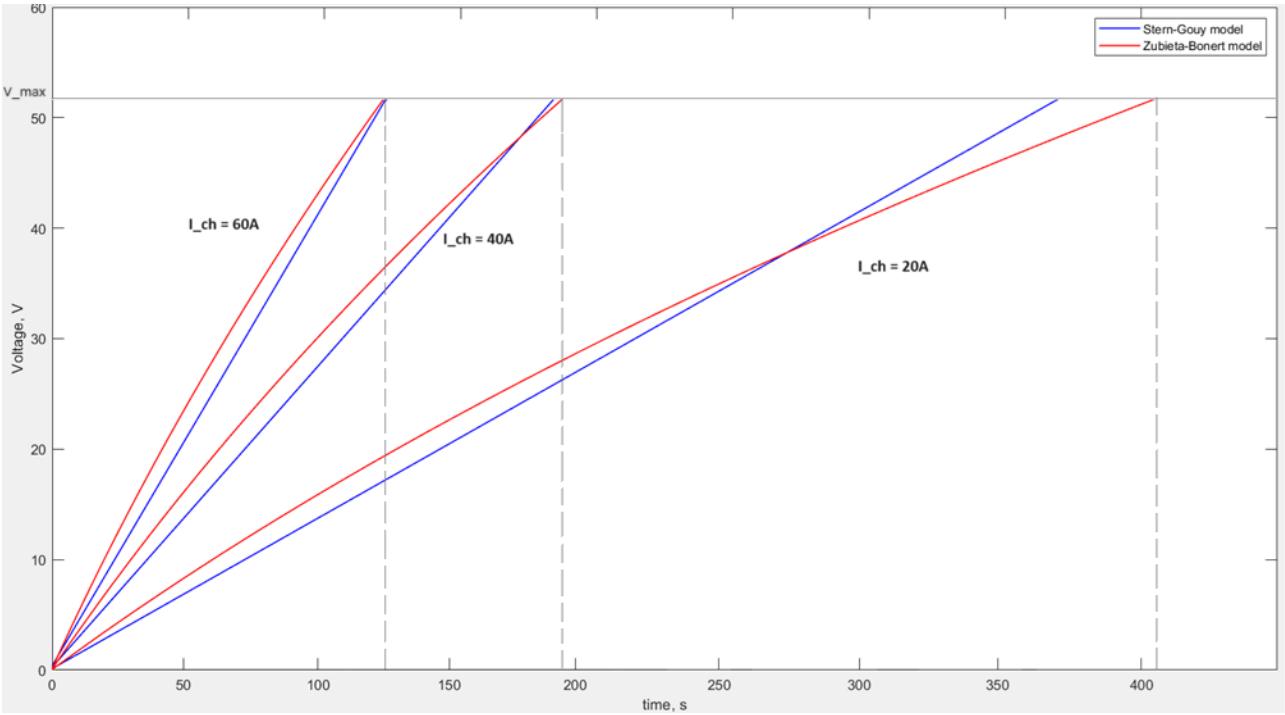

Figure 5.10: *Simulation results for different charging currents, Zubieta and Stern model comparison*

The same thing was done for the discharging phase. After every fully charge of the SC, it was discharged at different level of constant current at 20, 40, and 60 A. from experimental results [88], the total times of fully discharging a supercapacitor were (Figure 5.9):

- 121 seconds with a discharging current of 60 A
- 187 seconds with a discharging current of 40 A
- 370 seconds with a discharging current of 20 A

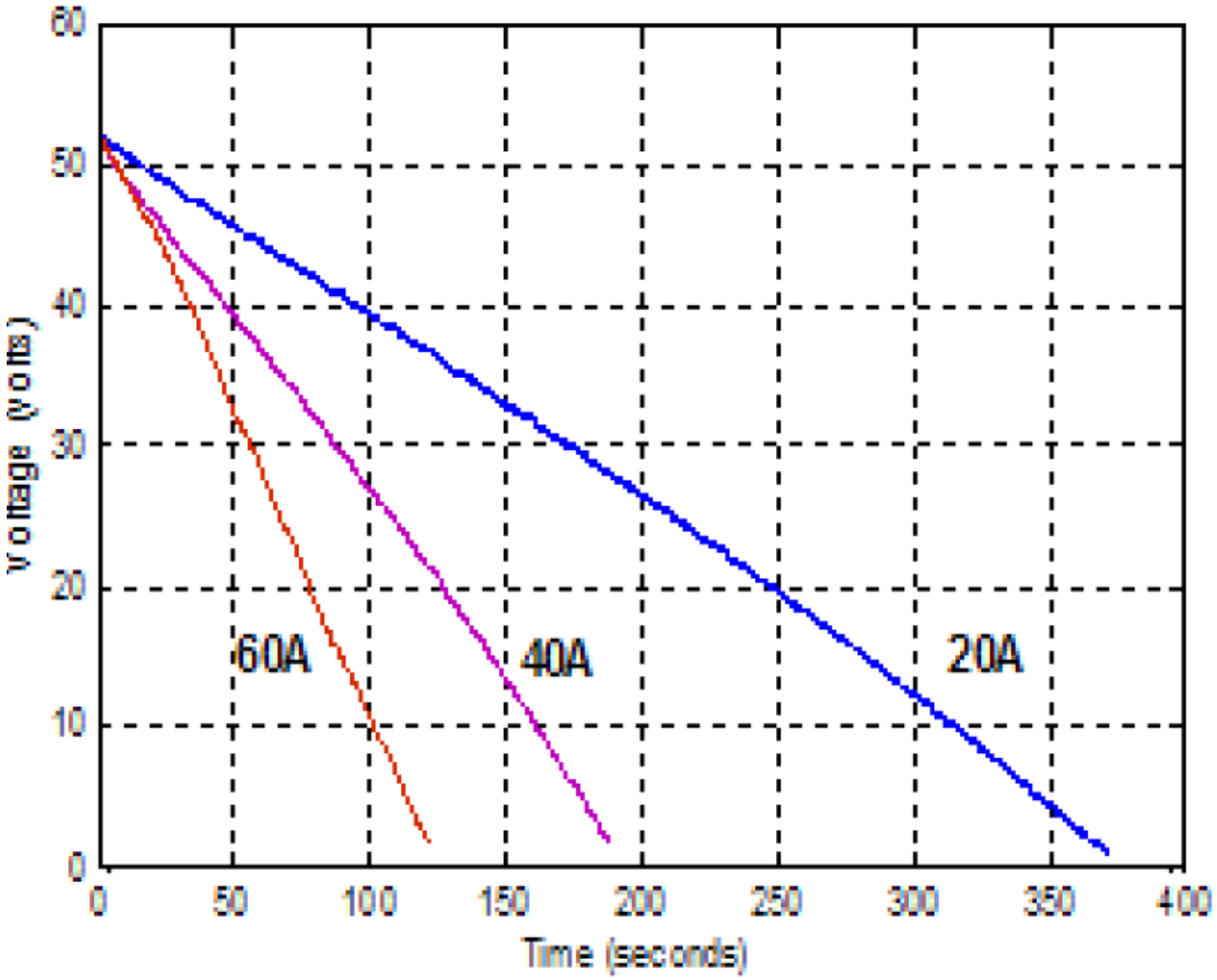

Figure 5.11: *Results of CCCD test with three different discharging currents [83]*

The results of the Zubieta and Stern model derived from Simulink simulations are shown in Figure 5.12.

The Zubieta model keeps the more curved trend even in discharging phase, but the difference between the two models is less visible in this case.

The total times for fully discharging the SC are similar for the two models, and rather corresponding to experimental data: around 122 seconds for 60 A, 185 seconds for 40 A and 370 seconds for 20 A.

It can be observed that the Stern model reports a voltage drop towards the end of the discharge, when the voltage level reaches values on the around of zero. Such a behaviour is not visible in experimental results, neither is reported in [88].

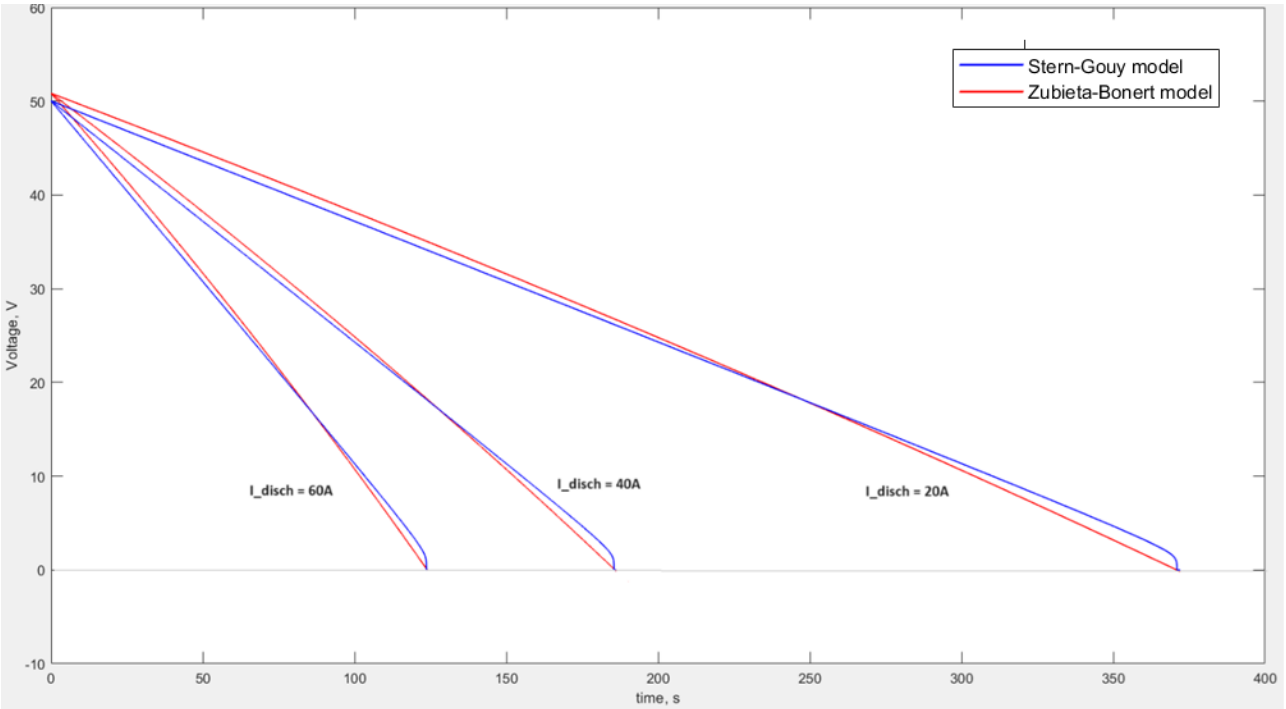

Figure 5.12: *Simulation results for different discharging currents, Zubieta and Stern model comparison*

The whole shape of the Zubieta model seems again more similar to the experimental one, as it happened for the charging phase, however, it is reasonable to say that both models can be considered as acceptable for our case, with regard to charging/discharging phases in the time-span of seconds/minutes.

5.3 Time-span of hours (self-discharge analysis)

One major obstacle for the application of EDLCs is the charge loss due to self-discharge mechanisms [93]. In this project, greater emphasis was put on the self-discharge behaviour of SCs. The self-discharge time-span was limited to few hours, as the duration of the EUROfusion cycle is around two hours and fifteen minutes. It should be noted that if the SC is required also during the two hours of reactor cycle, for instance to mantain frequence stability, the self-discharge effects would hardly affect the dynamic operations; instead, they

have major implications if the SC is kept at static setup during the 2 hours cycle of the reactor.

There are two main responsible effects of the voltage decay that occurs in SCs at rest: leakage current and charge redistribution, already discussed at paragraphs 3.6 and 4.1.2 respectively.

The charge redistribution effects are responsible of the voltage decay on the first stage [93]. The time during which their effect is visible can be variable, depending on the charge duration: In the case of a prolonged charging cycle the ions have enough time to migrate to the deeper pore structures; namely the meso- and micro-pores.

[95] showed that charging/discharging processes do not occur with the same time constant throughout the electrode material. This is due to the finite conductance of the electrolyte which leads to a voltage drop along the pore. As a result of this the macro-pores (which are at the mouth of the pore) have much smaller time constants than the meso- and micro-pores which are located in the deeper parts of the pore. This leads to the effect that the outer parts of the pores get charged/discharged much more quickly than the core pore structures.

In the case of short charging cycles most of the ions are still located at the pore opening which leads to a distinct gradient of ion concentration along the pore [93]. Figure 5.13 shows the experimental results of the self-discharge trend for a Nesscap 600F Supercapacitor, charged in three different times.

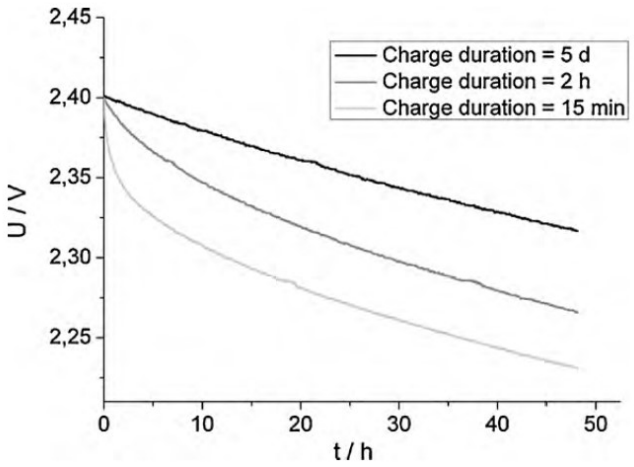

Figure 5.13: *Impact of charge duration on the open circuit voltage decay on a Nesscap 600F SC*

Hence the distinct open circuit voltage decay in the case of 15 min charge duration is no real charge loss due to self-discharge but is merely the effect of the redistribution of ions to areas of low ion concentration [96]. Approximately 50% of the open circuit voltage decay in the case the 15 min charge duration is caused by the redistribution effect within the first 48 h. The linear decline after the first 10–15 h of the open circuit voltage decay is assumed to be caused by real self-discharge mechanisms.

From figure 5.13, it can be observed that charge redistribution effet can be almost suppressed by charging the SC for quite a long time: indeed, the “5 d” curve (in black), shows a quite constant slope from the beginning.

In this project, the simulations on self-discharge were performed in MATLAB Simulink on a Maxwell Boostcap supercapacitor (2.7 V, 2600 F), and the experimental results taken from [90].

Figure 5.14 shows the voltage decay after the SC was charged with a current of 10 A up to its rated voltage. The experimental data are available for up to 30.000 s (around 8 hours) after the complete charging but, as mentioned before, we are interested in the around of the first 2 hours, so the simulation time was set to 10.000 s (charging phase included), for a total self-discharge time of around two hours and a half (left region in Figure 5.14).

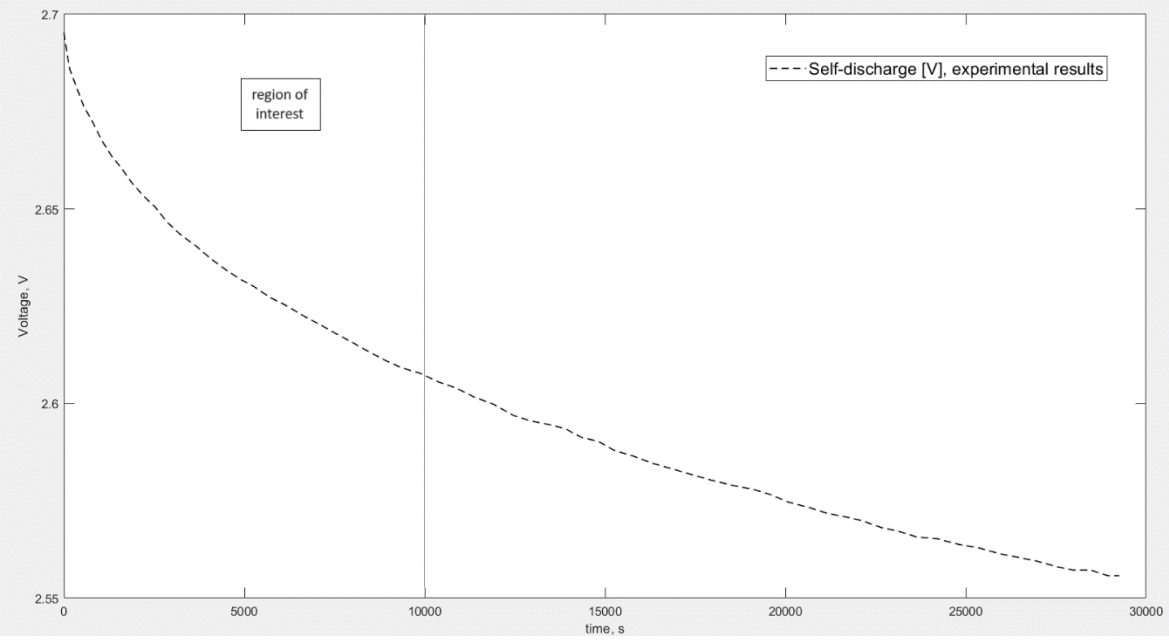

Figure 5.14: *Self discharge of a Maxwell 2600F, experimental results*

After 10.000 s, a voltage decay of around 0.1 V occurs. The trend is curved, as the charging phase was fast enough to make redistribution effects play a role in the first stage of open circuit.

Having experimental data on hand, the first simulation was carried out with the Stern model, in which experimental data can be put as input for the model in the window “Self-discharge”, as shown in Figure 5.15: one should specify the current prior open-circuit, and the voltage observed at 0, 10, 100 and 1000 seconds. Already by these input data, it can be supposed that the block properly models the self-discharge up to 1000 s (around 17 minutes), but it does not get any further than this.

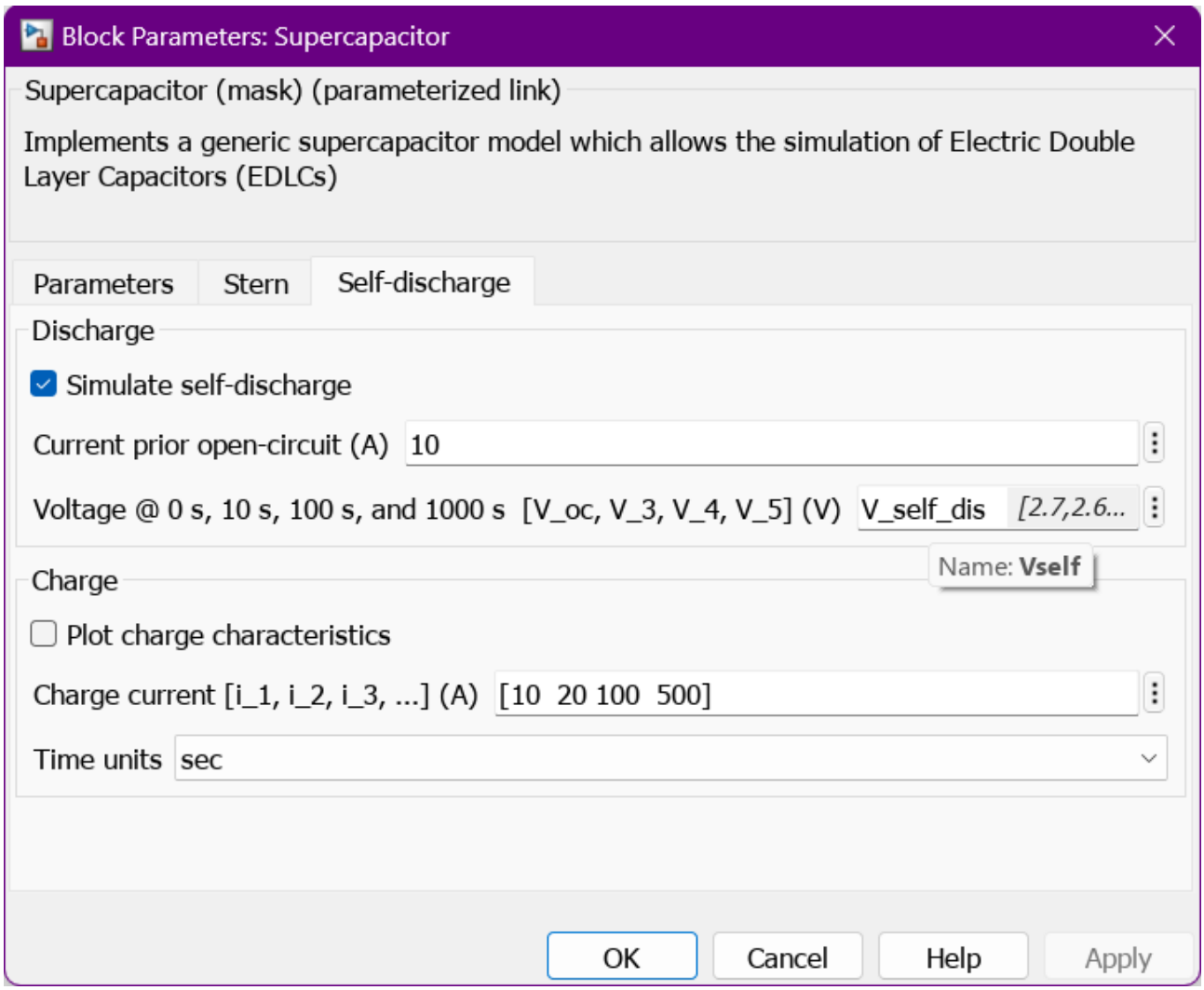

Figure 5.15: *Self-discharge window in Stern Simulink SC block*

After inputting the observed voltage values and running the simulation with a pattern similar to the one shown in Figure 5.9, the result is displayed in Figure 5.16.

As could be expected, the model works for the initial 1500-2000 s, but after that, it keeps a constant slope which is quite distant from the real one. At the end of the 10.000 seconds, a voltage loss of more than 0.2 V is reached, that is, more than double the voltage loss of experimental results.

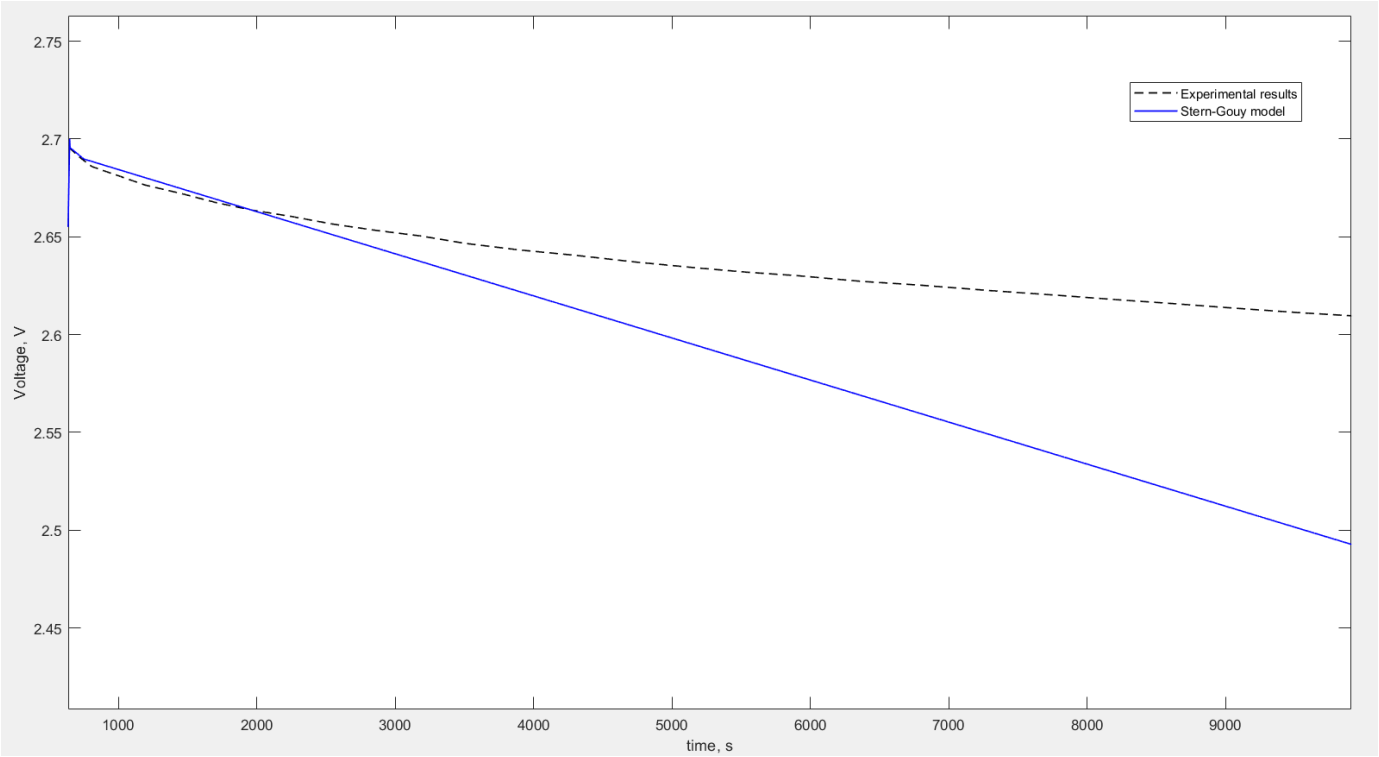

Figure 5.16: *Stern model self-discharge, comparison with experimental results*

Following this, the same simulation was run using the Zubieta model, formerly parameterized (the discharge resistance value was calculated as mentioned in [79]).

Figure 5.17 shows the results for Zubieta model in addition to the previous one.

As is evident from the plot, Zubieta model better represents the behaviour of the SC as the trend is rather similar to the experiments, although it results to be shifted up by around 0.02 V. It should be reminded that these simulations, such as the vast majority of simulations about self-discharge found in literature, are done on just one cell SC.

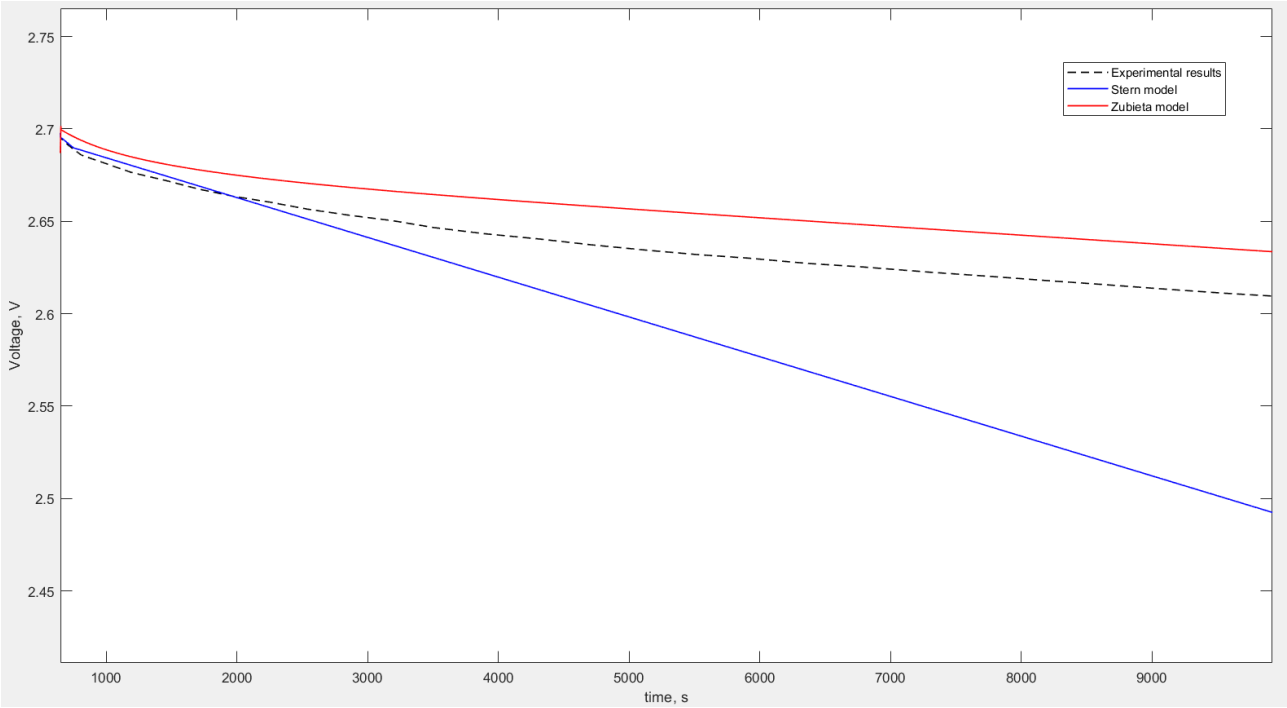

Figure 5.17: *Addition of Zubieta model results*

It means that the rated voltage is of around 2.7/3 V, and the error committed, although it seems to be small in absolute terms, should be considered relatively to the voltage application. Although the effective voltages of DEMOfusion network are not known yet, huge values can be predicted, in the order of kV or tens of kV: thus, the error is spread to several Volts, which means several kWh of stored energy losses (see section "Energy expression", paragraph 3.6).

In order to try to reduce the error on self-discharge, an additional model is proposed.

Since the slowest branch (third) of Zubieta model has a time constant in the order of thirty minutes, an fourth branch is added in the new model, with a time constant in the order of 100 minutes. The parameters R_4 and C_4 are calculated similarly to the metodology for the second and third branch.

As a matter of facts, this branch should take into account slower redistribution processes, in the order of hours. After three times the time constant of the branch, which means after roughly three hours, the branch reaches a situation of charge equilibrium.

Moreover, a voltage-dependent self-discharge resistance is added in series with the fixed leaked resistance of Zubieta model. A variable resistance for self-discharge is present in various models found in literature such as [90], [93]. As evident from experimental results,

higher voltage levels lead to more pronounced open circuit voltage decays: the voltage-dependent resistance is needed to model this behaviour.

The simulink implementation of this model is shown in Figure 5.18.

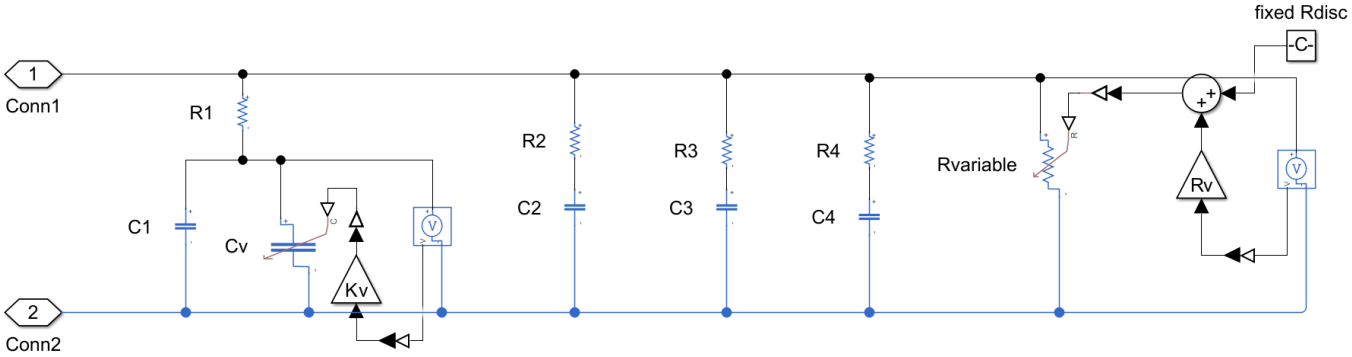

Figure 5.18: *Simulink implementation of 4-branches model*

The first three branches are rebuilt corresponding to Zubieta model.

It can be noticed an inner Voltage Sensor in the first branch, needed for the voltage-dependent capacitor (Cv); the measured voltage is multiplied by Kv by passing in the "gain" block. On the rightmost branch of the circuit, the voltage-dependent resistance is implemented, for which an other voltage sensor is needed.

The gain block "Rv", that is the resistance-voltage factor, is calculated in the MATLAB script by iterative calculation, based on the experimental results. Further analyses should be carried out for a more specific parameterization of this value. "R variable" is the sum of the voltage-dependent resistance and the fixed resistance, supposed to be in series with each other.

The same simulation as before was executed using this model, with the aim to get closer to experimental results. The results are shown in Figure 5.19.

This time, the voltage decay fits almost perfectly with experimental results. The voltage decay after 10.000 seconds corresponds, just as the overall voltage trend.

It can be noticed that the bent behaviour of the Zubieta model (in red), linked to the charge redistribution, ceases in between 2000 and 3000 seconds, becoming quite linear afterwards. The linear trend is due to the self-discharge resistance.

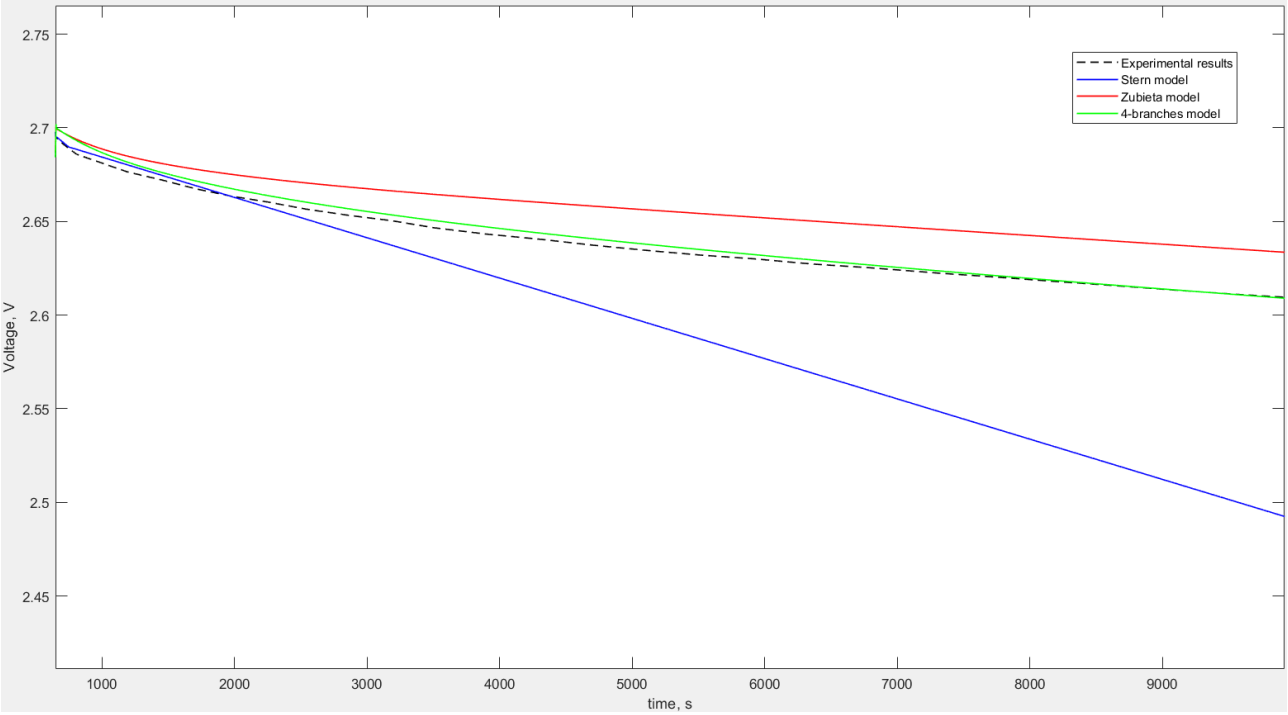

Figure 5.19: *4-branches model simulation results in comparison with other models*

On the contrary, the 4-branches model maintains a smoothly curved trend, like experimental results as well, nearly until the end of the simulation.

The fixed resistance contribution becomes more visible as getting closer to the end of the simulation, tending to flatten the voltage decay.

As previously noted, this model contains two voltage sensors which continuously measure the voltage across the first and last branch; moreover, an iterative calculation is implemented in MATLAB to calculate the voltage-dependent resistance gain. Therefore, the computational cost of simulations using this model is higher respect to the previous two.

As mentioned before, the charging current has an influence on the self-discharge of the SC. This should be modelled by the SC block, especially because extremely high values of current are handled in DEMOfusion network.

Figure 5.20 shows the voltage decay trends for two different charging current values, from experimental results [90]. The SC at stake is the same as before (Maxwell 2600 F).

The self-discharge curve is shifted from the initial voltage to zero, so that the voltage loss values can be observed more easily. By the way, the SC was charged up to its rated voltage of 2.7 V.

Again, we are interested only in the first 10.000 seconds of experimental results, they are available for a longer time-span though.

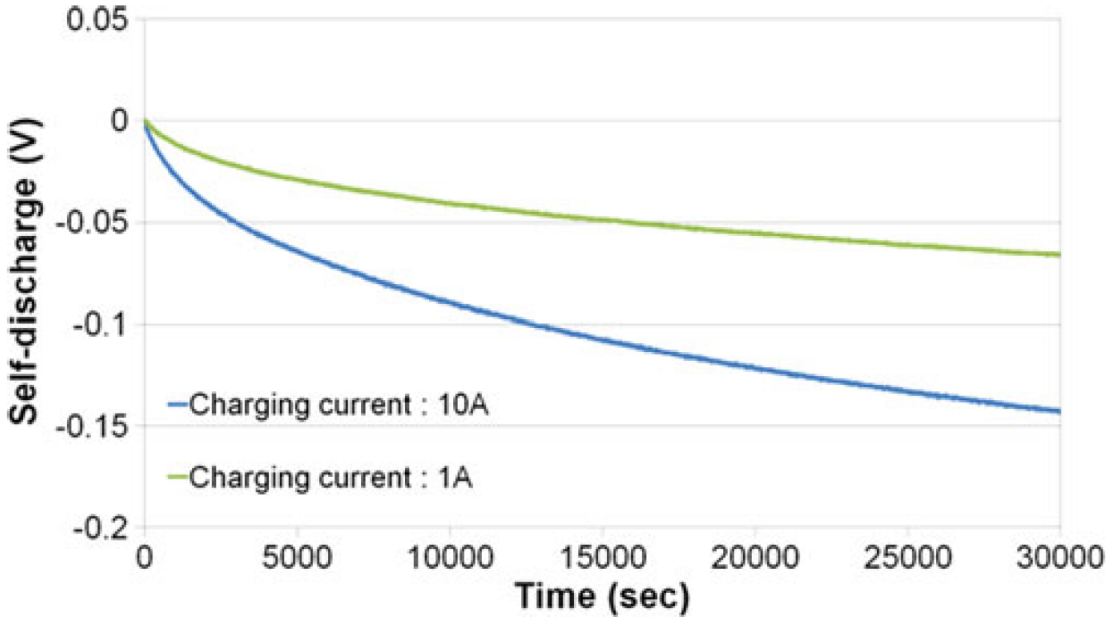

Figure 5.20: *Self-discharge of SC for different charging currents*

As predicted, the higher the charging current, the more noticeable the self discharge.

Figure 5.21, 5.22 and 5.23 show the results of the same test for the three different models.

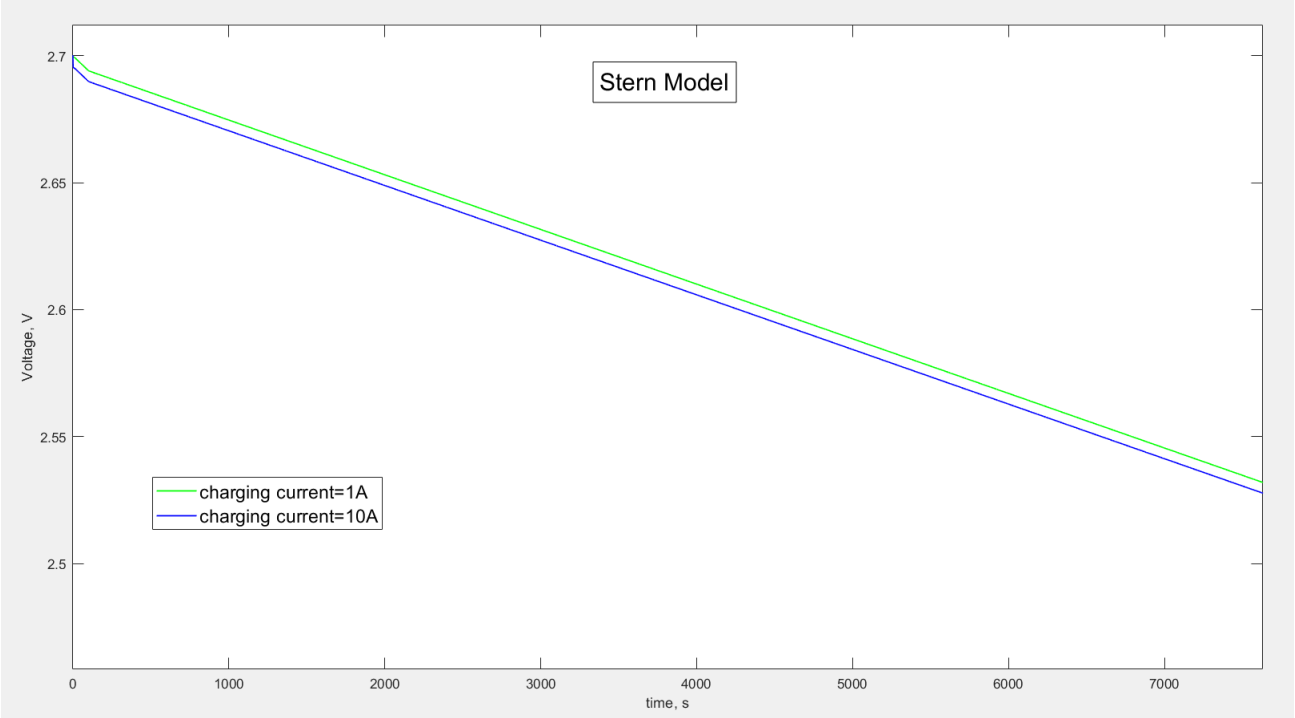

Figure 5.21: *Stern model results for different charging currents*

It is evident as the Stern SC does not make difference between the two charging currents modes. Only a larger IR voltage drop for is visible for charging current of 10 A, due to the Equivalent Series Resistance, not involved in the self-discharge.

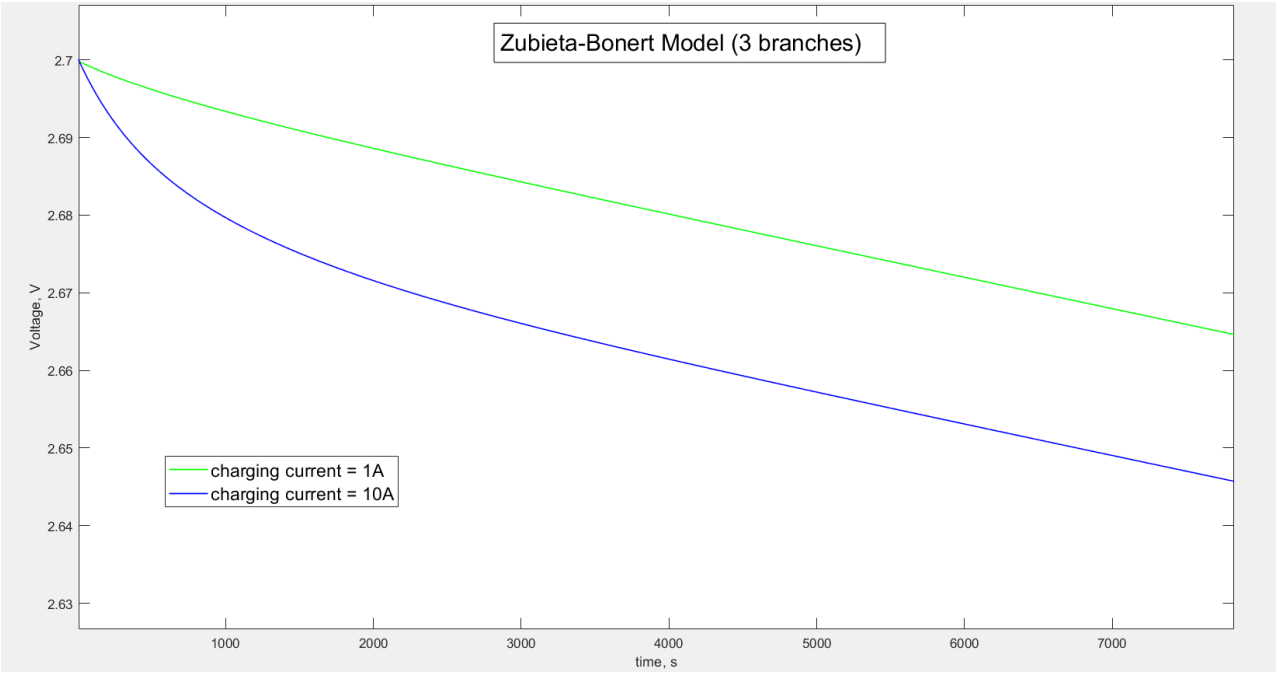

Figure 5.22: *Zubieta model results for different charging currents*

In Zubieta model simulation, a clear difference is visible. Nonetheless, the 1A plot is too flat respect to the experimental results in Figure 5.21.
Probably, the charging phase with 1 A is too long for a proper parameterization of the model; it should indeed be reminded that the charging phase should be as short as possible, in order to consider only the first branch capacitor to be affected by the charging, with the other two fully discharged [79].

The 4-branches model is again the closest one respect to experimental result (Figure 5.23). A noticeble difference between the two charging current modes can be seen, either the 1 A curve follows a similar trend to the experimental one.

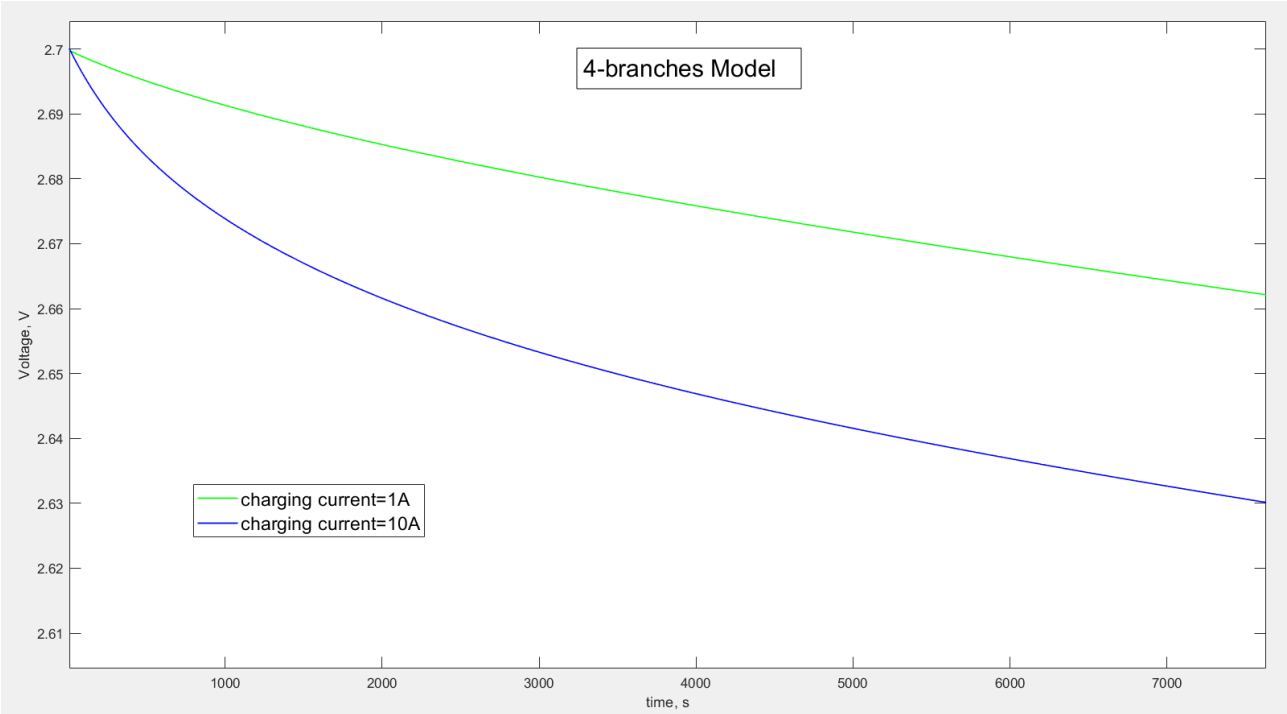

Figure 5.23: *4-branches model results for different charging currents*

Discarding the Stern model, too far from acceptable results, a comparison between Zubieta and 4-branches model is shown in Figure 5.24 about 1 A charging current.

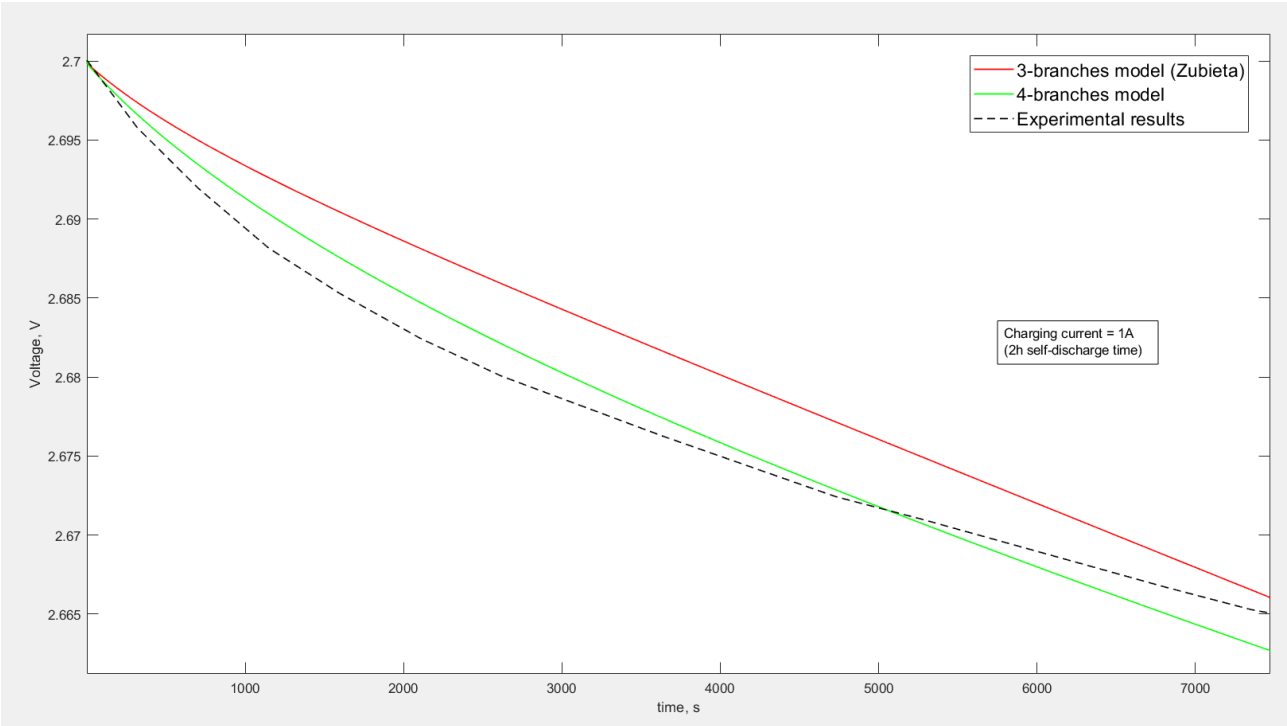

Figure 5.24: *Charging current = 1 A, results comparison*

Both models follow the experimental plot with acceptable precision.

A similar test was performed for what concerns the different initial voltage, from which the self-discharge phase begins. Higher voltage levels lead to more pronounced open circuit voltage decays [90], [93]. This can be observed in the experimental results in Figure 5.25, in which a current of 10 A was supplied to charge the SC up to 60% of rated voltage, and 100% of rated voltage.

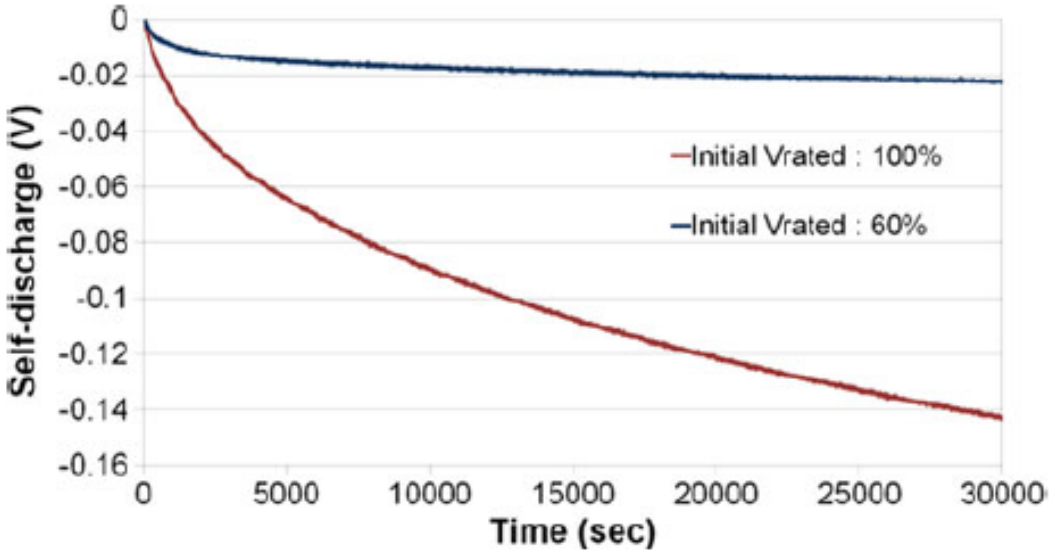

Figure 5.25: *Experimental results for self-discharge starting from different initial voltages*

The graphs of the following results are normalized by the two plots starting from zero.

As before, the Stern model did not represent this difference (Figure 5.26). Indeed, only one line is even visible as the Stern SC shaped the self-discharge trend exactly the same for the two different starting voltages.

Figure 5.27 and 5.28 display the results for Zubieta model and 4-branches model respectively.

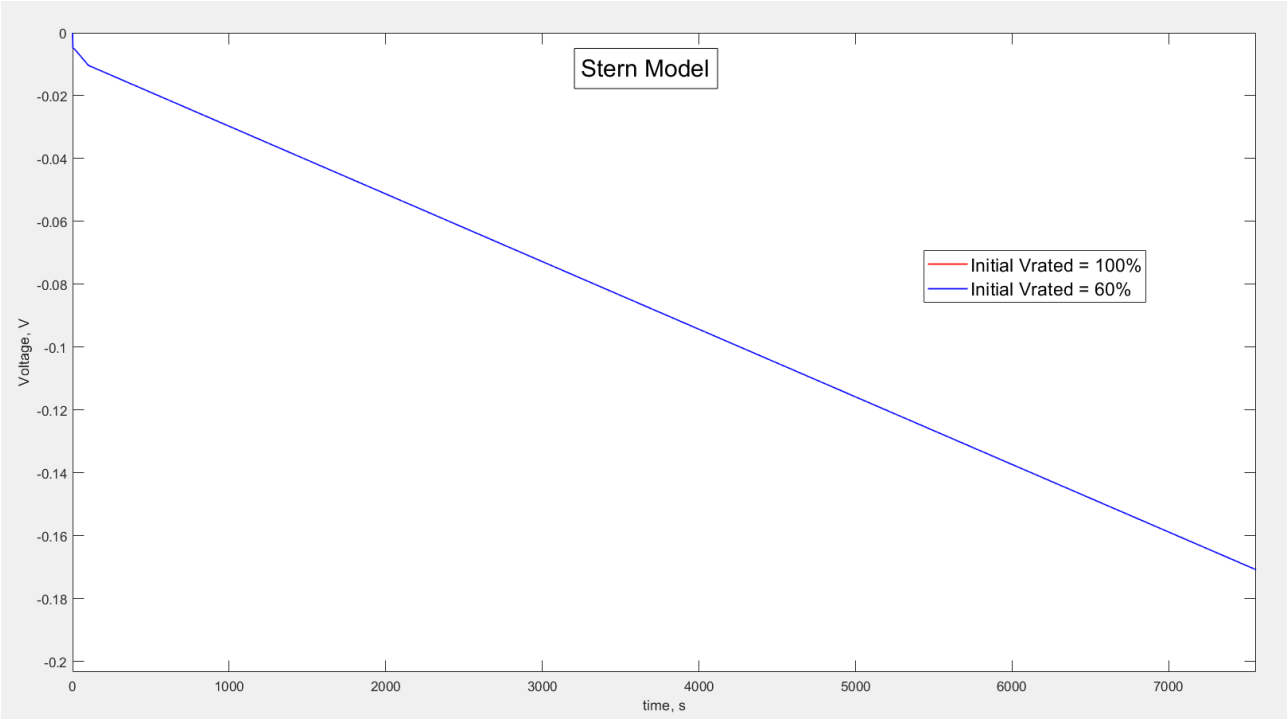

Figure 5.26: *Stern model results for self-discharge starting from different initial voltages*

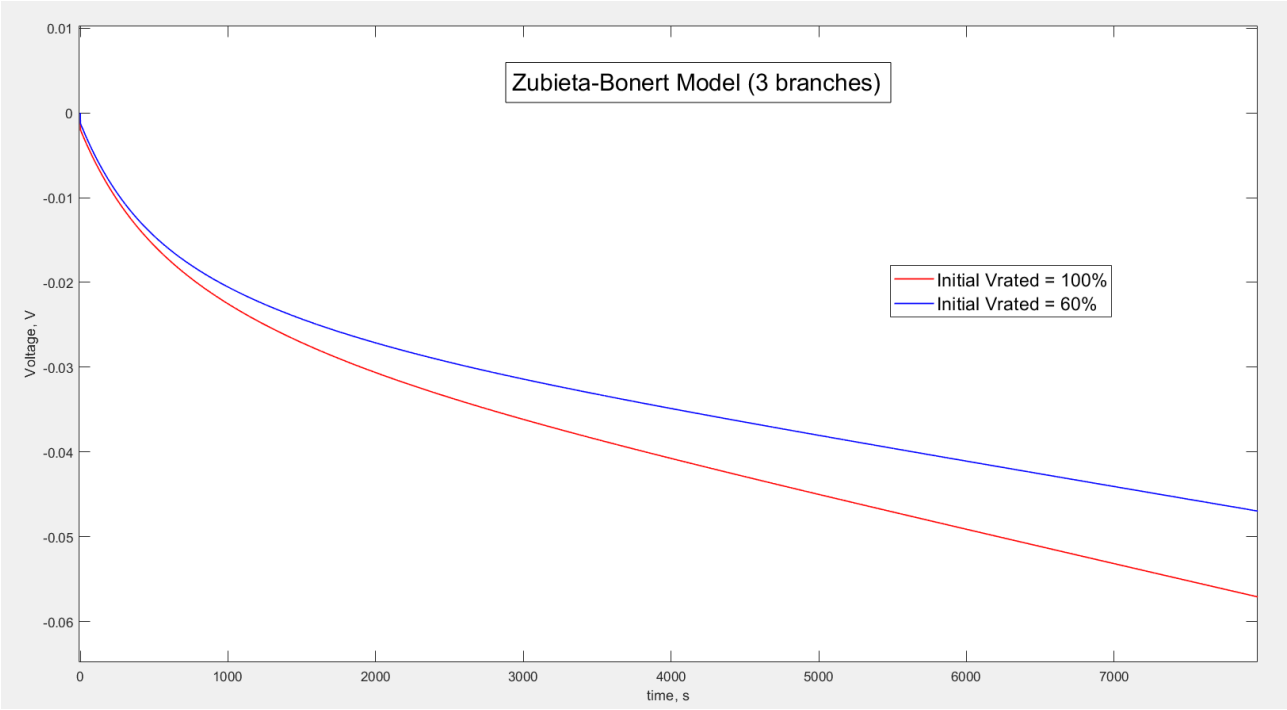

Figure 5.27: *Zubieta model results for self-discharge starting from different initial voltages*

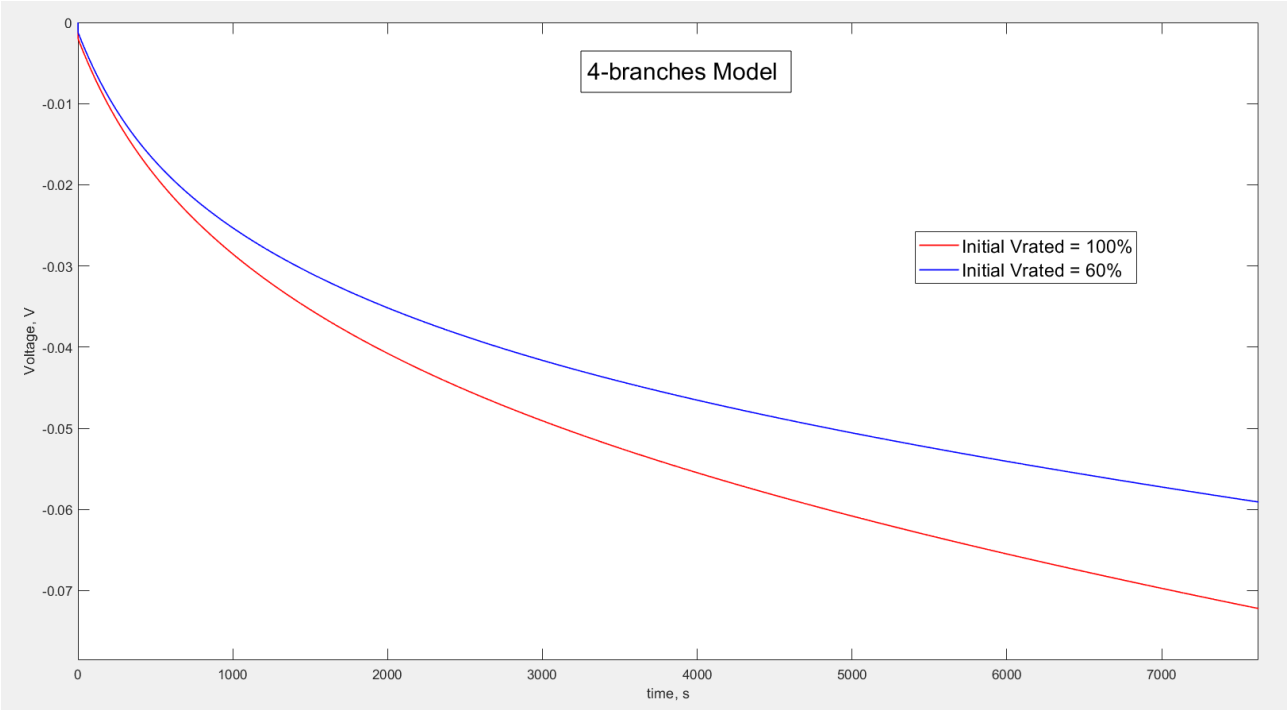

***Figure 5.28**: 4-branches model results for self-discharge starting from different initial voltages*

With these two models, a difference can be spotted between the two curves, although it is not as evident as in the experimental results of Figure 5.25.

As showed in Figure 5.19, the self-discharge profiles starting from 100% rated voltage are quite matched with experimental results, thus the difference is between the profiles from 60% voltage; a comparison between the two models can be seen in Figure 5.29.

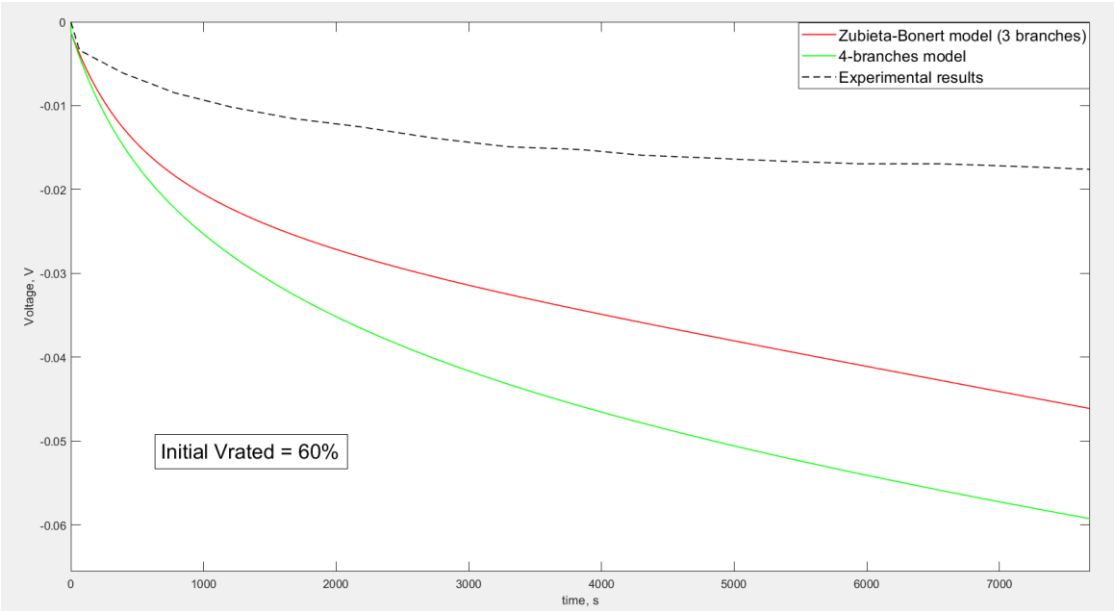

***Figure 5.29:** Initial voltage = 60%, results comparison*

This time, the Zubieta model gets closer to experimental results than the 4-branches model. Parameterization could play an important role in this experiment: it is usually done with a complete charging phase of the SC, and the parameters found could not properly work for other rated voltage tests, as in this case; yet, the final error is around 0.025 V for Zubieta model, and 0.04 V for 4-branches model, thus quite acceptable values.

Further refinements of the models should be carried out, in order to make them suitable within this aspect.

6. Conclusions

In this chapter, the conclusions of the project are drawn.

For starters, the reliability of the models depends on the quality of the assumptions.

Given the phase of development of DEMO, most assumptions are provisional. For instance, the active power profile of Figure 2.10, as well as derivative and step profile, consists of several subsystems of which final consumption is unknown; as a consequence, the real sizing and dynamic operation of the Energy Storage System results to be unknown yet.

As an example, if EES charging and discharging operations are required throughout all the cycle, for instance for frequence stability, the self-discharge modelling is deemed to be irrelevant in that case.

Moving on SC modelling taking these assumptions into account, the choice of the model to be used in future PES network simulations, is necessarily a tradeoff between accuracy and computational cost, as mentioned throughout the thesis.

Stern model is the most effortless to be used, since it can be given as an input all the main key parameters, findable in every commercial SC datasheet, as well as experimental data of constant current charging/discharging test and self-discharge test.

On the contrary, Zubieta and 4-branches model need a former parameterization, namely all the parameter values of their equivalent circuits need to be found before using them for simulations. The parameterization used for Zubieta and 4-branches models, described in paragraph 4.4 and implemented in a MATLAB script with Simulink/Simscape, led to satisfactory results, as visible in Figure 5.2. That was a solid starting point for these models to be further considered for the aim of this project.

In a short simulation period, so in the time-span of seconds or few minutes, all models provide enough accuracy results. The robustness of the results was confirmed for a variety of different SCs and initial conditions simulations.

However, the self-discharge analysis in the time-span of few hours led to differences among models; the Stern model, although given the correct experimental data as input, did not properly represent the voltage of the SC, as its voltage decay response was characterized by

a constant slope which cumulated voltage errors after around half an hour of open circuit, as displayed in Figure 5.13.

Hence, the Stern model is proper for a short simulations and as a first approximation, as its computational cost is rather low.

Conversely, Zubieta model represents self-discharge behaviour in acceptable way, at least for the first two hours of open circuit, *i.e.* the time cycle of the reactor.

The computational cost, not excessive, was comparable to Stern model's one.

Even more accurate results about self-discharge emerged from the 4-branches model, built during this graduation project for this purpose. It provided fine results with small errors for almost every simulation, but the computational cost was rather high, since it contains two voltage sensors within it, whose signals fall into a Simulink loop for voltage-dependent resistance and capacitance calculations, as explained in paragraph 5.3. This obviously leads to larger durations for simulations; in the up-coming project about DEMO, PES network simulations will be performed: PES network is an extremely complex system, and its Simulink model, even though is a simplified one, will require very high computational cost: there could be no chance to make it even heavier by connecting a complex Energy Storage System block to that.

However, the Zubieta model provides a good compromise between complexity and accuracy. In these terms, the best option would be to use this model for up-coming works, with the care of making a proper parameterization of the model before using it for simulations.

References

[1] V. Smil, Energy and civilization: a history. MIT press, 2018.

[2] IEA, “Key world statistics 2021”. “https://www.iea.org/reports/key-world-energy-statistics-2021”

[3] H. Ritchie, M. Roser, and P. Rosado, “Co and greenhouse gas emissions,” Our World in Data, 2020. “https://ourworldindata.org/co2-and-greenhouse-gas-emissions”.

[4] J. Ongena and Y. Ogawa, “Nuclear fusion: Status report and future prospects,” Energy Policy, vol. 96, pp. 770–778, 2016.

[5] Fusione nucleare, URL: https://nucleareeragione.org/fusione-nucleare-2

[6] D. Maradin, “Advantages and disadvantages of renewable energy sources utilization,” International Journal of Energy Economics and Policy, 2021

[7] M. Zucchetti, L. Candido, V. Khripunov, B. Kolbasov, and R. Testoni, “Fusion power plants, fission and conventional power plants. radioactivity, radiotoxicity, radioactive waste,” Fusion Engineering and Design, vol. 136, pp. 1529–1533, 2018. Special Issue: Proceedings of the 13th International Symposium on Fusion Nuclear Technology (ISFNT-13).

[8] S. Sandri, G. M. Contessa, M. D’Arienzo, M. Guardati, M. Guarracino, C. Poggi, and R. Villari, “A review of radioactive wastes production and potential environmental releases at experimental nuclear fusion facilities”, Environments, vol. 7, no. 1, 2020.

[9] D.Ward, I. Cook, Y. Lechon, and R. Saez, “The economic viability of fusion power” Fusion Engineering and Design, vol. 75-79, pp. 1221–1227, 2005. Proceedings of the 23rd Symposium of Fusion Technology.

[10] A. J. Donn´e, “Roadmap towards fusion electricity (editorial),” Journal of Fusion Energy, vol. 38, pp. 503–505, Dec 2019.

[11] International Atomic Energy Agency, https://www.iaea.org/newscenter/news/what-is-nuclear-fusion.

[12] EUROfusion, https://euro-fusion.org/eurofusion. 2023

[13] A. J. Donn’e, “Roadmap towards fusion electricity (editorial),” Journal of Fusion Energy, vol. 38, pp. 503-505, Dec 2019

[14] ITER, “What will ITER do”, https://www.iter.org/sci/Goals, 2023

[15] ITER, “Plasma heating”, https://www.iter.org/sci/plasmaheating, 2023

[16] S. Minucci, s. Panella, s. Ciattaglia, M.C. Falvo, A. Lampasi “Electrical loads and Power Systems for the DEMO Nuclear Fusion Project”, Energies, vol. 13, no. 9, p. 2269, 2020.

[17] H. Zohm, “On the size of tokamak fusion power plants”, Philosophical Transactions of the Royal Society, A, vol.377, no.2141, p. 20170437, 2019.

[18]C. C. Petty, J. C. DeBoo, R. J. L. Haye, T. C. Luce, P. A. Politzer, and C. P.-C.Wong, “Feasibility study of a compact ignition tokamak based upon gyrobohm scaling physics,” Fusion science and technology, vol. 43, no. 1, pp. 1–17, 2003.

[19] E. Gaio, A. Ferro, A. Lampasi, A. Maistrello, M. Dan, M. Falvo, F. Gasparini, F. Lunardon, A. Magnanimo, M. Manganelli, S. Minucci, S. Panella, M. Proietti Cosimi, D. Ratti, L. Barucca, S. Ciattaglia, T. Franke, G. Federici, and R. Piovan, “Status and challenges for the concept design development of the EU DEMO Plant Electrical System,” Fusion Engineering and Design, vol. 177, p. 113052, 2022.

[20] M. De Nardi and M. Recchia, “Studies on ecrh ps topology to reduce the power request on the ac side”

[21] A. Ferro, M. Dan, and F. Lunardon, “Update of the iter-like design of cs-pf power supplies and fdu”. Report IDM reference No. EFDA D 2Q6988.

[22]Ferro, A.; Lunardon, F.; Ciattaglia, S.; Gaio, E. “The reactive power demand in DEMO: Estimations and study of mitigation via a novel design approach for base converters”. *Fusion Eng. Des.* 2019, *146*, 2687–2691.

[23] I. Moscato, L. Barucca, E. Bubelis, G. Caruso, S. Ciattaglia, C. Ciurluini, A. Del Nevo, P. Di Maio, F. Giannetti, , W. Hering, P. Lorusso, E. Martelli, V. Narcisi, S. Norrman, T. Pinna, S. Perez-Martin, A. Quartararo, M. Szogradi, A. Tarallo, and E. Vallone, “Tokamak cooling systems and power conversion system options”, Fusion Engineering and Design, vol. 178, p. 113093, 2022.

[24] S. Minucci, “Update of the electrical load list”.

[25] M. Tran, P. Agostinetti, G. Aiello, K. Avramidis, B. Baiocchi, M. Barbisan, V. Bobkov, S. Briefi, A. Bruschi, R. Chavan, I. Chelis, C. Day, R. Delogu, B. Ell, F. Fanale, A. Fassina, U. Fantz, H. Faugel, L. Figini, and W. Zhang, “Status and future development of heating and current drive for eu demo”, Fusion Engineering and Design, vol. 180, p. 113159, 2022.

[26] M. De Nardi and M. Recchia, “Studies on ecrh ps topology to reduce the power request on the ac side”. Report IDM reference No. EFDA D 2Q8MEG.

[27] J. Markus “Electrical Energy Storage Systems at the DEMO Fusion Power Plant”, 2023.

[28] F. Ottonello, “Tg coordinator.”

[29] C. Falvo, “First outcomes from the study of the generator operation in the indirect and direct bb phts&pcs coupling option,” 2020. Report IDM reference No. EFDA D 2NUUWT.

[30] Comission Regulation (EU), “Establishing a network code on requirements for grid connection of generators”. “http://data.europa.eu/eli/reg/2016/631/oj”, 2016.

[31] J. Mitali, S. Dhinakaran, and A. Mohamad, “Energy storage systems: A review,” Energy Storage and Saving, 2022.

[32] A. Olabi, C. Onumaegbu, T. Wilberforce, M. Ramadan, M. A. Abdelkareem, and A. H. Al – Alami, “Critical review of energy storage systems,” Energy, vol. 214, p. 118987, 2021.

[33] Slides Prof. G. Comodi, https://learn.univpm.it/course/SAG_07, Univpm, 2023.

[34] Wang Y et al. “Recent progress in carbon-based materials for supercapacitor electrodes: A review”. Journal of of Materials Science, 2021.

[35] Kötz R, Carlen M. “Principles and applications of electrochemical capacitors”. Electrochimica Acta. 2000.

[36] Wang H et al. “Interconnected carbon nanosheets derived from hemp for ultrafast supercapacitors with high energy”. ACS Nano. 2013.

[37] An KH et al. “Supercapacitors using single-walled carbon nanotube electrodes”. Advanced Materials, 2001.

[38] Beidaghi M, Wang C. “Microsupercapacitors based on three dimensional interdigital polypyrrole/CMEMS electrodes”. Electrochimica Acta, 2011.

[39]Yun YS, Park HH, Jin H-J. “Pseudocapacitive effects of N-doped carbon nanotube electrodes in supercapacitors”. Materials, 2012

[40] Raza Wet al. “Recent advancements in supercapacitor technology” Nano Energy, 2018

[41] Bansal RC, Goyal M. “Activated Carbon Adsorption”. Boca Raton: CRC Press, 2005

[42] Imtiaz Ahmed Khan, Litty Thekkekara, Sania Waqar, Nauman Choudhry and Sabu John “Supercapacitors fabrication and performance evaluation techniques”.

[43] Zhang L et al. “Porous 3D graphenebased bulk materials with exceptional high surface area and excellent conductivity for supercapacitors”. Scientific Reports, 2013.

[44] Basnayaka PA, Ram MK, Stefanakos L and Kumar A. “Graphene/polypyrrole nanocomposite as electrochemical supercapacitor electrode: Electrochemical impedance studies”. 2013.

[45] Forouzandeh P, Kumaravel V, Pillai SC. “Electrode materials for supercapacitors: A review of recent advances”. Catalysts, 2020.

[46] Ma Z, Zheng R, Liu Y, Ying Y, Shi W. “Carbon nanotubes interpenetrating MOFs-derived Co-Ni-S composite spheres with interconnected architecture for high performance hybrid supercapacitor”. Journal of Colloid and Interface Science, 2021.

[47]Wang G, Zhang L, Zhang J. “A review of electrode materials for electrochemical supercapacitors”. Chemical Society Reviews. 2012.

[48]Verma KD, Sinha P, Banerjee S, Kar KK, Ghorai MK. “Characteristics of separator materials for supercapacitors”. In: Handbook of Nanocomposite Supercapacitor Materials I. Switzerland AG: Springer; 2020.

[49] F. Nadeem, S. M. S. Hussain, P. K. Tiwari, A. K. Goswami, and T. S. Ustun, “Comparative review of energy storage systems, their roles, and impacts on future power systems,” IEEE Access, vol. 7, pp. 4555–4585, 2019.

[50] Z. Sanliang, P. Ning “Supercapacitors Performance Evaluation”, Advanced Energy Materials, 1614-6832, 2015.

[51] Wang J., et al., “Pseudocapacitive contributions to electrochemical energy storage in TiO_2 (Anatase) nanoparticles”, The journal of physical chemistry, 2007.

[52] Khomenko, V., E. Frackowiak, and F. Béguin, “Determination of the specific capacitance of conducting polymer/nanotubes composite electrodes using different cell configurations”. Electrochimica Acta, 2005.

[53] Liu, T.-C., et al., “Behavior of Molybdenum Nitrides as Materials for Electrochemical Capacitors”. J. Electrochem. Soc., 1998.

[54] Miller, J.R., R.A. Outlaw, and B.C. Holloway, “Graphene double-layer capacitor with AC line-filtering performance”. Science, 2010.

[55] Du, C. and N. Pan, “Supercapacitors using carbon nanotube films by electrophoretic deposition”. Journal of Power Sources, 2006.

[56] Taberna, P.L., P. Simon, and J.F. Fauvarque, “Electrochemical Characteristics and Impedance Spectroscopy Studies of Carbon-Carbon Supercapacitors”. Journal of The Electrochemical Society, 2003.

[57] Dupont, M.F., A.F. Hollenkamp, and S.W. Donne, “Large Amplitude Electrochemical Impedance Spectroscopy for Characterizing the Performance of Electrochemical Capacitors”. Journal of The Electrochemical Society, 2014.

[58] Zhu, Y., et al., “Carbon-based supercapacitors produced by activation of graphene”. Science, 2011.

[59] Burke, A., & Miller, M. “Testing of electrochemical capacitors: Capacitance, resistance, energy density, and power capability”. *Electrochimica Acta, 2010.*

[60] Maxwell Technologies, Inc. “Test procedures for capacitance, ESR, leakage current and self-discharging characterizations of ultracapacitors”. *2009.*

[61] Vicentini, R., Da Silva, L. M., Cecilio Junior, E. P., Alves, T. A., Nunes, W. G., & Zanin, H. “How to measure and calculate equivalent series resistance of electric double-layer capacitors”. *Molecules, 24*(8), 2019

[62] Lu, M *“New materials for sustainable energy and development”.* Supercapacitors - Materials, systems, and applications, 2013.

[63] Kurzweil, P., & Chwistek, M. “Electrochemical stability of organic electrolytes in supercapacitors: Spectroscopy and gas analysis of decomposition products”. *Journal of Power Sources, 2008.*

[64] Ong, S. P., & Ceder, G. “ Investigation of the effect of functional group substitutions on the gas-phase electron affinities and ionization energies of room-temperature ionic liquids ions using density functional theory”. *Electrochimica Acta, 2010.*

[65] Armand, M., et al. “Ionic-liquid materials for the electrochemical challenges of the future”. *Nature Materials*. 2009.

[66] Qu, Q. T., et al. “Study on electrochemical performance of activated carbon in aqueous Li2SO4, Na2SO4 and K2SO4 electrolytes”. *Electrochemistry Communications, 2008.*

[67] Burke A. and Miller M. “The power capability of ultracapacitors and lithium batteries for electric and hybrid vehicle applications”. Journal of Power Sources, 2011.

[68] Thompson Phillips (2009-05-30), Dynamo-Electric Machinery; A Manual for Students of Electrotechnics, BiblioBazaar, LLC, ISBN 978-1-110-35104-6

[69] IOXUS, “Notes on supercapacitors supecifications”, https://ioxus.com.

[70] IOXUS,“Representative Test Procedures for Customer Evaluations”, https://ioxus.com.

[71] Ma, N., Yang, D., Riaz, S., Wang, L., & Wang, K. “Aging Mechanism and Models of Supercapacitors: A Review”. School of Electrical Engineering, Weihai Innovation Research Institute, Qingdao University, 2023.

[72]Ayadi, M.; Briat, B.; Lallemand, R.; Eddahech, A.; German, R.; Coquery, G.; Vinassa, J.M. “Description of supercapacitor performance degradation rate during thermal cycling under constant voltage ageing test”. *Microelectron. Reliab.* 2014.

[73]Bohlen, O.; Kowal, J.; Sauer, D.U. “Ageing behaviour of electrochemical double layer capacitors—Part II. Lifetime simulation model for dynamic applications”. *J. Power Sources* 2007.

[74] Zheng, F.H.; Li, Y.X.; Wang, X.S. “Study on effects of applied current and voltage on the ageing of supercapacitors”. *Electrochim. Acta* 2018.

[75] Sedlakova, V.; Sikula, J.; Majzner, J.; Sedlak, P.; Kuparowitz, T.; Buergler, B.; Vasina, P. “Supercapacitor degradation assesment by power cycling and calendar life tests”. *Metrol. Meas. Syst.* 2016

[76] Arkadiusz Szewczyk, Josef Sikula, Vlasta Sedlakova, Jiri Majzner, Petr Sedlak, Tomas Kuparowitz “ Voltage dependence of supercapacitor capacitance”. Gdańsk University of Technology, Faculty of Electronics, Telecommunications and Informatics, 201

[77] Lee, J.; Yi, J.; Kim, D.; Shin, C.; Min, K.S.; Choi, J.; Lee, H.Y. “Modeling of the Electrical and Thermal Behaviors of an Ultracapacitor”. Energies. 2014.

[78] Ayao Kitahara And Akira Watanabe . "Electrical Phenomena At Interfaces. Fundamentals, Measurements And Applications", 1984.

[79] Zubieta, L. and R. Bonert. “Characterization of Double-Layer Capacitors for Power Electronics Applications.” *IEEE Transactions on Industry Applications*, Vol. 36, No. 1, 2000, pp. 199–205.

[80] E. Gileadi, E. Kirowa Eisner And J Pemciner. "Interfacial Electro-Chemistry. An Experimental Approach.", 1975

[81] Shao-Long Zhong, Zhi-Min Dang, Wen-Ying Zhou, Hui-Wu Cai, “Past and future on nanodieletrics”. State Key Laboratory of Power System and Department of Electrical Engineering, Tsinghua University, Beijing

[82] R. Morrison. "The chemical physics of surfaces, " 1990. Plenum Press.

[83] F. Licht, M.A. Davis, A.H. Andreas, “Charge redistribution and electrode history impact galvanostatic charging/discharging and associated figures of merit”. Journal of Power Sources, 2020.

[84] Sedlakova, V., Sikula, J., Majzner, J., Sedlak, P., Kuparowitz, T., Buergler, B., Vasina, P. (2015). “Supercapacitor equivalent electrical circuit model based on charges redistribution by diffusion”. J. Power Sources, 286, 58–65

[85] Xu, N.; Riley, J. “Nonlinear analysis of a classical system: The double-layer capacitor”. *Electrochem. Commun.* 2011.

[86] Kang, J.; Wen, J.; Jayaram, S.H.; Yu, A.; Wang, X. “Development of an equivalent circuit model for electrochemical double layer capacitors (EDLCs) with distinct electrolytes”. Electrochim. Acta 2014.

[87] Oldham, K.B. “A Gouy–Chapman–Stern model of the double layer at a (metal)/(ionic liquid) interface”. J. Electroanal. Chem. 2008.

[88] Z. M. Salameh, AB cultura ll, “Modeling, evaluation and simulation of a Supercapacitor module for energy storage application”

[89] Pankaj Saha, Munmun Khanra "Equivalent Circuit Model of Supercapacitor for Self-Discharge Analysis - A Comparative Study". International conference on Signal Processing, Communication, Power and Embedded System. 2016.

[90] Kim, Sang-Hyun, Woojin Choi, Kyo-Bum Lee, and Sewan Choi. "Advanced Dynamic Simulation of Supercapacitors Considering Parameter Variation and Self-Discharge." IEEE Transactions on Industrial Electronics, vol. 61, no. 7, 2014.

[91] Mathworks documentation, https://nl.mathworks.com/help/sps/ug/supercapacitor-parameter-identification.html.

[92] IOXUS X-SERIES, https://ioxus.com/product/imod128v041a23.

[93] Kaus, M., Kowal, J., & Sauer, D. U. “Modelling the effects of charge redistribution during self-discharge of supercapacitors”. *Electrochemical Energy Conversion and Storage Systems Group, Institute for Power Electronics and Electrical Drives (ISEA), RWTH Aachen University, Jagerstr. 2010.*

[94] B.W. Ricketts, C. Ton-That, “Self-discharge of carbon-based supercapacitors with organic electrolytes”. J. Power Sources 89 2000.

[95] R. De Levie, “On porous electrodes in electrolyte solutions: Capacitance effects”. Electrochim, Acta, 1963.

[96] J. Kowal, E. Avaroglu, F. Chamekh, A. “Senfelds, T. Thien, D. Wijaya, D.U. Sauer, “Detailed analysis of the self-discharge of supercapacitors” J. Power Sources, 2009.